



**AALBORG UNIVERSITY**  
DENMARK

**Aalborg Universitet**

## **Applications of electron deficient hetero aromatic moieties**

*In donor-acceptor polymers and small molecule acceptors towards roll coated solar cells*

Brandt, Rasmus Guldbæk

DOI (link to publication from Publisher):  
[10.5278/vbn.phd.engsci.00047](https://doi.org/10.5278/vbn.phd.engsci.00047)

Publication date:  
2016

Document Version  
Publisher's PDF, also known as Version of record

[Link to publication from Aalborg University](#)

Citation for published version (APA):

Brandt, R. G. (2016). *Applications of electron deficient hetero aromatic moieties: In donor-acceptor polymers and small molecule acceptors towards roll coated solar cells*. Aalborg Universitetsforlag. <https://doi.org/10.5278/vbn.phd.engsci.00047>

### **General rights**

Copyright and moral rights for the publications made accessible in the public portal are retained by the authors and/or other copyright owners and it is a condition of accessing publications that users recognise and abide by the legal requirements associated with these rights.

- Users may download and print one copy of any publication from the public portal for the purpose of private study or research.
- You may not further distribute the material or use it for any profit-making activity or commercial gain
- You may freely distribute the URL identifying the publication in the public portal -

### **Take down policy**

If you believe that this document breaches copyright please contact us at [vbn@aub.aau.dk](mailto:vbn@aub.aau.dk) providing details, and we will remove access to the work immediately and investigate your claim.



**APPLICATIONS OF ELECTRON DEFICIENT  
HETERO AROMATIC MOIETIES:  
IN DONORACCEPTOR POLYMERS  
AND SMALL MOLECULE ACCEPTORS  
TOWARDS ROLL COATED SOLAR CELLS**

**BY  
RASMUS GULDBÆK BRANDT**

DISSERTATION SUBMITTED 2016



**AALBORG UNIVERSITY**  
DENMARK



# **APPLICATIONS OF ELECTRON DEFICIENT HETERO AROMATIC MOIETIES: IN DONOR- ACCEPTOR POLYMERS AND SMALL MOLECULE ACCEPTORS TOWARDS ROLL COATED SOLAR CELLS**

by

Rasmus Guldbæk Brandt



**AALBORG UNIVERSITY**  
DENMARK

Dissertation submitted

Dissertation submitted: February, 2016

PhD supervisor: Associate Prof. Donghong Yu  
Aalborg University

PhD committee: Associate Professor Vittorio Boffa (chairman)  
Aalborg University, Denmark

Director Peter Sommer-Larsen  
Danish Technological Institute, Denmark

Professor Zhishan Bo  
Beijing Normal University, China

PhD Series: Faculty of Engineering and Science, Aalborg University

ISSN (online): 2246-1248  
ISBN (online): 978-87-7112-518-4

Published by:  
Aalborg University Press  
Skjernvej 4A, 2nd floor  
DK – 9220 Aalborg Ø  
Phone: +45 99407140  
aauf@forlag.aau.dk  
forlag.aau.dk

© Copyright: Rasmus Guldbæk Brandt

Printed in Denmark by Rosendahls, 2016

# ENGLISH SUMMARY

Organic photovoltaics are a field of science that has attracted great interest throughout several decades with strong reasons. The demand for energy is ever growing, while fossil fuels are getting scarcer. Therefore, developing renewable energy sources is instrumental in achieving an alternative, fossil fuel free, and sustainable future. Within the field of organic photovoltaics, there is several interesting disciplines. The three most predominate are synthesis of light-harvesting materials, the scaling of production, and stability of devices. In this PhD-thesis, the focus will be on the application of novel hetero atomic semiconducting conjugated materials and the transition from small area spin-coated organic photovoltaic devices to large area devices. The topics covered in this thesis are, rational molecular design, syntheses, and characterization of novel low bandgap conjugated polymers, boron containing conjugated polymers, and small molecule acceptors for roll coated organic photovoltaic devices, and lastly the synthesis and characterization of water-processable conjugated polymer nanoparticles for organic photovoltaic fabrication.

In this thesis, a series of benzodipyrrolidone-based low band gap polymers have been designed, synthesized, and characterized in regards to both structure and photo-physical properties. The photovoltaic device in small areas were tested and reached power conversion efficiencies around 0.6%, however, the scalable roll-coated solar cells obtained limited success. In parallel, two isoindigo based low band gap polymers were synthesized and characterized. While one of the polymers showed little potential, the other, an isoindigo-dithienopyrrole polymer, showed great potential affording a power conversion efficiency of 0.25% in a small area device. The potential became even greater as an all solution processed, ITO- and vacuum-free large area device exhibited a power conversion efficiency approaching 1%. Due to the absorbance characteristics of the promising polymer, roll coated tandem photovoltaic devices have been constructed together with the high bandgap polymer PBDTTTz-4. The resulting device showed an efficiency of 1.73% with an open circuit voltage of 1.08V.

Furthermore, a novel borylated carbazole conjugated monomer has been reported and fully characterized both structurally and photo-physically. This novel monomer has been polymerized with both donor and acceptor monomers. Molecular dynamics simulations indicated an interesting pseudo-acceptor characteristic. The synthesized polymers were characterized both in regards to structure and photo-physical properties. The combination of the borylated carbazole and an alkylthienyl-substituted-benzodithiophene donor resulted in a polymer that was tested in an organic photovoltaic device with a power conversion efficiency of 3.8%, which clearly emphasized the great potential of the novel monomer for future incorporation with various donor moieties.

One key barrier associated with the scaling of organic photovoltaic technology is the utilization of fullerenes as the electron acceptor in the active layer materials of the photovoltaic devices. This is an issue due to the energy intensity of these fullerenes, and an alternative electron acceptor must therefore be developed. Small molecule acceptors are a possible approach, and this has been studied extensively. Very few studies have been made investigating the transferal of these types of molecules from small area spin-coated devices to

the scalable roll-coated devices. In this study three simple small molecule acceptors have been investigated and both structurally and photo-physically characterized. It was shown that their molecular geometry has a great impact on the transferal from spin coated to roll-coated ones.

Lastly, efforts have been made to construct prearranged all-in-one polymer nanoparticles in order to reduce the usage of organic solvents in the synthesis of the polymers and, therefore, in solar cell fabrication, too. This was attempted via the *in situ* emulsion Suzuki cross-coupling polymerization of dialkyl fluorene and benzothiadiazole. The polymer particles were investigated with SEM and DLS, yielding particle diameters around 130 nm. Particles with and without PC<sub>61</sub>BM were synthesized. Fluorescence studies were made to investigate the effects of the introduction of such an electron acceptor. These showed a good energy transfer between the donor and acceptor component of these particles. Attempts to make functioning organic photovoltaic devices were made but not achieved.

# DANSK RESUME

Organiske solceller er et videnskabeligt område, der har tiltrukket en stor interesse de sidste årtier med god grund. Der er et evigt voksende behov for energi samtidig med, at fossile brændsler bliver færre. Derfor er udviklingen af en vedvarende energikilde essentiel for at opnå en alternativ, fossilt brændselsfri, bæredygtig fremtid. Organiske solceller som videnskabeligt område har flere interessante discipliner. De tre mest dominerende er syntesen af lyshøstende materialer, skalering af produktionen samt stabiliteten af enheder. I denne ph.d.-afhandling er fokus på anvendelse af nye heteroatomiske, halvledende, konjugerede materialer og overgangen fra lille-areal spin-coatede organiske solceller til stor-areals enheder. Belyste emner vil være det rationelle molekylære design, syntese samt karakterisering af nye lav-båndgab konjugerede polymerer, konjugerede polymerer indeholdende bor, småmolekyle acceptorer til roll coatede organiske solceller samt syntese og karakterisering af vandbearbejdelige, konjugerede polymer nanopartikler til fabrikationen af organiske solceller.

I denne tese er en serie af benzodipyrrolidone baserede lav-båndgab polymerer blevet designet, syntetiseret samt karakteriseret i forhold til både struktur og fotofysiske egenskaber. Disse polymerer blev testet i lille-arealsolceller og opnåede nyttevirkningsgrader på cirka 0,6%. Anvendelsen af disse polymerer i skalerbare roll-coatede organiske solceller havde begrænset succes. Samtidigt blev to isoindigo baserede lav-båndgab polymerer syntetiseret og karakteriseret. Mens den ene af disse polymere udviste meget lille potentiale, viste den anden, en isoindigo-ditheinopyrrole polymer, stort potentiale ved at give en nyttevirkningsgrad på 0,25% for lille-arealsolceller. Potentialet blev desto mere tydeligt, da en indiumtinoxid- og vakuumfri stor-arealsolcelle viste en nyttevirkningsgrads på næsten 1%. På grund af polymerens absorptionskarakteristika blev denne testet som lav-båndgabskomponent i en organisk roll-coated tandemsolcelle sammen med høj-båndgab polymeren PBDTTTz-4. Denne tandemsolcelle viste en nyttevirkningsgrad på 1,73% med en åbent kredsløbs spænding på 1,08V.

Ydermere er en ny konjugeret boryleret carbazol monomer blevet rapporteret og fuldt karakteriseret med hensyn til både struktur og fotofysiske egenskaber. Denne nye monomer blev polymeriseret sammen med både donor- og acceptortype monomerer. Molekylære simuleringer indikerede en interessant pseudo-acceptor karakteristisk. De resulterende polymerer blev karakteriseret med hensyn til både struktur og fotofysiske egenskaber. Kombinationen af den boryleret carbazole og en alkylthienyl substitueret benzodithiophene donormonomer resulterede i en polymer, der blev testet i en organisk solcelle, som præsterede en nyttevirkningsgrad på cirka 3,8 %. Dette fremhæver det store potentiale for denne nye monomer for fremtidig inkorporering med andre donormonomere.

En af nøglebarriererne forbundet med skalering af organisk solcelleteknologi er benyttelsen af fullerener som elektronacceptor i det aktive lag af de organiske solceller. Dette er en udfordring på grund af energiintensiteten af disse fullerener, og derfor bør der udvikles alternative acceptormolekyler. Småmolekyleacceptorer, er en mulig løsning og er blevet studeret ekstensivt. Meget få studier er blevet udført på overførslen af disse fra lille-areals spin-coated til stor-areals roll-coated solceller. I denne tese er tre simple småmolekyle acceptorer blevet undersøgt med hensyn til både strukturelle og fotofysiske egenskaber. Det

blev vist at deres molekylære geometri har stor indvirkning på overførslen fra spin-coated til roll-coated enheder

Endeligt, er det forsøgt at fremstille organiske konjugerede alt-i-en nano-partikel med en forudbestemt morfologi. Dette blev gjort for at reducere den brugte mængde af organiske solventer i fremstillingen af organisk solceller. Nano-partiklerne blev fremstillet via en *in situ* emulsions Suzuki krydskoblings-polymerisation af dialkyl flourene og benzothiadiazole. Partiklerne blev undersøgt med henholdsvis SEM og DLS, der viste en partikeldiameter på omtrent 130 nm. Partikler med og uden PC<sub>61</sub>BM blev fremstillet. Fluorescensspektroskopi blev foretaget for at evaluere effekten af introduktionen af denne elektronacceptor. Der blev fundet en god energioverførsel mellem donor og acceptor i partiklerne men fremstillingen af funktionsdygtige organiske solceller blev ikke opnået.

# ACKNOWLEDGEMENTS

First of all, I would like to express my deepest felt gratitude towards my supervisor Associate Professor *Donghong Yu* for guidance, collaboration and support throughout the process of the PhD-study. Thank you for helping me define my own project and path, while continuously showing support and help in achieving the goals.

The greatest of gratitude should be directed towards my unofficial cosupervisor *Thomas Rieks Andersen (Dr. T-rex)* for his constant feedback, experimental help, proof-reading, technical expertise, sparring and optimistic attitude. Without *Thomas* this thesis would not have been possible. For that and being a supporting friend, I thank you. Thank you, *Fei, Du, Wei* and *Lasse* for your inspiration and help with the experimental dimension of the Ph.D.-work. Especially thanks to *Du* for practical assistance and friendship during my stay in Qingdao.

I also direct my gratitude at Professor *Yanhou Geng* and his group at Changchun Institute of Applied Chemistry in China for welcoming me in the very early days of my Ph.D.-study. Despite the lack of results, the stay still broadened my horizon and gave me valuable insights.

A large gratitude towards Professor *Renqiang Yang* and his group at Qingdao Institute of Bioenergy and Bioprocess Technology, for assisting me in producing devices and characterization of materials during my stay in Qingdao. Special thanks should be directed towards *Manjun* for the tireless assistance in the laboratory and letting me leech of his device fabrication knowledge.

Sincere thanks should be directed towards Professor *Frederik C. Krebs* and Senior Scientist *Jens W. Andreasen* their coworkers at DTU Energy Conversion, for opening up their laboratories for me to conduct experiments on state-of-art equipment. Special thanks should be directed towards *Dechan* and *Thue* for assisting me with experiments during my visits at DTU and in general.

I would also like to thank my colleagues at Section of Chemistry, and especially the members of the Lunch Club; *Ludmilla, Thorbjørn, Lars, Mads* and *Bugge* for the daily breaks, frivolous discussions and friendship through the years.

To *Jackie, Skipper, Buch, Martin, Mikkel, Carsten, Lene* and *Line*, you have my gratitude for your never ending procrastinations and friendship throughout the Ph.D., thank you.

To my family I would also like to extend gratitude for your support and especially to my dear mother for letting me move home for the last year of the Ph.D., thank you!

Lastly, I would acknowledge my loving girlfriend *Helga* and our dear son *Arthur*. *Helga*, I cannot thank you enough for the endless support and taking care of our beautiful son while I buried myself in the Ph.D.-studies.

I dedicate this thesis to you, *Helga* – *All my tomorrows belong to you!*

**List of Publications:**(underlined if 1<sup>st</sup> author)

- Paper I:** An isoindigo containing donor-acceptor polymer: synthesis and photovoltaic properties of all-solution-processed ITO- and vacuum-free large area roll-coated single junction and tandem solar cells. Brandt, Rasmus Guldbæk; Yue, Wei; Andersen, Thomas Rieks; Larsen-Olsen, Thue Trofod; Hinge, Mogens; Bundgaard, Eva; Krebs, Frederik C; Yu, Donghong. Journal of Materials Chemistry C, Nr. 3, 16.01.2015, s. 1633-1639.
- Paper II:** The effect of molecular geometry on the photovoltaic property of diketopyrrolopyrrole based non-fullerene acceptors. Zhang, Fei / Brandt, Rasmus Guldbæk; Gu, Zhuowei; Wu, Shasha; Andersen, Thomas Rieks; Minmin, Shi; Yu, Donghong; Chen, Hongzheng. Synthetic Metals, Vol. 203, 24.02.2015, s. 249-254.

**Under preparation / review:**

- Paper III:** Novel high bandgap pendant-borylated carbazole polymers with deep HOMO level through +N=B- interactions for Organic photovoltaics. Rasmus G. Brandt, Steffen G. Sveegaard, Manjun Xiao, Wei Yue, Zhengkun Du, Meng Qiu, Thomas R. Andersen, Renqiang Yang and Donghong Yu. Chemical Science
- Paper IV:** Roll coated large area ITO- and vacuum-free all organic solar cells from diketopyrrolopyrrole based non-fullerene acceptors with molecular geometry effects. Rasmus Guldbæk Brandt, Fei Zhang, Thomas Rieks Andersen, Dechan Angmo, Minmin Shi, Hongzhen Chen, Leonid Gurevich, Jens Wenzel Andreasen, and Donghong Yu. RSC Advances

**Not included in the thesis:**

**Theoretical Study on the Rational Design of Cyano-Substituted P3HT Materials for OSCs: Substitution Effect on the Improvement of Photovoltaic Performance.** Qiu, Meng ; Brandt, Rasmus Guldbæk; Niu, Yingli; Bao, Xichang; Yu, Donghong; Wang, Ning; Han, Liangliang; Yu, Liangmin; Xia, Shuwei; Yang, Renqiang. The Journal of Physical Chemistry Part C: Nanomaterials, Interfaces and Hard Matter, Vol. 119, Nr. 16, 31.03.2015, s. 8501-8511.

**Structure and crystallinity of water dispersible photoactive nanoparticles for organic solar cells.** Pedersen, Emil B.L.; Pedersen, M.C.; Simonsen, Søren B.; Brandt, Rasmus Guldbæk; Böttiger, Arvid P.L.; Andersen, Thomas Rieks; Jiang, W.; Xie, Zhiyuan; Krebs, Frederik C.; Arleth, Lise; Andreasen, Jens W. I: Journal of Materials Chemistry A, 13.07.2015, s. 17022 - 17031.

# TABLE OF CONTENTS

<b>Chapter 1. Introduction.....</b>	<b>11</b>
1.1. Motivation.....	11
1.2. Conjugated systems.....	12
1.2.1. Concept of a conjugated molecule .....	12
1.2.2. Absorbance of conjugated molecules.....	13
1.2.3. Band gap engineering.....	15
1.3. Organic photovoltaic devices.....	18
1.3.1. Device characterization.....	21
1.4. Limitations and paths to overcome these .....	22
1.5. Scalability of production.....	25
1.6. Focus of the thesis.....	27
<b>Chapter 2. Low Bandgap D-A polymers.....</b>	<b>29</b>
2.1. benzodipyrrolidone-based low band gap polymers.....	29
2.1.1. Materials and Methods .....	31
2.1.2. Materials characterization .....	35
2.1.3. Device performance .....	39
2.1.4. Summary of the BDPDP – polymers .....	43
2.2. Isoindigo-based Low bandgap polymers.....	44
2.2.1. Materials and methods .....	45
2.2.2. Materials characterization .....	47
2.2.3. PFI Devices .....	50
2.2.4. PDTPI devices .....	53
2.2.5. Summary of the isoindigo containing OPV devices.....	57
<b>Chapter 3. Novel N-borylated carbazole for high performance OPVs .....</b>	<b>59</b>
3.1. Motivation.....	59
3.2. Materials and methods .....	61
3.3. Materials characterization .....	64
3.3.1. Molecular simulations of borylated compounds .....	65
3.3.2. Photophysical properties .....	69
3.4. Device performance .....	72
3.4.1. Rollcoated devices .....	79

3.5. Summarization .....	80
<b>Chapter 4. Small molecule acceptors: going from small to large area OPVs .....</b>	<b>81</b>
4.1. Introduction .....	81
4.1. Materials and methods .....	84
4.2. Materials characterization .....	87
4.2.1. Molecular simulations .....	88
4.2.2. Photophysical properties .....	90
4.2.3. Device performance .....	92
4.3. Summarization .....	99
<b>Chapter 5. Nanoparticles via <i>In situ</i> micro-emulsion polymerization towards water processable OPVs.....</b>	<b>101</b>
5.1. Motivation.....	101
5.1.1. Precipitation technique.....	102
5.1.2. Micro-emulsion technique .....	103
5.1.3. Micro-emulsion polymerization .....	103
5.2. Materials and methods .....	105
5.3. Results and discussion .....	106
5.3.1. Characterization of particles .....	106
5.3.2. Attempts to make Nanoparticle devices .....	108
5.4. Summary .....	109
<b>Chapter 6. Conclusion and perspective.....</b>	<b>111</b>
<b>References.....</b>	<b>115</b>
<b>Appendices - Papers.....</b>	<b>131</b>

# CHAPTER 1. INTRODUCTION

## 1.1. MOTIVATION

We live in a world, with an ever growing wealth and prosperity of the majority of the world; and with this the demand for energy increases globally[1]. While the energy demand ever increases, the fossil based fuels reservoirs are considered finite. This combined with the volatility of the prices of fossil based fuels and large environmental impact, makes it essential to find a sustainable, renewable, and environmentally safe alternative energy source. The search for an alternative energy source has, for the last decade or so, been a major area of focus for researchers and politicians alike. And there is no other energy resource that is comparable to the solar energy since energy types such as wind energy are secondary, deriving from the sun. There are only two techniques to harvest the solar energy directly, one being solar heating applied widely in the household (and larger facilities) to heat water and the other being photovoltaics converting the incident lights directly into electricity.

The first photovoltaic effect was discovered by E. Becquerel in 1839, when he observed a photo induced current when illuminating an AgCl electrode in an electrolyte[2]. But it was not until 1954 that the first commercial photovoltaic device was presented by researchers at Bell Laboratories showing a power conversion efficiency of approximate 6% [3]. The researchers at Bell applied Silicon single crystal wafers which are still used today and have by now reached an efficiency of 25.6% [4] at laboratory scale, and reached 10 to 12 % or even higher for commercial available modules, a life time exceeding 25 years [5], [6]. Despite the life time and efficiency, energy consumed to produce these devices; makes the energy produced by the devices, more costly than energy produced by fossil fuel based technologies[7].

To address the issues associated with the large energy requirements of the single crystal silicon based technology, there has been a shift in technology towards lower energy requirements, these being thin-films of amorphous silicon, CIGS (Copper Indium Gallium Selenide), cadmium telluride etc. All the above mentioned devices are fabricated using sputtering or a vapor-depositing technique, which to some extent influences the production price and the energy consumption of the manufacturing process of these materials. They have reached power conversion efficiency (PCE) of 27.7 % at laboratory scale [1], and approximately 10% in commercially available modules, these also have a life time exceeding two decades[4]. A common denominator of the above mentioned technologies is that they all rely on pure inorganic materials, which are energy intensive to manufacture. To reduce price and energy consumption of the production of the devices, a new generation of solar cells has been explored. The main idea is to switch the high energy intensive solar cell production of inorganic material to low energy processing via solution techniques from organic materials, combined with a rethinking of device structure. The organic based devices consist of materials that can be solution processed onto a flexible substrate, which allow fast production via Roll-to-Roll (R2R) printing which again shortens the road to commercialization by reducing the production price and embodied energy. The idea of organic photovoltaics is not a new one as it was firstly discovered when Pochetton in 1906 and Volmer in 1913 observed the photovoltaic effect of anthracene [8], but the true versatility of the organic photovoltaics (OPV) has been shown in last couple of decades as there has been a large interesting focus from the research communities[8].

The power conversion efficiency has risen from approximately 4% to 10.5 % within the last decade, the scalability for the OPVs have still not reached its potential. The focuses of these applications are still majorly on the academic understanding of the molecular structure of the active layer materials which are commonly conjugated systems, e.g. conjugated electron donors (D) and electron acceptors (A) as p-n junctions from both organic polymers and small molecules, which become the main focus of this PhD dissertation.

## 1.2. CONJUGATED SYSTEMS

### 1.2.1. CONCEPT OF A CONJUGATED MOLECULE

In the previous section, the idea of OPV is shortly introduced. There it is mentioned that the heart of the OPV device is the conjugated material (either small molecule (SM) or polymer based), where the photons are absorbed for creating available charge carriers. A conjugated system contains interconnected  $\pi$ -orbitals where the electrons can delocalize thus lowering the energy level. Conjugation is normally attained by alternating single and double bonds or by aromaticity as shown in Figure 1.

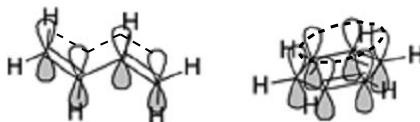


Figure 1: Illustration of orbitals in both a linear and cyclic aromatic constellation. The dot line illustrates the conjugation concept.

The conjugation affords an environment that facilitates sharing the  $\pi$ -electrons over the entirety of the conjugation. The orientation is essential for this delocalization, this becomes especially clear when observing allene ( $\text{H}_2\text{C}=\text{C}=\text{CH}_2$ ) despite it containing two double bonds, this structure is not fully conjugated as the two  $\pi$ -orbitals at the  $sp$ -hybridized center-carbon atom are perpendicular to each other thus the necessary orientation is not fulfilled. This orientation can only occur when there is a single bond in between the two double bonds (so the carbon atoms are  $sp^2$ -hybridized). But conjugation does not only have to be through carbon-carbon bonds, the conjugation can also include other atoms such as oxygen or nitrogen; as long as they have correct orbital orientation that facilitates the  $\pi$ - $\pi$  electron delocalization. An example of this can be observed in a molecule such as propenal where the double bond is conjugated with the  $I^2$  hybridized carbonyl and oxygen atom. The simplest conjugated hydrocarbon is 1,3-butadiene (shown in Figure 1) it can also exist in a 1,2-butadiene isomer, but for the reasons described above, that is not conjugated. With the two double bonds of the 1,3-butadiene there are 4  $\pi$ -electrons in the system. When filling out the molecular orbital diagram of the conjugated molecule as shown in Figure 2. It becomes clear that the  $\psi_{1-2}$  both are bonding orbital configurations, as there is no out of phase orbitals in  $\psi_1$  while there is one in  $\psi_2$ , affording 3 and 2 bonding interactions out of 3, respectively. While for the levels  $\psi_{3-4}$  both are anti-bonding orbital configurations. In  $\psi_4$  all 4 orbital are out of phase (thus have the highest energy level i.e. the most unstable). While  $\psi_3$  has 2 anti-bonding and 1 bonding orbital, it is overall antibonding orbital configuration, but with a lower energy than  $\psi_4$ . Therefore the virtual level of  $\psi_3$  is denoted the Lowest Unoccupied Molecular Orbital

(LUMO). The  $\psi_2$  has the single anti-bonding interaction which will be slightly less favorable (i.e. slightly higher energy), thereby being the Highest Occupied Molecular Orbital (HOMO). The effects of the orbital interactions are therefore that the overall molecule becomes more thermodynamically stable ( $\psi_1$ ), but also more reactive towards nucleophiles and electrophiles. The increased reactivity towards nucleophiles comes from the decrease of the LUMO energy, while the increased reactivity towards electrophiles derives from the increased HOMO level.

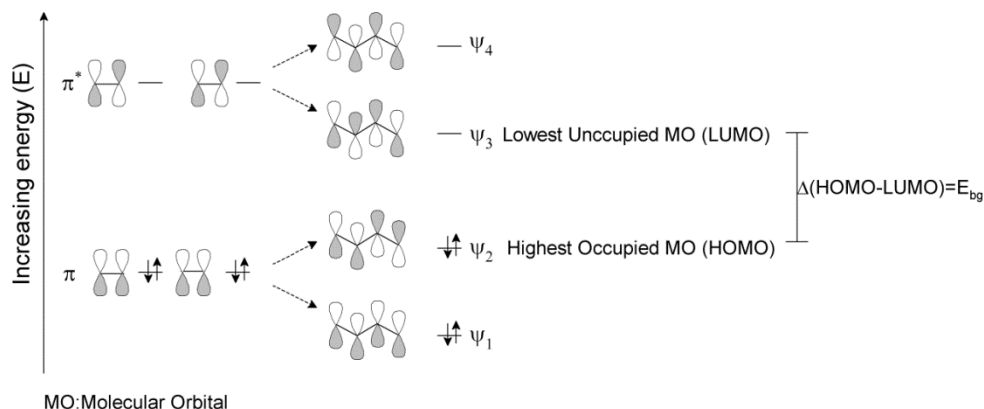


Figure 2: Energy orbital diagram of  $\pi$  orbital interactions of 1,3-butadiene inspired by Clayden et al.[9]

This increase of the HOMO and decrease of the LUMO facilitates the overall lowering of the bandgap ( $E_g$ , defined by absolute difference between energy level of HOMO and LUMO, as shown in Figure 2). The further implications of the lowering of the bandgap will be discussed in a later paragraph.

## 1.2.2. ABSORBANCE OF CONJUGATED MOLECULES

If the conjugation of these  $\pi$ -orbitals is extended further by simply adding a longer consecutive alternating double bonds, the lowering of the band gap will continue to some extent as expected to go towards a finite value [10]. The bandgap as described in Figure 2 is inverse proportional to the maximum wavelength at which a given material can absorb. The process of absorbance is that an electron is excited via photon energy from the HOMO to LUMO level. In inorganic material the energy levels are denoted as valence band (VB) and conductive band (CB), even though these possess some comparable characteristics, they still differ in the fact that for inorganic materials the CB is continuous while the LUMO of conjugated organic materials are discrete values; this is illustrated in Figure 3.

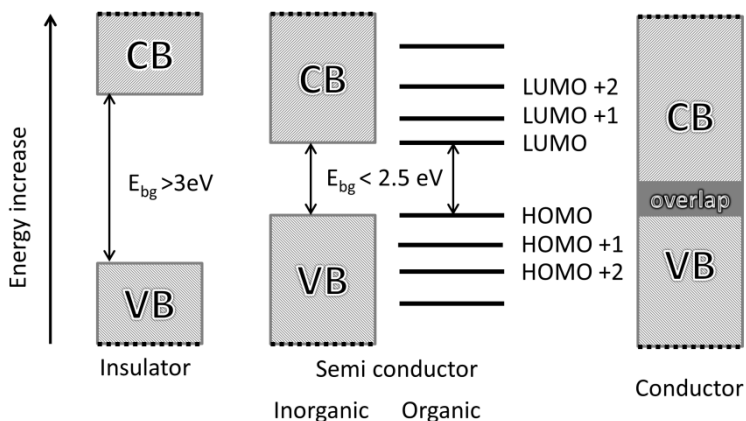


Figure 3: Representation of the energy levels of an insulator, the semiconductors (both Inorganic and Organic) and a conductor, where CB is short for Conduction Band and VB is short for Valence Band. The overlap of the conductors is the Fermi energy level.

The procedure of absorbance is essential of the OPVs, as the entire concept of OPV is to absorb photons from the sunlight and then convert these into an electrical current. But as illustrated above in Figure 3, it is apparent that the semiconducting properties of inorganic materials and the organic materials utilized in the OPV are quite similar, in the sense that the  $E_g$  is excluding low energy photons thus prohibits the usage of them in the fabrication of photocurrent.

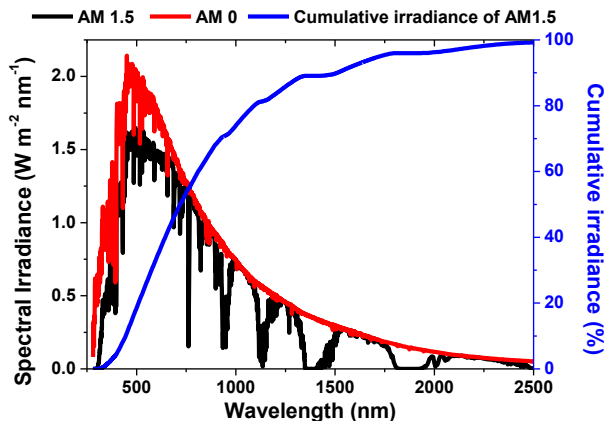


Figure 4: The solar irradiance spectrum at Air mass (AM) 0 (red) and AM 1.5 (black). The cumulative irradiance of AM 1.5 (blue).[11]

The discreet nature of the organic semiconductors allows for the low bandgap conjugated materials to be transparent for higher energy photons; this is a characteristic of the conjugated material, which should be taken into consideration when designing the structure of the conjugated material.

As mentioned above; it is essential to fit the absorbance of the conjugated material with the solar spectrum as shown in Figure 4. Such fitting to the air-mass 1.5 (AM 1.5) solar spectrum is a keystone to developing conjugated materials for OPVs. The AM 1.5 spectrum is the solar radiation at ground level with a solar zenith angle of  $48.19^\circ$ , while AM 0 is just outside the atmosphere at zenith angle of  $0^\circ$ . This angle is equivalent to the surface irradiance of Europe and Northern America. The cumulative irradiance shows that if a material can absorb light with a wavelength of approximately 720 nm ( $E_g \sim 1.7$  eV), which is equivalent to 50% of the solar spectrum. To reach an absorbance 75% of the solar spectrum, the onset absorbance must be around 1000 nm ( $E_g \sim 1.23$  eV).

### 1.2.3. BAND GAP ENGINEERING

Besides alternating double bonding in polyacetylene; other units can be applied to extend the  $\pi$ -conjugation such as aromatic units. These aromatic units can be phenyl based (benzene, naphthalene, and anthracene etc.) but also hetero aromatic units such as thiophene, pyridine, pyrrole etc. While thiophene is the most widely used monomer (and building block) for conjugated molecule, other candidates and moieties can be seen in Figure 5.

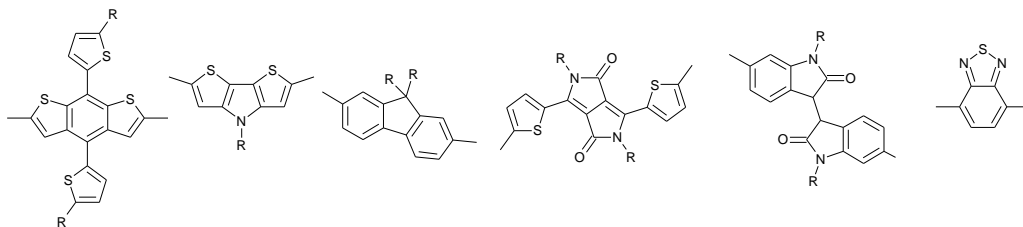


Figure 5: Different molecular structures of conjugated molecules being both donor and acceptor types

The different units have different effects on the energy levels, thus the bandgap; some of the units has a high electron density whilst others have lower density, which manipulate either the HOMO or the LUMO level when combined. This effect induced by changing the units is one of several parameters affecting the bandgap of an organic chromophore. Below are listed different factors affecting the band gap, which have been presented by Bundgaard *et al.*[12] and Winder *et al.*[13]:

1. Aromaticity
2.  $\pi$  - conjugation length
3. Torsion
4. Bond length alteration
5. Intra-chain interactions
6. Substitution effects
7. Inter-molecular / spatial interactions

The aromaticity (1) and  $\pi$ -conjugation length (2) are to some extent correlated, as mentioned before. The extension of the conjugation via alternating double bonds has limitations in regards to stability and practicalities. Therefore using aromatic units to extend the conjugation is a straightforward strategy, and the aromatic units can both be homo- or hetero-atomic. While the aromatic units extend the available  $\pi$ -orbitals, the delocalization is slightly hindered

compared to the same amount of “free” standing  $\pi$ -orbitals simple alternating double bonds. Due to the nature of the aromatic units, the shared electrons of the structure are also confined within the unit which in turn increases the stability. This combined with the planarity of these aromatic units makes these structures a great scaffold, for the conjugated organic material, in assisting the lowering  $E_g$  of the resulting materials.

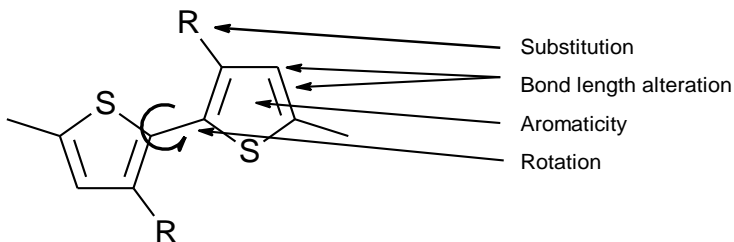


Figure 6: Different characteristics and molecular geometries that influences the energy levels of a conjugated organic material. Inspired by Winder et al.[13].

For most of the listed factors that influences the  $E_g$ , it is common that one modification has an effect on the other and vice versa. For instance, this is seen when looking into torsion (3): the torsion between two conjugated units can be affected by substitutions (6), more discussion will be made later in the chapter. The effect of torsion is clear for previously introduced allene molecule, where the perpendicularly oriented  $\pi$ -orbitals do not show the same delocalization and therefore are not conjugated. Thus a high degree of torsion between two units, even though the units themselves are conjugated, will result in the broken conjugation thus affording an increase in  $E_g$ .

Bond length alternation (4) derives from a type of Peierls instability [14], where the given bond structure changes in the way that the bonds are alternating between single and double bond. This alternation for poly(thiophene) is not a lowering of the  $E_g$ , but for such molecules as poly(benzo[c]thiophene) with the fused ring structure stabilizes the quinoid form and thus affords a lowered  $E_g$ . The  $E_g$  for poly(thiophene) is approximately 2.0 eV, while the  $E_g$  for poly(benzo[c]thiophene) is about 1.0 eV. Therefore a fused ring approach that enables and stabilizes the quinoid form is favorable when designing a low band gap organic molecule.

The existence of high and low electron density influences the intra-chain interactions (5). The approach is often denoted as push-pull or the donor-acceptor (D-A) approach. The donor moieties are electron rich, while the acceptors being electron deficient. The electron rich donors will fill up higher occupied MO thus increasing the HOMO. Electron deficient acceptors facilitate the lowering of the available virtual MO; thus lowering the LUMO, therefore combining the donor and acceptor moieties will lower the  $E_g$  to afford a low band gap material, which is illustrated on Figure 7.

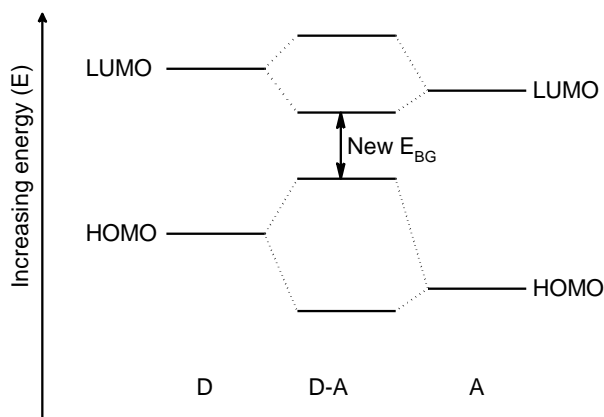


Figure 7:  $E_g$  lowering via D-A orbital interactions.

Substitution effects (6) is an ambiguous concept as these cover both substituents that aid dissolving the conjugated molecule and substituents that tune the MOs of the molecule. Due to the rigid structure of the organic molecules (backbone of a polymer), the intermolecular interactions are quite strong and this limits their solubility in common organic solvents which are essential for device fabrication via solution processing.

Therefore nearly all conjugated molecules/polymers are equipped with either linear or branched alkyl groups that ensure solubility. The introduction of any substituents can have an effect on not only the torsion (3) but also on the spatial stacking of the molecules i.e. intermolecular /spatial interactions (7). These solubilizing substituents lower the relative amount of photoactive material in the matrix which is not favorable for the application, but this is a necessary trade-off. Another function of substituents is the fine tuning of the MOs of the resulting conjugated molecules. To manipulate the LUMO level, electron withdrawing functional groups such as cyano (-CN), nitro (-NO<sub>2</sub>), and fluorine (F) can be applied. While regulating the HOMO is realized by applying electron donating functional groups, e.g., thiophenes, ethers or even hydroxyl. Chen *et al.* [15] showed that the LUMO level could be tuned -0.1 eV by the introduction of fluorine to thieno[3,4-b]thiophene acceptor moiety compared to the native moiety.

The  $\pi$ -orbital interactions are not only defined by the conjugated bond, but also by intermolecular / spatial interactions (7); these interactions also influences the  $E_g$ . If the material are allowed to form a rigid structure, this can facilitate the formation of either crystalline or semi crystalline domains. The planar structure of the conjugated molecules can also facilitate the molecular orbital overlap, thus allowing a lowering of the  $E_g$ .

This is of course not relevant for the ideal solubilized molecule as each molecule in this case would be isolated and surrounded by solvent molecules. For the ideally solubilized molecule the attached sidechains will although still have an effect, as the introduction a sidechain can have an effect on the torsion as described before. When considering the  $\pi$ - $\pi$  interactions, the  $\pi$ - $\pi$  stacking is an intermolecular force that ensures the arranging of aromatic molecules. This is a parameter that has to weight when designing a conjugated molecule, as a large aromatic moiety with a high degree of  $\pi$ - $\pi$  stacking makes it impossible to dissolve thus hindering processing. The easiest way to evaluate a given conjugated molecules ability to  $\pi$ - $\pi$  stack is

going from solution to solid form, where for most of the molecules a red shift is observed meaning aggregation occurs.

### 1.3. ORGANIC PHOTOVOLTAIC DEVICES

An OPV device can be referred to a reversed light emitting diode (LED). For a LED, an electron is injected into the electrode with a lower laying work function (WF), similarly a hole is injected into the electrode with the higher WF. This injection will result in the recombination affording a photon with the wavelength of the  $E_g$ . While an OPV devices perform in a complete reversed manner, as exhibited in Figure 8 which covers five general steps. As shown in Figure 3, the difference between an organic and an inorganic absorber is firstly the nature of the LUMO and VB, respectively.

When a photon is absorbed by the inorganic semiconductor free charge carriers (CC) are formed and the photo induced current can then be collected at the respective electrodes. This is not the case for an organic molecule, when a photon with the correct energy strikes a conjugated molecule, it is excited (an electron is moved from the HOMO to the LUMO) and thereby forming a so-called exciton. An exciton is a coulombic bound electron-hole pair, that is formed within the excited material and due to the binding energy of the exciton (ranging from 0.2-2.0eV [16], [17]) direct dissociation into free CC is limited.

Generally the conductivity and charge carrier mobility in the organic conjugated molecule is relatively low (compared to inorganic semiconductors) therefore the diffusion length of the excitons are in the range of 10-20 nm[10], [18]. The short diffusion lengths also lead to high degree recombination and this is not favorable when the goal of the excitation is to generate a photocurrent. Therefore the introduction of a material that can facilitate the splitting of the exciton and thus the dissociation into free charges, should be an n-type material (Acceptor (A)) with a relative high electron affinity and an energy level that aligns appropriately with the absorber the p-type material (donor, (D)).

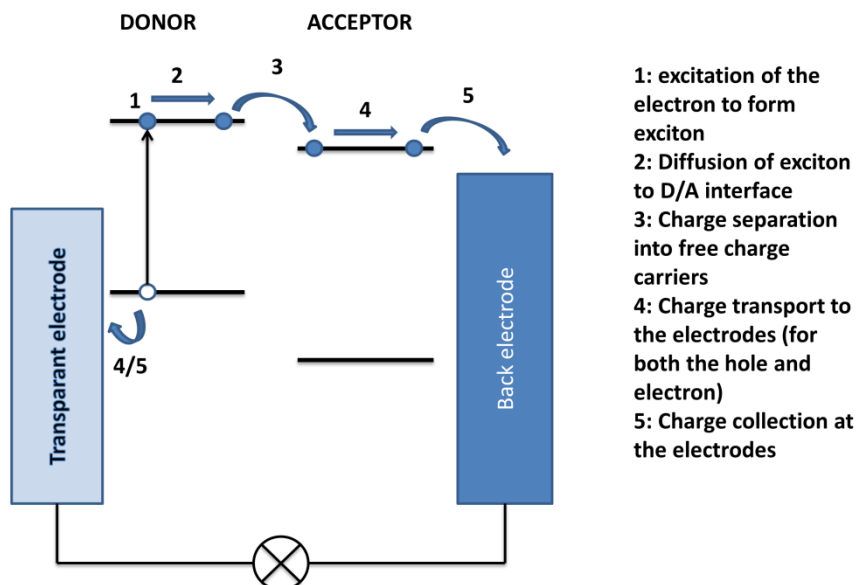


Figure 8: Photo-physical procedure of an OPV device under solar illumination with asymmetrical electrodes

In order to achieve the charge separation, the electrodes with asymmetric WFs are applied; this is done by using two different materials for the charge collection. The uses of asymmetric electrodes facilitate the electron flow from the low WF electrode to the high WF electrode. The absorbance coefficients of conjugated molecules are in the range of  $10^5 \text{cm}^{-1}$ , thus films with thicknesses of 100 nm will ensure an absorbance approaching nearly a hundred percent absorbance of most of the photons from solar radiation, when a reflective back electrode is applied [19]. The introduction of an electron acceptor (often fullerene based) facilitates this dissociation by introducing an internal built-in electric field due to the LUMO-LUMO difference between the two materials D and A. In order to achieve an efficient device, the A must have a high electron affinity (EA, low lying LUMO) and the D must have a high lying ionization potential (IP, high HOMO). Thus the most straight forward approach is to use of the D-A bilayer structure as illustrated in Figure 10, while this facilitates the charge extraction due to the large continuous domain of the phases; but the large shortcoming is that due to the limited diffusion lengths of the exciton this approach is only conceptual rather than optimal.

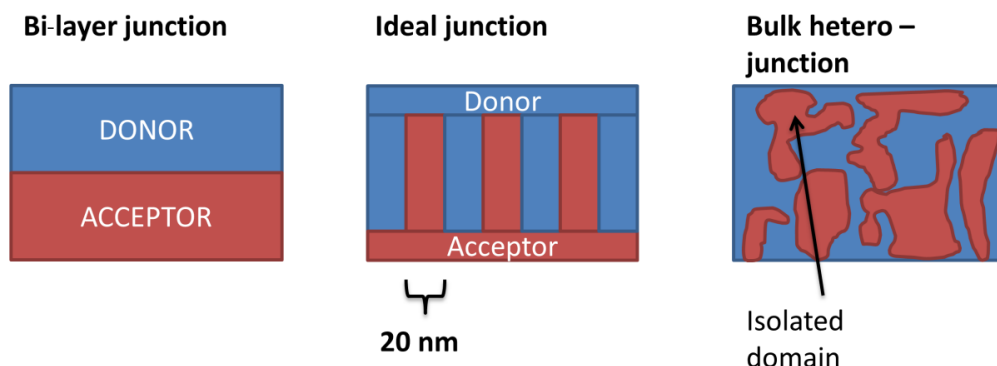


Figure 9: Active layer morphology of; a bi-layer device junction, an ideal D/A junction, and a bulk hetero-junction.

To circumvent the low interfacial area of the bilayer OPV, a method where the dispersing A material into D-phase will facilitate a much larger D-A interface. Upon thermodynamic phase separation, micro- or nano-meter scaled domains are formed, thereby improving the dissociation of the exciton and then ultimately increasing the photo-induced current. Such structured solar cell is called the bulk heterojunction (BHJ) device, and is the mostly applied technique to manufacture OPV devices. The D-materials and A-materials are mixed and domains of approximately the exciton lifetime intended to be formed, this being in the sub 100 nm scale (10-20 nm preferably). Such method with the nanophase morphology is tricky and is normally indirectly controlled by processing parameters, which will be discussed later. Also this approach can result in isolated domains where the dissociated exciton does not reach the electrodes and is lost to decay mechanisms. For the BHJ, opposite to the bilayer device, it does not have an internal electric field that dictates the current direction. This can be achieved via the previously mentioned asymmetric electrodes and further (as shown in the Figure 10) assisted by using barrier layers that exclude and/or favors either holes or electrons.

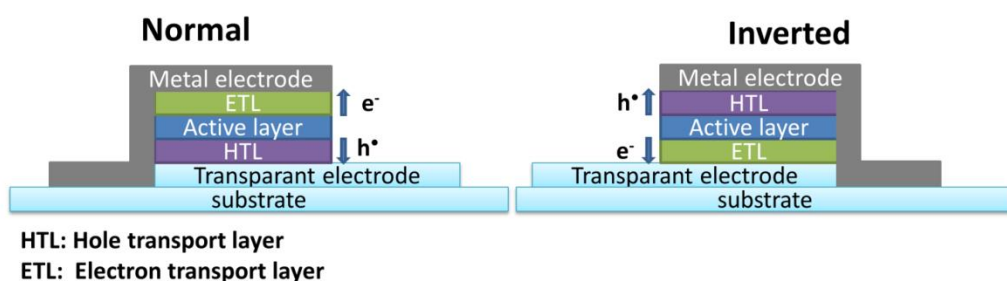


Figure 10: Normal and inverted device geometries, the charge carrier flow-direction is illustrated by the arrows for both geometries.

An OPV can be produced with a sandwich structure consisting of a semi-transparent front electrode, an active layer (AL, with the D and A phase) and a back electrode. This is the simplest design, as the front electrode allows the light to be transported and absorbed by the AL. Generally architecture of the device can be divided into normal or inverted geometry as shown in Figure 10. For the normal geometry devices, the transparent electrode is the anode,

meaning that the current flows away from the front electrode. For the inverted geometry the process reversed so the front transparent electrode act as cathode, thus the current flows towards it.

### 1.3.1. DEVICE CHARACTERIZATION

To evaluate the device performance, a voltage-current (I/V) diagram is measured. The current is measured at a forced voltage starting in a negative bias going towards a positive bias. The different parameters of the I/V curve are interlinked and represent different physical and chemical properties of the device. The current (I, A) can be normalized against the area, so the current is transformed into a current density (J, A•cm<sup>-2</sup>); making trans-experimental comparison easier. Another of the key parameters of a J/V is the V<sub>oc</sub> which is associated with the MOs of the applied materials. The V<sub>oc</sub> is ultimately defined by the difference between the HOMO of the D and the LUMO of the A, thus it is correlated to the choices of molecular components of the device (i.e. molecular dynamics).

The short circuit current (J<sub>sc</sub>) is the current flowing at V=0. The J<sub>sc</sub> is associated with the photocurrent which is related to photon absorption and charge separation. The last parameter is the Fill Factor (FF), and this is a parameter to evaluate how the device is performing against the ideality. In an ideal case the Voltage of maximum power (V<sub>mp</sub>) should be V<sub>oc</sub>, but this is not the case and the same for the current of maximum power (I<sub>mp</sub>) and I<sub>sc</sub>. The FF of the OPVs is normally ranging from 0.25-0.80 (the higher the better device). The FF is given by the Equation 1-1:

$$FF = \frac{I_{mp} \cdot V_{mp}}{I_{sc} \cdot V_{oc}} \quad \text{Equation 1-1}$$

The FF is an indicator of the proximity to the ideal conditions thus representing a summarization of the device characteristics and is a parameter that can be changed by modifying e.g. the morphology amongst others. The parameter that the OPV normally is evaluated with is the power conversion efficiency (PCE, %). The PCE is determined by measuring the power at the point of maximum power and divided by the power of incident lights (P<sub>in</sub>), the photon flux applied is the AM 1.5 defined in section 1.2.2.

$$PCE(\%) = \frac{I_{sc} \cdot V_{oc} \cdot FF}{P_{in}} \cdot 100 \quad \text{Equation 1-2}$$

To give a more detailed understanding of the OPV device another important parameter evaluating the device performance is the external quantum efficiency (EQE, %), this is the number of collected electrons at a given wavelength (λ) divided by the number of the irradiated photons at that given wavelength.

$$EQE(\lambda) = \frac{N_{electrons}(\lambda)}{N_{photons}(\lambda)} \cdot 100 \quad \text{Equation 1-3}$$

## 1.4. LIMITATIONS AND PATHS TO OVERCOME THESE

Only after clarifying the limitations of the OPV, can these be addressed. The largest hurdle with OPV is the low PCE, compared to the inorganic counter parts. This can be done by finding the optimal value of the conjugated molecules, to optimize and tune the band gap of the components of the OPV. Aligning the conjugated molecules; absorbance to the solar spectrum to increase the generated current ( $J_{sc}$ ), but as described below (in Figure 11) the narrowing of the bandgap will also affect the obtainable  $V_{oc}$ . This correlation and limitation was investigated theoretically by Shockley and Queisser in 1961 [20]. They worked within the following assumptions to determine the effect of such parameters on the PCE ( $\eta$ ):

1. Only photons with energy equal or higher than the bandgap (of photovoltaic material) can be absorbed, thus contribute to the photovoltaic current.
2. “Hot” CC can be formed by absorbing photons with a higher energy than the  $E_g$ , these excessively energized CC can then relax via “thermalization”.

Using the previously described energy diagram model, the model assumptions parameters can be described by the following graphic (Figure 11):

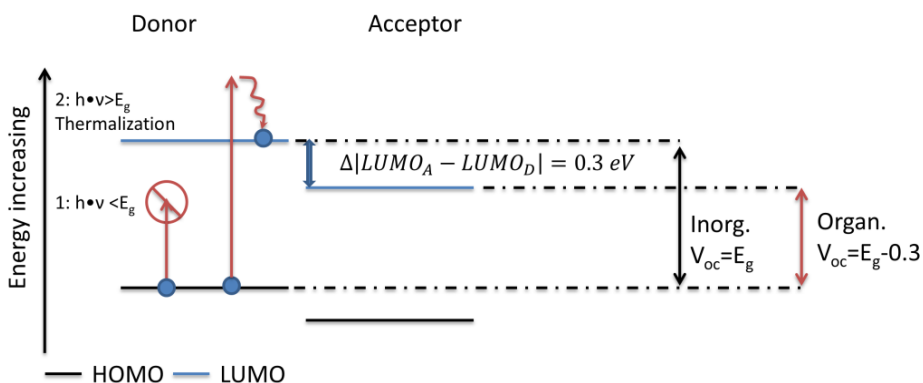


Figure 11: Graphical illustrations of Shockly-Queisser model assumptions, where the two losses are illustrated.

Given these assumptions, the maximum obtained  $V_{oc}$  is given by the  $E_g$  of the photovoltaic material. To simplify the model, the FF of the ideal case is 1 and the EQE of the material is 100% meaning that, when light irradiated is directly converted into a free CC.

$$\eta(E_G) = J_{SC}(E_G) \cdot V_{OC}(E_G) \cdot FF \quad \text{Equation 1-4}$$

The short circuit current ( $J_{sc}$ ) is also related to the assumption stating that all incident photons with energy larger than the  $E_g$  is converted to current. This is given by the following equation:

$$J_{SC}(E_G) = \int_{E_{in}}^{E_G} N_{PH}(E_{BG}) \cdot EQE(E_{BG}) \, dE \quad \text{Equation 1-5}$$

The number of incident photons ( $N_{PH}$ ) is calculated from the AM 1.5 emission spectrum describe in section 1.2.2. Combining the two equations the *ultimate efficiency* can be determined, although this is assuming ideality. The relationship between  $P$  (or PCE, i.e.,  $P/100$ ),  $V_{oc}$  and  $J_{sc}$  as function wavelength can be seen in Figure 12.

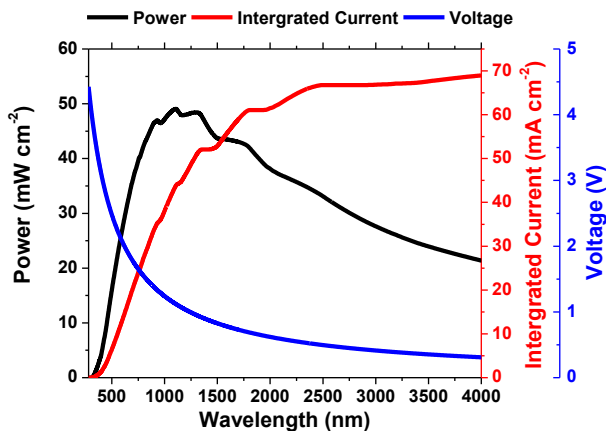


Figure 12: The maximum obtainable power ( $P$ , **black**), current ( $J$ , **red**) and voltage ( $V$ , **blue**) as function of the wavelength ( $\lambda$ ) simulated via the Shockley-Queisser model. The emission spectrum used is the AM 1.5G. Ideality is assumed ( $EQE=100$ ,  $FF=1$  and  $V_{oc}=E_g$ )

The maximum PCE is afforded at 1100 nm (1.12 eV), with a value of ~48%. Adding different decay losses Shockley and Queisser proposed that the more realistic single junction PV efficiency to be 31 % [20]. While this model is simple and straight forward, this model cannot be directly transferred to the OPVs, as the light absorbed by the conjugated molecule does not afford free CC but rather the bound excitons. As a consequence the introduction of a heterojunction, also change the parameters of the model, it has been experimentally determined that the optimal  $LUMO_{DONOR} - LUMO_{ACCEPTOR}$  offset to ensure an efficient charge separation (CS) is 0.3 eV [21], this effectively lowers the optimal bandgap of the OPV, the new bandgap for the ultimate efficiency is then 1.4 eV (shown in Figure 13) and also lowering the ultimate PCE to ~35%.

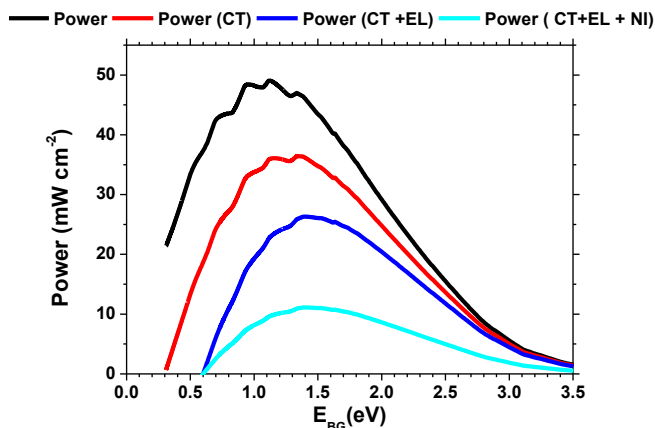


Figure 13: The ultimate power as function of wavelength calculated using the Shockley-Queisser model and the emission spectrum 1.5 AM. Ultimate power (**black**), Power with the 0.3 eV deduction to ensure charge transfer (CT, **red**), the power the 0.3 eV CT loss and the 0.3 V experimental loss (**blue**) and last the power under none-ideal conditions with a FF of 0.7 and EQE of 70% (**cyan**).

According to Ameri *et al.*[22] it has been shown an experimental loss of 0.3 eV which origin is still under debate[23], [24], but still further lowers the ultimate PCE to approximately 26%. Further improving the power model, could be done by include the less ideal conditions, in Figure 13 the ultimate PCE of a system with a FF of 0.7 and EQE of 70% is shown; and the obtained maximum PCE is 11.1%, the conditions chosen are similar to what has been reported in literature[25], [26]. According the Shockley-Queisser model the two largest loses are related to the lack of absorbance in the low energy photons and the relaxation of the “hot” CC (illustrated on Figure 11). To further increase the efficiency of the OPV a multi-junction (tandem) approach could be applied. The potentials and limitations of such tandem PV systems were discussed by De Vos in 1980[27]. There it was found that a double junction device with a material with a band gap of 1.9 eV and 1.0 eV could ideally afford an ultimate effect of 40%. When presenting the conjugated molecule, the fact that the absorbance of these materials are not continuous results in low band gap materials with poor absorbance in the UV region while having strong absorbance in the near-IR region, this is illustrated on Figure 14.

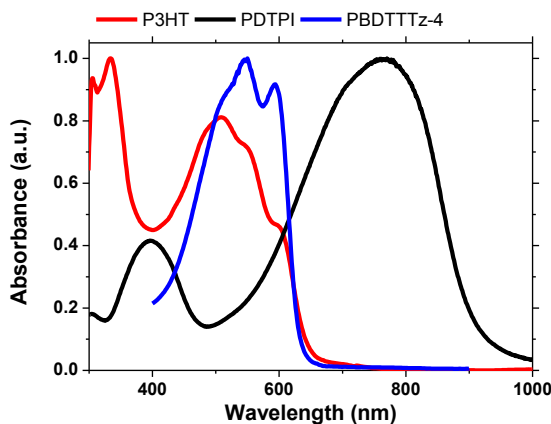


Figure 14: The combined absorbance spectra of the polymers PDTPI (**black**), P3HT (**red**) and PBDTTTz-4 (**blue**) in  $\text{CHCl}_3$  adapted from paper I.

Using a multiple junction device structure will therefore afford a larger spectral overlap with the sun emission spectrum. So taking the design parameters into considerations, to further improve the efficiency of the OPV devices, conjugated molecules should be synthesized with a bandgap of approximately 1.5 eV, to afford the maximum performance. But it is essential to modify not only the donor (light harvesting phase), but also the acceptor material to fit the energy levels of donor. As shown in Figure 11 and discussed above, the optimal difference has empirically been determined to be 0.3 eV[21], thus energy level alignment of the acceptors is essential to be tunable for suiting a wider range of the conjugated materials. This is in great contrast to the fact that fullerene based materials can be hardly modified in regards to the energy levels[28]–[30].

## 1.5. SCALABILITY OF PRODUCTION

For commercialization of the OPV technology, one of the most important aspects is the scalability of manufacturing. There is a lack of common knowledge of how those new breeds of high performing materials will behave in an upscaled processing. In contrast, it has been argued that due to the inherent differences in processing, many of the achievements of small area OPVs are proven difficult to retain using scaled-up methods, e.g., from small area devices ( $>0.1 \text{ cm}^2$ ) to medium / large area devices ( $<1 \text{ cm}^2$ ) and even larger. Generally small area device are produced via the application of ITO glass (glass sputtered with Indium tin oxide (ITO)), spin-coating the organic materials, and final evaporating the back metal electrode. The ITO sputtering is largely scalable but very energy intensive, thus the use of ITO is not energy-preferable in an industrial production[31]. Spin-coating method (presented in Figure 16) is advantageous for its economical setup, and the fabrication is fast for a single device. The strong drawback of spin-coating is that such method is only viable for relative small area and cannot be done in a continuous manner, which is essential for the application in large scale production like R2R techniques[32]–[34].

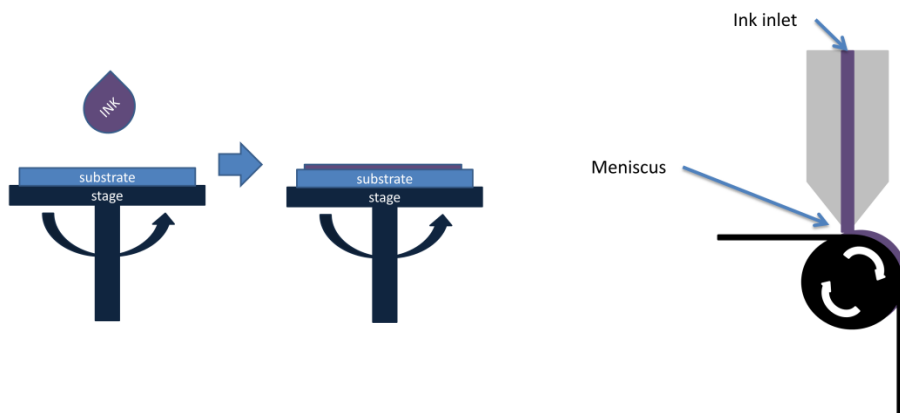


Figure 15: A schematic illustration of spin coating    Figure 16: A slot die coater head process

Despite there being a large array of large area printing methods, the one method that works the best in the field of organic photovoltaics is slot die coating (seen in Figure 16). Slot die coating allows 2 dimensional printing (2D, being the film thickness and width) and facilitates large area and fast production in the scale of  $\text{m} \cdot \text{min}^{-1}$ . The large disadvantage with the R2R approach is that the investment in the technology is relative cost intensive. The R2R setup deposited metal electrode flexographically (and normally consists of silver (Ag)).

Krebs and coworkers, at DTU Risoe campus, have pioneered the application of the R2R coating technique and established a spin-off company *Infinity PV*<sup>1</sup>. The major issue with the R2R technology is that it is material intensive to test new materials where the availability of material is a limiting factor. The solution to this issue is using a benchtop roll-coater (RC) that simulates the large scale apparatus, while conserving materials.

Despite the successes in applying the CM in the large scale R2R processing, the gap between the best performing large scale devices and the small area devices is still large. The difference between the two methods of production, are influencing a large array of different parameters regarding layer thickness, morphology amongst some. Therefore a better understanding of the parameters that have an influence on the performance of the devices is essential. Another hurdle in regards to making the OPV commercial available is to reduce inherent energy of the different components of the devices; the first obstacle was the removal of the ITO as mentioned before, the ITO was the largest contributor to the embodied energy which has been done [35]. Another disadvantage is the application of organic solvents, which generally contributes to the embodied energy in a negative manner [36]. Therefore one possible solution to facilitate the commercialization of the OPV technology is to get rid of such organic solvents (as primary solvent) by using aqueous systems.

<sup>1</sup> <http://www.infinitypv.com/>

## 1.6. FOCUS OF THE THESIS

In this thesis, four major topics will be investigated in order to get a further understanding for the hurdles, limitations and perspectives in the commercialization of the OPV technology. The three overall topics are considered from a chemistry approach, and the topics can overall be considered as follows:

1. The synthesis and characterization of novel low bandgap polymers, towards efficient OPVs both single- and multi-junction. Investigation of new polymeric monomers, to design high efficiency polymeric compounds for OPV applications using novel molecular compositions.
2. Understanding and investigation on the effect of bandgap alignment of the electron acceptor in an OPV device, the design and understanding of 3D implications of the molecular dynamics on small molecule acceptor going from small area devices to large area ones via spin-coating and roll coating
3. Lowering the embodied energy and the number of processing steps by applications of *in situ* nano particles formation during polymerization

**Chapter 2 – Novel low band gap polymers:** The focus has been on investigating novel combinations of donor and acceptor moieties. To afford lower band gap polymers possessing characteristics absorption band – but going from the interesting absorbance characteristics to device performance is not always straight forward. The polymers presented contain either isoindigo and benzodipyrrolidone based acceptor moieties, which have been combined with a wide array of different donors to afford AL materials, and have been characterized photo-physically and chemically. These polymers have then been applied in firstly small area devices and the best candidates have then been characterized using the mini-roll coater for both single- and tandem-junction. This work has been presented in the paper **I** and unpublished works.

**Chapter 3 – Novel N-Borylated carbazole for high performance OPVs:** In the pursue of high efficient conjugated materials for OPV applications, investigation and discovery of novel electronic compounds is essential to move forward. In this chapter a novel monomer N-borylated carbazole is presented with ambipolar characteristics. The synthesized monomer was used as a pseudo-acceptor with different donor moieties; and showed a high  $V_{oc}$  and moderately high efficiency. This work has been presented in the paper **III** and unpublished works.

**Chapter 4 – Small molecule acceptors, going from small to large area devices:** An important perspective of the development of conjugated materials for the application in OPV technology is the scalability of the components. In this chapter three different simple DPP based small molecule acceptors have been synthesized and photo-physically characterized. Devices going from the small area spin-coated devices to medium area devices are investigated. This is done to explore the molecular geometry dependence on their PV performance. The morphology was characterized using X-ray and AFM to correlate materials structure and the device morphology. This has been presented in the papers **II** and **IV**.

**Chapter 5 – Nanoparticle via *In situ* micro-emulsion polymerization towards water processable OPVs:** To ensure the environmental friendly processing OPVs, it is favorable to attempt to fabricate polymer particles in mesoscale *in situ* to avoid the use of expensive organic solvents. An array of polymers, photo physical properties, and quenching characteristics has been shown. The work presented is unpublished work.

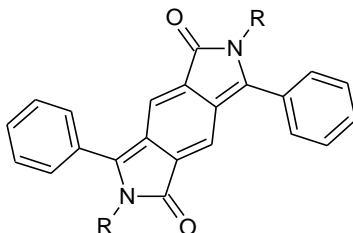
**Chapter 6 – Conclusion and perspectives:** The perspective of the findings in this thesis is summarized.

# CHAPTER 2. LOW BANDGAP D-A POLYMERS

As discussed in the introduction, low band gap (LBG) materials are of great importance for the further development and progress of OPVs. The LBG materials are, as mentioned, obtained by incorporating moieties with an electron donating (D) and accepting (A) nature; within the given organic molecule being either a small molecule or a large polymer. Generally these types of polymerization are conducted via transition metal catalyzed cross-coupling reactions such as Suzuki cross-coupling or Stille cross-coupling[37], [38]. The donor units are numerous, and these are moieties such as thiophene, pyrrole, flourene[39], carbazole[40], [41], dithienopyrrole[42], dithienosilole[43], and so on[44]. These donor moieties are associated with the depth of the HOMO of a given polymer and thereby also partly for the stability of the polymer; while the acceptor moiety directs the LUMO level of the polymer that is associated with the charge dissociation between the donor polymer and acceptor in the device. There has in recent years been a large interest in and focus on, the development of novel hetero atomic acceptor monomers for application in LGB systems. To mention a few of these acceptors are, benzothiadiazole (BT)[12], diketopyrrollopyrrollo (DPP)[45], thieno[3,4-*c*]pyrrollo-4,6-dione (TPD)[46] and pyrene and perylene derivatives [47]. In this work the focus has primarily been combining state-of-art donor units with novel acceptor moieties being isoindigo (*i*-ID)[48] and benzodipyrrolidone (BDPDP) [49]. Both of these have shown high potentials in regards to photovoltaic performance. But little work has been conducted to convert small area spin coating into the more scalable setup of RC without neither ITO nor vacuum techniques in the fabrication. Therefore these acceptor monomers have been polymerized with different donor moieties to afford LBG polymers and devices have been prepared with both small and large area, to investigate the up-scalability of these LBG polymers.

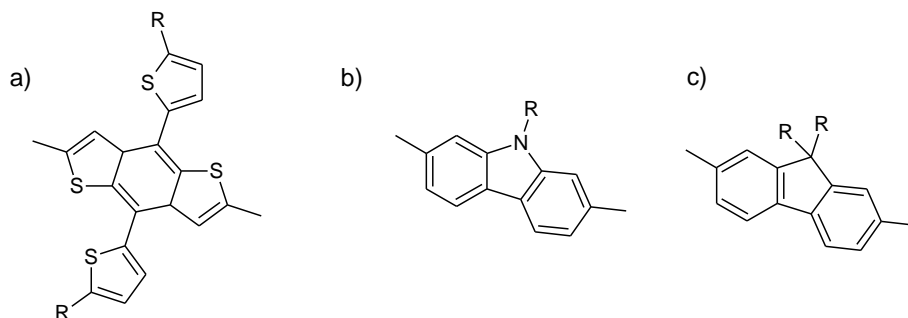
## 2.1. BENZODIPYRROLIDONE-BASED LOW BAND GAP POLYMERS

A possible acceptor candidate for an efficient LBG polymer; is the monomer benzodipyrrolidone (BDPDP), since Wudl *et al.*[49] in 2011 reported two simple polymeric compounds consisting of BDPDP and phenylene and thiophene, which showed a bandgap of 1.9 eV and 1.68 eV, respectively. This combined with a high ambipolar mobility in the order of  $10^{-3} \text{ cm}^2 \text{ V}^{-1} \text{ s}^{-1}$ , indicated that BDPDP could be a valuable acceptor candidate for low band gap polymers[50]. The LUMO level of the reported polymers is -3.35 and -3.50 eV for BDPDT with phenyl and thiophene, respectively. This energy level matches the LUMO level of around -3.7 eV of [6,6]-phenyl-C(61)-butyric acid methyl ester (PC<sub>61</sub>BM) [51], which is a commonly used acceptor in BHJ devices. This alignment determines that thiophenedipyrrolidone is not as ideal a candidate, as the LUMO level of an array of polymers presented by Rumer *et al.* [52] and Cui *et al.* [53] have been reported being in the range of -3.75 eV to -4.24 eV. The electron affinity of these compounds will therefore not allow the needed potential difference to facilitate the charge separation, at least not when using the fullerene based acceptors. A literature study rapidly shows that little work has been done on the BDPDP based polymers, two reviews only report a total of 10 different combinations of BDPDP and various donors[47], [50]. Deng *et al.*[54] have made a further evolving of the BDPDP moiety by an N-acylation, they found that an N-acylation lowered the LUMO of the resulting polymer compared to native BDPDP containing polymer.



Scheme 1: Chemical structure of benzodipyrrolidone (BDPDP) as an acceptor moiety for low band gap polymers

The structure as seen in Scheme 1, is similar to that of diketopyrrolopyrrole (DPP), but differs due to the extended nature with interconnected five-membered lactam ring. For DPP molecules, the lactam rings are directly connected whilst for BDPDP the lactam rings are bridged by a 1,4-cyclohexadiene ring, that extends the conjugation. This extension of the fused ring structure enlarge the  $\pi$ -conjugation, such combined planar structure of the BDPDP moiety is expected to facilitate a high degree of  $\pi$ - $\pi$  stacking, thus intermolecular interactions[55], [56]. The high  $\pi$ - $\pi$  intermolecular interactions are also one of the reasons for the relative high mobility that characterizes polymers with BDPDP incorporated [49], [57]. Due to the interesting characteristics of BDPDP; co-polymers of BDPDP and an electron donating moiety have been synthesized and utilized in the production of organic field transistors (OFET), and pronounced interesting mobilities [57], [58]. Despite the obvious advantages of BDPDP as a candidate for making efficient donor polymers via the D-A approach, there has only been reported one instance of the utilization a BDPDP copolymer in an OPV. Yue *et al.*[59] constructed a LBG D/A polymer of N-(1-pentylhexyl) substituted dithieno[3,2-b:2',3'-d]pyrrole (DTP) and BDPDP via a Stille coupling to afford the polymer PBDPDP-DTP. The reported polymer had a bandgap of 1.39 eV and the frontier orbitals -5.27 eV/-3.83 eV (HOMO/LUMO), this LUMO is slightly too low for perfect alignment with LUMO<sub>PC<sub>61</sub>BM</sub>. The resulting device with the structure ITO/PEDOT:PSS/PBDPDP-DTP:PC<sub>61</sub>BM (1:1.5) /LiF/Al presented a PCE of 2.6 % with a  $V_{oc}$  of 0.74 V and a  $J_{sc}$  of -7.87 mA cm<sup>-2</sup>. This clearly shows a potential of the BDPDP moiety in efficient OPV applications. The donor (DTP) applied in the polymer is considered one of the strongest donating moieties[44], therefore it could be interesting to use an array different donor moieties ranging from strong to weaker donors to investigate the effect on the bandgap, energy levels and the performance of the final OPV devices.



Scheme 2: Donor candidates a) 4,8-bis(5-(2'-alkyl)thiophen-2-yl)benzo[1,2-*b*;4,5-*b'*]dithiophene; b) 9-(9-alkyl)-9*H*-carbazole; c) 9,9-dialkylfluorene.

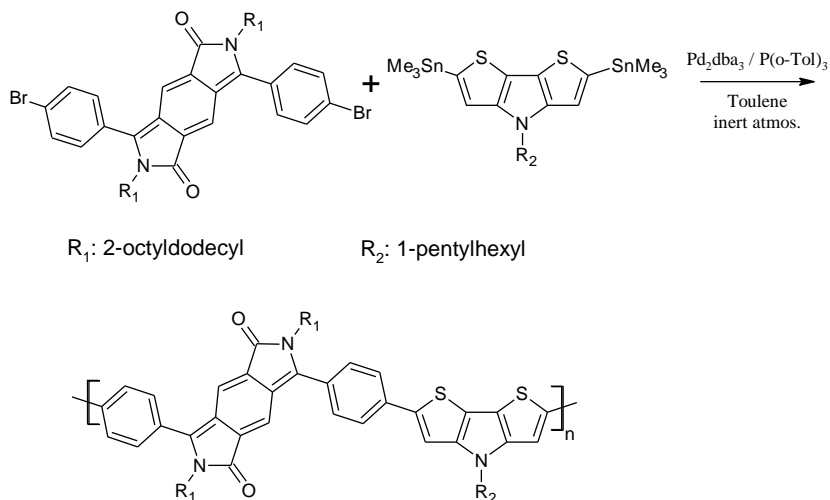
In this study copolymers of BDPDP have been synthesized using the candidates shown in Scheme 2. The donor moieties are (ranging in donor strength, highest firstly) DTP, 4,8-bis(5-(2-ethylhexyl)thiophen-2-yl)benzo[1,2-*b*;4,5-*b'*]dithiophene (BDTTT), 9-(9-heptadecanyl)-9*H*-carbazole (C) and 9,9-dioctylfluorene (F).

## 2.1.1. MATERIALS AND METHODS

### 2.1.1.1 Materials:

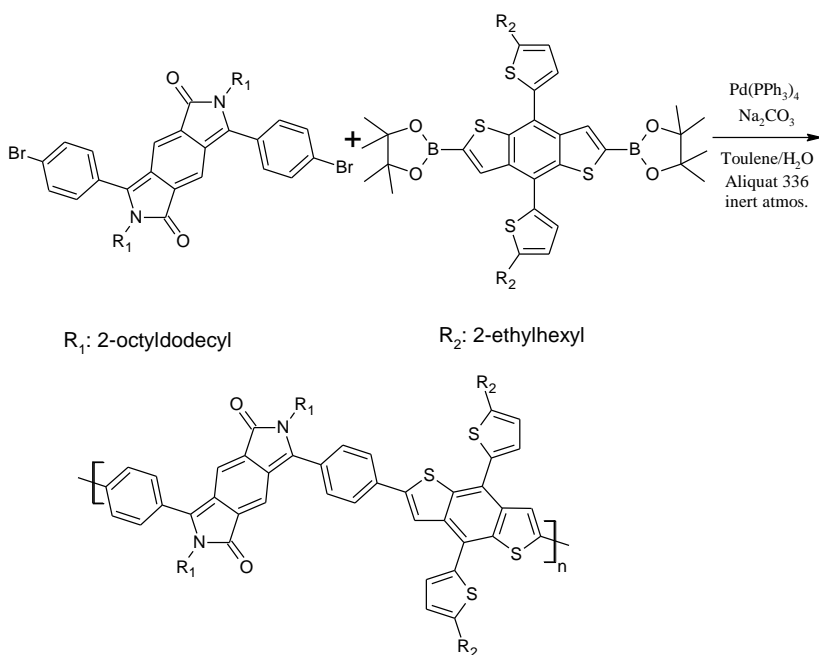
The BDPDP was synthesized according to literature procedure [49]. Chemicals used were of commercial grade, and used without further purification, if not state otherwise.

### 2.1.1.2 Syntheses:



Scheme 3: Synthesis of BDPDP-DTP via Stille polymerization of 2,6-di(trimethyltin)-*N*-(1-pentylhexyl)dithieno[3,2-*b*:2',3'-*d*]pyrrole (93.3 mg, 0.142 mol) and 3,7-bis(4-bromophenyl)-1,5-bis(2-octyldecyl)pyrrolo[2,3-*f*]indole-2,6(1*H*,5*H*)-dione.

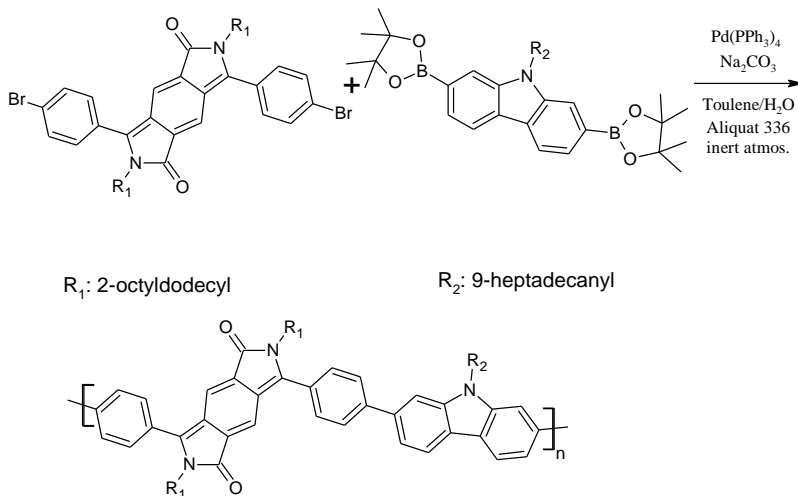
**PBDPDP-DTP.** As presented in Scheme 3, a mixture of 2,6-di(trimethyltin)-N-(1-pentylhexyl)dithieno[3,2-b:2',3'-d]-pyrrole (93.3 mg, 0.142 mol), 3,7-bis(4-bromophenyl)-1,5-bis(2-octyldodecyl)pyrrolo[2,3-f]indole-2,6(1H,5H)-dione (100 mg, 0.139 mol), tris(dibenzylideneacetone)dipalladium ( $\text{Pd}_2\text{dba}_3$ , 2.60 mg,  $2.80 \cdot 10^{-3}$  mmol), and tri-*o*-tolylphosphine ( $\text{P}(\text{o-Tol})_3$ , 6.80 mg,  $2.22 \times 10^{-2}$  mmol) was degassed with  $\text{N}_2$ , and then toluene (14 mL) was added. The mixture was further purged with  $\text{N}_2$  for 20 min and heated to  $120^\circ\text{C}$  for 48 h. After being cooled to room temperature, the solution was precipitated into methanol. The crude polymer was collected by filtration and then extracted on a Soxhlet's extractor with acetone, and hexane in succession. The final polymer was obtained by precipitating the hexane solution in methanol as a dark brown sheet with a yield of 72% (90.0 mg). GPC:  $M_n$  29000; PDI 3.65.  $^1\text{H}$  NMR (600 MHz,  $\text{CDCl}_3$ ,  $\delta$ , ppm): 7.42-7.83 (m, 8 H), 7.17-7.26 (m, 2 H), 6.27 (s, 2H), 4.28 (s, br, 1 H), 3.58-3.63 (m, 4 H), 1.80-2.16 (m, br, 6 H), 1.16-1.50 (m, br, 28 H), 0.84-0.99 (m, br, 18 H). Anal. Calcd for  $\text{C}_{57}\text{H}_{71}\text{N}_3\text{O}_2\text{S}_2$ (%): C, 76.55; H, 8.00; N, 4.70. Found (%): C, 76.41; H, 8.11; N, 4.76



*Scheme 4: Synthesis of BDPDP-BDITT via Suzuki polymerization 3,7-bis(4-bromophenyl)-1,5-bis(2-octyldodecyl)pyrrolo[2,3-f]indole-2,6(1H,5H)-dione 4,8-bis(5-(2-ethylhexyl)thiophen-2-yl)benzo[1,2-b;4,5-b']dithiophene boronic acid bis(pinacol) ester.*

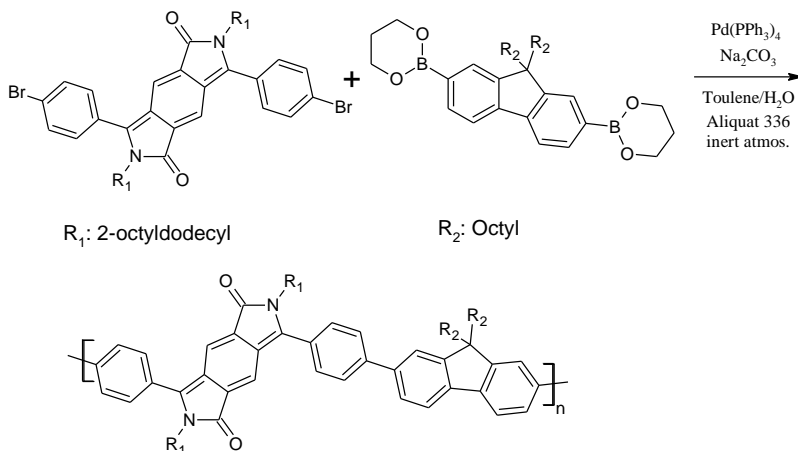
**PBDPDP-BDITT.** A flask was charged with 3,7-bis(4-bromophenyl)-1,5-bis(2-ethylhexyl)pyrrolo[2,3-f]indole-2,6(1H,5H)-dione (147 mg, 0.139 mmol), 4,8-bis(5-(2-ethylhexyl)thiophen-2-yl)benzo[1,2-*b*;4,5-*b'*]dithiophene boronic acid bis(pinacol) ester (115.5 mg, 0.139 mmol),  $\text{Pd}(\text{PPh}_3)_4$  (2.40 mg,  $2.09 \cdot 10^{-3}$  mmol),  $\text{Na}_2\text{CO}_3$  (530 mg, 5 mmol) and a drop of Aliquat 336 was degassed with nitrogen, then toluene (7.5 mL) and oxygen freed  $\text{H}_2\text{O}$  (2.5 mL) were added. The resulting mixture was heated at  $90^\circ\text{C}$  for 48 h by following the reaction presented in Scheme 4. After being cooled to room temperature, the mixture was precipitated in methanol. The crude polymer was collected by filtration and then

extracted on a Soxhlet's extractor with acetone, hexane and chloroform in succession. The final polymer was obtained by precipitating the chloroform solution in methanol. GPC:  $M_n = 5155$ ,  $M_w = 7741$ , PDI = 1.50  $^1\text{H NMR}$  (600 MHz,  $\text{CDCl}_3$ ,  $\delta$ , ppm): 7.42-7.83 (m, 12 H), 6.95-7.1 (m, 2 H), 6.25-6.50 (m, 2H), 3.55 (m, br, 4 H), 2.9-3 (m, 4 H), 1.70-2.16 (m, br, 4 H), 1.1-1.60 (m, br, 48 H), 0.84-0.99 (m, br, 24 H).



*Scheme 5: Synthesis of BDPDP-C via a Suzuki polymerization of 3,7-bis(4-bromophenyl)-1,5-bis(2-octyldodecyl)pyrrolo[2,3-f]indole-2,6(1H,5H)-dione and 9-(9-heptadecanyl)-9H-carbazole-2,7-diboronic acid bis(pinacol) ester.*

**PBDPDP-C.** A flask was charged with 3,7-bis(4-bromophenyl)-1,5-bis(2-ethylhexyl)pyrrolo[2,3-f]indole-2,6(1H,5H)-dione (147 mg, 0.139 mmol), 9-(9-heptadecanyl)-9H-carbazole-2,7-diboronic acid bis(pinacol) ester (91.3 mg, 0.139 mmol),  $\text{Pd}(\text{PPh}_3)_4$  (2.40 mg,  $2.09 \cdot 10^{-3}$  mmol),  $\text{Na}_2\text{CO}_3$  (530 mg, 5 mmol) and a drop of Aliquat 336 was degassed with nitrogen, then toluene (7.5 mL) and oxygen freed  $\text{H}_2\text{O}$  (2.5 mL) were added. The resulting mixture was heated at 90 °C for 48 h, as found in Scheme 5. After being cooled to room temperature, the mixture was precipitated in methanol. The crude polymer was collected by filtration and then extracted on a Soxhlet's extractor with acetone, hexane and chloroform in succession. The final polymer was obtained by precipitating the chloroform solution in methanol.  $^1\text{H NMR}$  (600 MHz,  $\text{CDCl}_3$ ,  $\delta$ , ppm): 7.78-8.00 (m, 10 H), 7.61-7.79 (m, 4 H), 6.52 (m, 2H), 3.6 (d, br, 5 H), 1.1-1.67 (m, br, 50 H), 0.84-0.99 (m, br, 28 H).



Scheme 6: Synthesis of BDPDP-F via a Suzuki polymerization of 3,7-bis(4-bromophenyl)-1,5-bis(2-octyldodecyl)pyrrolo[2,3-f]indole-2,6(1H,5H)-dione and 9,9-dioctylfluorene-2,7-diboric acid bis(1,3-propanediol) ester.

**PBDPDP-F.** Being described in Scheme 6, a mixture of 3,7-bis(4-bromophenyl)-1,5-bis(2-octyldodecyl)pyrrolo[2,3-f]indole-2,6(1H,5H)-dione (147 mg, 0.139 mmol), 9,9-dioctylfluorene-2,7-diboric acid bis(1,3-propanediol) ester (77.6 mg, 0.139 mmol), Pd(PPh<sub>3</sub>)<sub>4</sub> (2.40 mg, 2.09 × 10<sup>-3</sup> mmol), Na<sub>2</sub>CO<sub>3</sub> (530 mg, 5 mmol) and a drop of Aliquat 336 was degassed with nitrogen, then toluene (7.5 mL) and oxygen-free H<sub>2</sub>O (2.5 mL) were added. The resulting mixture was heated at 90 °C for 24 h. After cooled to room temperature, the mixture was precipitated in methanol. The crude polymer was collected by filtration and then extracted on a Soxhlet's extractor with acetone, hexane and chloroform in succession. The final polymer was obtained by precipitating the chloroform solution in methanol. <sup>1</sup>H NMR (600 MHz, CDCl<sub>3</sub>, δ, ppm): 8.15-8.35 (m, 2 H), 7.8-8.02 (m, 8 H), 7.39-7.76 (m, 4H), 6.54 (m, 2H), 3.6 (d, br, 4 H), 1.1-1.67 (m, br, 52 H), 0.84-0.99 (m, br, 20 H).

### 2.1.1.3 Methods:

<sup>1</sup>H NMR spectra were recorded on a Bruker AvanceIII 600 MHz spectrometer. The molecular weight of the synthesized polymers were determined by high temperature gel permeation chromatography (HT-GPC) at a temperature of 150 °C with 1,2,4-trichlorobenzene as an eluent against polystyrene standards. Thermogravimetric analysis (TGA) was performed on a TI TGA Q50, using a platinum pan, under nitrogen atmosphere. The samples were measured with a ramp of 10 °C min<sup>-1</sup> from 20°C to 800°C. The cyclic voltammetry (CV) was performed by a CHI 660D System with a three-electrode cell in a solution of 0.10 M tetrabutylammonium hexafluorophosphate (TBAPF6) in acetonitrile as the electrolyte at a scan rate of 100 mV/s, the electrodes consisted of a glassy carbon electrode (working electrode) on which the polymer film was drop casted, a platinum wire (counter electrode) and a saturated calomel reference electrode. UV-vis spectra were measured on a Varian Cary 50 UV/vis spectrometer. The device type was BHJ OPVs and fabricated using the polymers as the donor combined with different amounts of PC<sub>71</sub>BM as the acceptor. The manufactured devices were of a normal geometry, and the device structure applied was ITO/PEDOT:PSS/active layer/Ca/Al. The active-area of the devices were 0.1 cm<sup>2</sup>, the current density-voltage (J-V) characteristics were recorded with a Keithley 2420 source measurement

unit under simulated  $100 \text{ mW cm}^{-2}$  (AM 1.5G) irradiation from a Newport solar simulator. Experiments with additives were conducted, and it was found that the effect of the additive diiodooctane (DIO) was very depended on the polymer material. The method used to evaluate the charge carrier mobility is called space-charge limited charge (SCLC), this gives an estimation of the charge carrier mobility for the PBDPDP-DTP, PBDPDP-BDTTT, PBDPDP-C, and PBDPDP-F. The devices where constructed for the hole only device ITO/PEDOT:PSS/active layer/MoO/Ag and the electron only device ITO/ZnO/Active layer/Ca/Al.

## 2.1.2. MATERIALS CHARACTERIZATION

The number averaged molecular weight were determined to be 29 kDa (PDI = 3.7) for PBDPDP-DTP, 5.1 kDa (PDI = 1.5) for PBDPDP-BDTTT, 5155 kDa (PDI = 1.5) for PBDPDP-C, and  $M_n$  for PBDPDP-F was not determined.

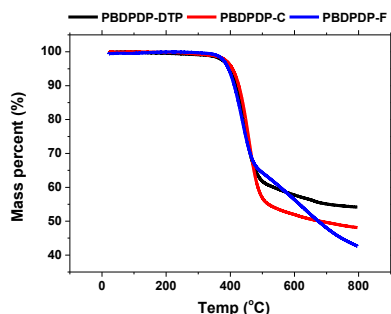


Figure 17: Thermogravimetric analysis (TGA) of the polymers PBDPDP-DTP (black) PBDPDP-C (red) and PBDPDP-F (blue). The scan rate was  $10^\circ\text{C min}^{-1}$  in a platinum pan under inert nitrogen atmosphere.

As seen in Figure 17 the TGA shows a thermal stability of approximately  $400^\circ\text{C}$  which is safe under conditions for manufacturing devices. Even though the TGA analysis of PBDPDP-BDTTT is not available; the thermal stability is expected to be in the same range as the 3 other materials due to its higher rigidity on BDTTT moiety. Yue *et al.*[59] showed that PBDPDP-DTP had a low band gap of 1.39 eV, this is according to the calculations conducted in the introduction section 1.4, slightly too low in order to reach the maximum efficiency as a function of the duality of the  $V_{oc}$  and  $J_{sc}$  of the devices.

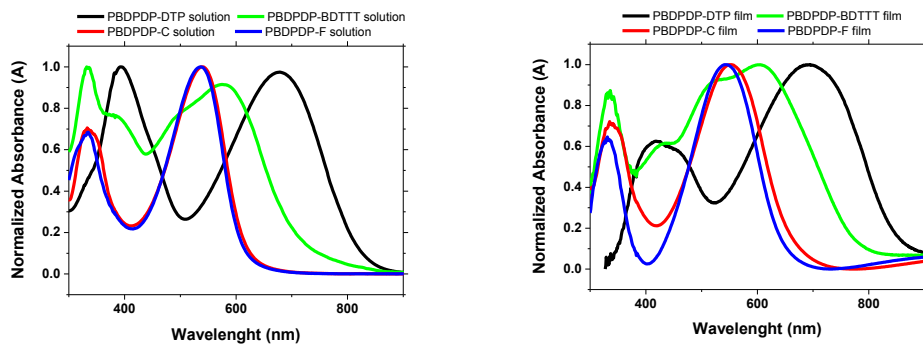


Figure 18: Absorbance of the polymers in solution (in  $\text{CHCl}_3$ ) (left) and as a spin coated film (right). The polymers being of PBDPDP-DTP (black) PBDPDP-BDTTT (green), PBDPDP-C (red) and PBDPDP-F (blue).

The absorbance spectra of the 4 compounds can be seen in Figure 18. For the first glance, the absorbance of PBDPDP-C and PBDPDP-F are nearly identical with a slight difference of approximately 5 nm between their onsets. The entire absorbance spectra are still identical, with a maximum absorbance at 540 nm and a secondary local maximum at 340 nm. This double absorbance is evidence of a strong intramolecular charge transfer (ICT), which is a clear indication of a D-A relationship between the moieties of the polymers. The high energy maximum derives from the  $\pi$ - $\pi^*$  transition of the donor moiety[49]. As expected the peak absorption of polymer films showed a large red shift of the onset, going from 610 nm to an onset that exceeds 650 nm, when comparing those of solutions. The red shift is expected, as the BDPDP monomer has a planar structure which will facilitate the intermolecular interactions thus lowering the  $E_g$  and resulting in a redshift[60]. The  $E_g$  difference between PBDPDP-C and PBDPDP-F becomes clearer when going from solution to film, the onset of PBDPDP-C is 673 nm while the PBDPDP-F is 650 nm, this difference derives from the more planar structure of carbazole compared to the fluorene used. The major structural difference is the nitrogen at the 9 position of the 3 fused rings of the carbazole compared to tertiary substituted carbon of the fluorene, i.e. possessing 2  $\pi$ -electrons for conjugation at N-atom rather than pseudo- (or hyper-)conjugation caused by the  $sp^3$  hybridized lone pair electrons at C-C ( $\sigma$ -bonding). The similar absorbance of PBDPDP-F and PBDPDP-C indicates the similar donor strength. The PBDPDP-DTP polymer showed as expected similar absorbance trends as the one reported by Yue *et al.*[59] with an onset of the film of 848 nm, the PBDPDP-DTP showed the lowest red shift as function of the solution-film transition. Since the red shift on BDPDP-F and PBDPDP-C can be ascribed to the planarity of the given polymer system, therefore it is interesting that PBDPDP-DTP has the lowest redshift of 4 reported polymers. The red shift of PBDPDP-DTP is 24 nm compared with the 45 nm red shift of PBDPDP-BDTTT, 56 nm of PBDPDP-C and 39 of PBDPDP-F. This low red shift could also indicate a steric hindrance from the branched alkyl substituent of the DTP. The high absorbance edge clearly demonstrates that the DTP is by far the strongest donating moiety of the 4 applied donor moieties. The onset is approximately 70 nm higher than PBDPDP-BDTTT which is the second strongest donor and the PBDPDP-C and PBDPDP-F are the two weakest ones.

The absorbance of PBDPDP-DTP exhibits a clear ICT with a primary maximum at approx. 700 nm and a secondary maximum at approx. 400 nm; in between these two maxima the absorbance is relative low. The ratio between the two maxima is also interesting, as the first and second

maxima are of identical size indicating a very strong D-A interaction. When the film is coated, the ratio between the two peaks changes, this is associated with the film formation and intermolecular interactions deriving from the  $\pi$ - $\pi$  interactions. Such a change in relative absorption indicates the molecular interactions such as localized  $\pi$ - $\pi$  interaction and therefore there is not as large redshift as expected. The ditch between the two maxima is also an illustration of the none-continuous behavior of the LUMO of an organic material. For the PBDPDP-BDTTT polymer the absorbance is about the same strength throughout the absorbance spectrum, starting at 776 nm. Despite the rather uniform absorbance there are still two maxima, as expected for a D-A polymer. While PBDPDP-DTP could be a candidate for a tandem OPV, PBDPDP-BDTTT is not suitable due to the relative uniform absorbance spectrum. From Equation 2-1 the optical  $E_g$  has been determined, using the  $\lambda_{onset}$  of the film absorbance. The optical  $E_g$  for the polymers are; 1.46 eV for PBDPDP-DTP, 1.59 eV for PBDPDP-BDTTT, 1.85 eV for PBDPDP-C and 1.91 eV for PBDPDP-F.

$$E_g = \frac{h \cdot \nu}{\lambda} \cong \frac{1240}{\lambda_{onset}} \quad \text{Equation 2-1}$$

But determination of the  $E_g$  is not enough, as an essential parameter of a conjugated polymer, this will be the alignment of the energy levels. The energy levels have been determined using CV on drop-casted polymer films. The CV scans of the four polymer film can be seen on Figure 19.

$$E_{HOMO} = -(E_{ox\ onset} + 4.8)eV \quad \text{Equation 2-2}$$

The first thing that should be noticed is the lack of reversibility of the four polymers. This indicates an electrochemically facilitated reaction occurring under the oxidation of the polymers. This is presumably also why there is no clear reduction occurring in at least PBDPDP-C and PBDPDP-F, and the current output of the reduction of PBDPDP-BDTTT is very low compared to the oxidation. Therefore determining the LUMO level (electron affinity) cannot be done directly from the CV. But the ionization potential ( $E_{ox\ onset}$ ) can be used to determine the HOMO level of the materials; this is done using the empirical equation shown in Equation 2-2. The LUMO level is then determined by adding the  $E_g$  with the HOMO. The summarized photo physical- and electrochemical-parameters can be seen in Table 1.

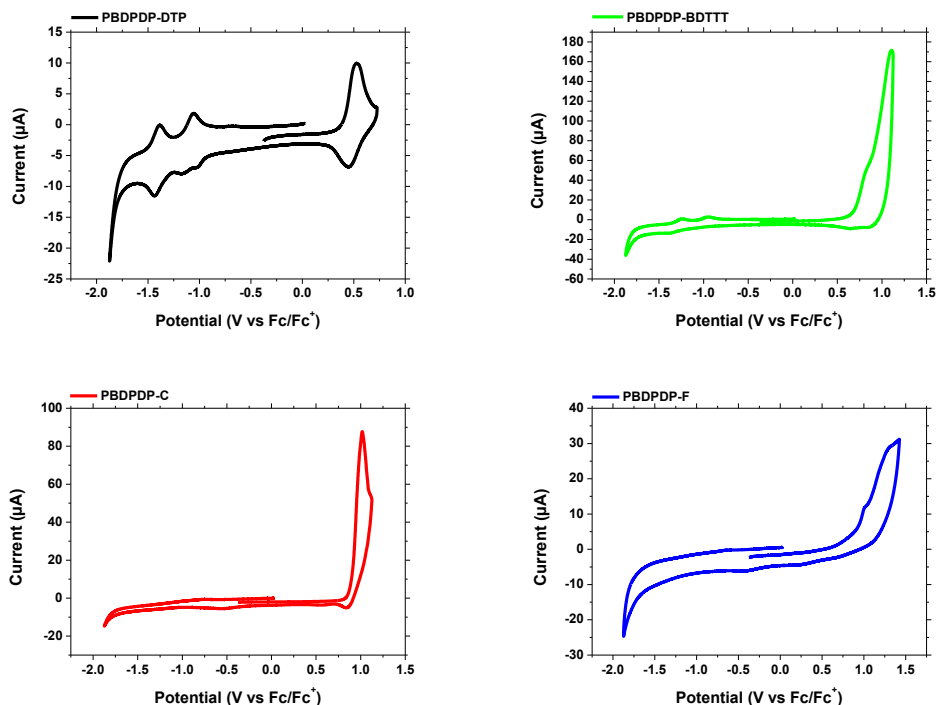


Figure 19: Cyclic voltammety (CV) of the four different polymer film of PBDPDP-DTP (black, upper left) PBDPDP-BDTTT (green, upper right), PBDPDP-C (red, lower left) and PBDPDP-F (blue, lower right).

In regard to the energy alignment as mentioned before, the LUMO level of the PC<sub>61</sub>BM is 3.7 eV, and to ensure an efficient charge separation a difference between the  $\Delta|LUMO_{\text{Acceptor}} - LUMO_{\text{Donor}}| = 0.3$  eV is required.

Table 1: Photo-physical properties of the four conjugated polymers, PBDPDP-DTP, PBDPDP-BDTTT, PBDPDP-C and PBDPDP-F found by combining absorbance onset and the ionization potential found via CV.

Sample name	$\lambda_{\text{onset}}$ [nm]	$E_g$ [eV]	$E_{\text{ox onset}}$ [V]	$E_{\text{HOMO}}$ [eV]	$E_{\text{LUMO}}$ [eV]
PBDPDP-DTP	848	1.46	0.42	-5.22	-3.76
PBDPDP-BDTTT	780	1.59	0.68	-5.48	-3.89
PBDPDP-C	673	1.85	0.89	-5.69	-3.84
PBDPDP-F	650	1.91	0.83	-5.63	-3.72

This compared with the LUMO levels found in Table 1, which ranges from -3.72 eV for PBDPDP-F to -3.89 for PBDPDP-BDTTT, shows that despite PC<sub>61</sub>BM being the mostly used acceptor in OPV, the energy levels does not match the energy levels of the BDPDP-family, preventing the usage of PC<sub>61</sub>BM, although it should be noted that the LUMO is estimated thus the true value might be more appropriate. But taking the energy levels into consideration, another electron acceptor could be chosen. One of the other interesting acceptor candidates that can be used is [6,6]-phenyl-C71-butyric acid ester (PC<sub>71</sub>BM), whose LUMO level has been reported to be -3.9 eV [61]. The LUMO levels of the synthesized polymers are also slightly deeper than expected when making a literature survey. With the unfavorable LUMO level value, the efficiencies of the devices are not expected to good, but using the polymeric material as an electron acceptor could be a possibility, due to the high electron affinity.

### 2.1.3. DEVICE PERFORMANCE

When fabricating the devices, DIO is used as an additive due to its slow evaporation that facilitates the crystallization of the coated material. As expected the PBDPDP-C and PBDPDP-F polymers both pronounced a low PCE, with the maximum performance being 0.066 % for PBDPDP-C and even lower 0.016% for PBDPDP-F. The two mentioned polymers show moderated  $V_{oc}$ 's around 0.63V, which does not account for the low efficiency of the two polymers.

Table 2: Device performance of the organic photovoltaics, using the four polymers PBDPDP-DTP, PBDPDP-BDTTT, PBDPDP-C and PBDPDP-F as the donor against the acceptor PC<sub>71</sub>BM; in various weight ratios. The polymer:fullerene films is spin-coated from ortho-dichlorobenzene (o-DCB) with a dry content of 30 mg mL<sup>-1</sup>. The values shown are the average of at least 4 devices.

Polymer sample	Spin speed [RPM]	Ratio [D:A]	DIO [%]	Voc [V]	Jsc [mAcm <sup>-2</sup> ]	FF [%]	PCE [%]	PCE <sub>best</sub> [%]
PBDPDP-DTP	1500	1:1	-	0.58 ± 0.11	1.22 ± 0.06	38 ± 1.7	0.27 ± 0.07	0.406
		1:2	-	0.57 ± 0.17	1.58 ± 0.04	40.5 ± 5.1	0.38 ± 0.16	<b>0.614</b>
	2000	1		0.37 ± 0.18	0.33 ± 0.08	33.8 ± 4.1	0.04 ± 0.02	0.084
		2		0.64 ± 0.10	0.16 ± 0.002	40.5 ± 2.9	0.05 ± 0.004	0.056
		3		0.20 ± 0.11	0.27 ± 0.01	29.8 ± 3.6	0.02 ± 0.01	0.037
		3		0.60 ± 0.07	1.37 ± 0.01	33.6 ± 2.5	0.28 ± 0.05	0.406
		1:3	-	0.60 ± 0.07	1.37 ± 0.01	33.6 ± 2.5	0.28 ± 0.05	0.406
PBDPDP-BDTTT	1500	1:1	-	0.48 ± 0.22	0.67 ± 0.03	38.3 ± 8.5	0.14 ± 0.08	0.218
	1500	1:2	-	0.77 ± 0.02	0.99 ± 0.03	41.8 ± 0.8	0.32 ± 0.02	0.423
		1		0.80 ± 0.01	1.33 ± 0.02	47.1 ± 0.7	0.50 ± 0.02	0.639
		2		0.79 ± 0.02	1.20 ± 0.02	44.7 ± 2.6	0.50 ± 0.05	0.585
		3		0.80 ± 0.03	1.43 ± 0.01	47.6 ± 0.3	0.55 ± 0.03	<b>0.682</b>
	4		0.78 ± 0.02	1.16 ± 0.03	48.1 ± 0.8	0.52 ± 0.02	0.652	
	1000	1:3	-	0.83 ± 0.004	0.83 ± 0.009	42.6 ± 0.2	0.29 ± 0.004	0.300
PBDPDP-C	1500	1:1	-	0.58 ± 0.13	0.03 ± 0.002	31.1 ± 0.9	0.005 ± 0.001	0.007
	1500	1:2	-	0.50 ± 0.01	0.08 ± 0.01	31.2 ± 0.1	0.018 ± 0.002	0.020
		3		0.62 ± 0.16	0.22 ± 0.03	36.0 ± 1.8	0.050 ± 0.016	<b>0.066</b>
	1500	1:3	-	0.62 ± 0.13	0.11 ± 0.01	30.1 ± 0.3	0.024 ± 0.004	0.029
	1500	1:3	-	0.62 ± 0.13	0.11 ± 0.01	30.1 ± 0.3	0.024 ± 0.004	0.029
PBDPDP-F <sup>a</sup>	2000	1:1	-	0.58 ± 0.15	0.04 ± 0.00	30.3 ± 0.4	0.006 ± 0.002	0.007
	2000	1:2	-	0.63 ± 0.01	0.07 ± 0.002	33.9 ± 0.4	0.016 ± 0.001	<b>0.016</b>

a. Only average of 2 devices due to bad film formation.

The poor efficiency derives mostly from low photocurrents, which for PBDPDP-C and PBDPDP-F are only  $0.22\pm 0.03$   $\text{mAcm}^{-2}$  and  $0.074\pm 0.002$   $\text{mAcm}^{-2}$ , respectively. This low photocurrent can in part be argued to derive from a low charge separation which in turn is a result of the small difference between the donor LUMO and the acceptor LUMO.

But if this was true the resulting efficiency of PBDPDP-DTP and PBDPDP-BDTHTT should also be comparably low, which is not the case as one can observe from Table 2. The explanation can be found in the low FF of the manufactured devices, for PBDPDP-C and PBDPDP-F the FF is in the mid to low thirties (in percentage) while for the PBDPDP-DTP and PBDPDP-BDTHTT polymers they are in the mid to the high forties. The FF is an indication of a favorable morphology. The I/V curves of the best performing devices can be seen in Figure 20.

PBDPDP-DTP showed a worse performance than what has been reported by Yue *et al*[59]., due to a much lower  $V_{oc}$  and  $J_{sc}$ . The PCE reported Yue *et al.* was of 2.60 %, with a  $J_{sc}$  of 7.83  $\text{mAcm}^{-2}$  and  $V_{oc}$  of 0.74 V. The average  $V_{oc}$  found in this study was only 0.57 V, the best performing device also showed a comparable  $V_{oc}$  of 0.74V. Therefore it becomes apparent that the  $J_{sc}$  is the key-source (or reason for the worse performance), for the best performing device a  $J_{sc}$  1.73  $\text{mAcm}^{-2}$  was found. This might be due to not only the LUMO – LUMO difference but also a non-optimal morphology. Despite the photo-physical properties being similar, the PBDPDP-DTP synthesized in this study has a slightly different alkyl modification which might affect the morphology of the devices, this non-optimal morphology most likely originates from the usage of different sidechain 2-octyldodecyl compared to the 2-ethylhexyl presented in the work of Yue *et al.* [59].

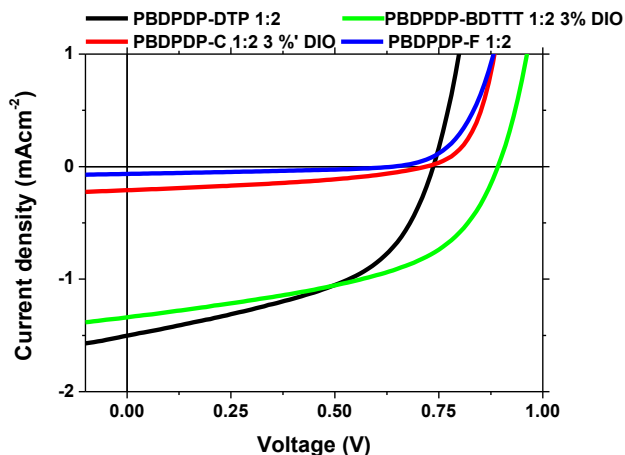


Figure 20: I/V characteristics of the PBDPDP-DTP (black,) PBDPDP-BDTHTT(green), PBDPDP-C (red) and PBDPDP-F(blue). The devices shown are the best performing of the population. All with the weight ratio (Donor:Acceptor) of 1:2 and with a DIO content of 3 % for the devices PBDPDP-BDTHTT(green) and PBDPDP-C (red).

PBDPDP-BDTHTT showed the overall best performance of the four polymers, with an average PCE of  $0.55\pm 0.03\%$  and a maximum performance of 0.682%, the best performance was achieved when 3% of DIO was added as additive. The  $V_{oc}$  was found to be  $0.80\pm 0.03$  V,

which is relative high compared to the other devices. The best performing devices had a  $V_{oc}$  0.89 V, which is much higher than that of the DTP based polymer. But as for all the polymers, the main reason for the relative low performance is the  $J_{sc}$ , even for the best performing devices; it did not exceed  $2 \text{ mAcm}^{-2}$ , with a  $J_{sc}$   $1.43 \pm 0.01 \text{ mAcm}^{-2}$  and a maximum performance of  $1.55 \text{ mAcm}^{-2}$ . The low photocurrent does most likely derive from the poor morphology and charge carrier mobility of the polymer film. The issue with the charge carrier mobility has been investigated by making hole only and electron only devices and thereby determining the charge carrier mobility by SCLC.

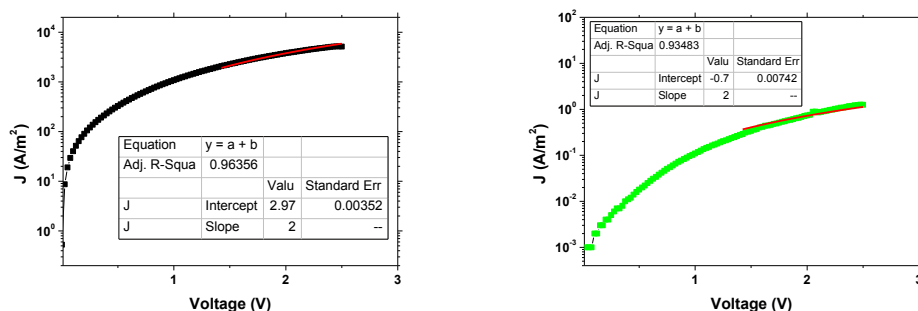


Figure 21: Space-charge limited current for **hole** only devices (ITO/PEDOT:PSS/active layer/MoO/Ag), these device are prepared using the optimized active layer composition. The active layers being of PBDPDP-DTP:PC<sub>71</sub>BM 1:2 (black, left) and PBDPDP-BDTTT:PC<sub>71</sub>BM 1:2 (green, right).

Figure 21 and Figure 22, present the hole- and electron-only device for the two best performing devices from the SCLC measurements, which are PBDPDP-DTP:PC<sub>71</sub>BM 1:2 spin coated at 2000 rpm and PBDPDP-BDTTT:PC<sub>71</sub>BM 1:2 spin coated at 1500 rpm.

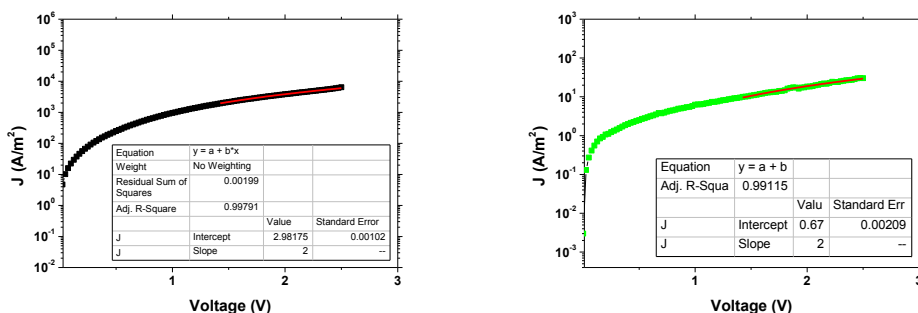


Figure 22: Space-charge limited current for **electron** only devices (ITO/ZnO/Active layer/Ca/Al), these device are prepared using the optimized active layer composition. The The active layers being of PBDPDP-DTP:PC<sub>71</sub>BM 1:2 (black, left) and PBDPDP-BDTTT:PC<sub>71</sub>BM 1:2 (green, right).

Using the equation presented in Equation 2-3, the charge carrier mobility can be determined:

$$J = \frac{9}{8} \mu \epsilon_0 \epsilon_R \frac{V^2}{L^3} \quad \text{Equation 2-3}$$

Where  $\mu$  is the charge carrier mobility (either hole or electron),  $L$  is the layer thickness,  $\epsilon_0$  is the free-space permittivity and  $\epsilon_r$  is the dielectric constant of the semiconductor,  $V$  is the applied voltage and  $J$  is the current density measured. The  $\epsilon_0$  is  $8.454 \cdot 10^{-12}$  F m<sup>-1</sup> and  $\epsilon_r$  is 3. Using the linear region of the  $I/V$ -curves with a constant slope of 2, the mobilities are calculated. The determined mobilities of the PBDPDP-DTP, PBDPDP-BDTTT, PBDPDP-C and PBDPDP-F are listed in Table 3.

Table 3: The space charge limited current mobility data of selected BDPDP based polymers, the bold are the devices presented in the Figure 21 and Figure 22. The weight-ratio 1:2 polymer:PC<sub>71</sub>BM in the active layer spin coated from chlorobenzene.

Sample name	Spin speed [rpm]	DIO [%]	Thickness [nm] <sup>a</sup>	Hole mobility [cm <sup>2</sup> V <sup>-1</sup> s <sup>-1</sup> ]	Electron mobility [cm <sup>2</sup> V <sup>-1</sup> s <sup>-1</sup> ]
<b>PBDPDP-DTP</b>	<b>2000</b>	-	<b>75</b>	<b>1.33•10<sup>-4</sup></b>	<b>1.35•10<sup>-4</sup></b>
	2000	3	83	1.66•10 <sup>-4</sup>	1.28•10 <sup>-6</sup>
<b>PBDPDP-BDTTT</b>	1500	-	100	1.10•10 <sup>-5</sup>	2.59•10 <sup>-4</sup>
	<b>1500</b>	<b>3</b>	<b>85</b>	<b>3.72•10<sup>-8</sup></b>	<b>9.68•10<sup>-7</sup></b>
<b>PBDPDP-C</b>	1500	-	115	3.43•10 <sup>-6</sup>	5.79•10 <sup>-6</sup>
	1500	3	100	6.39•10 <sup>-8</sup>	1.02•10 <sup>-4</sup>
<b>PBDPDP-F</b>	2000	-	70	1.01•10 <sup>-6</sup>	5.94•10 <sup>-6</sup>
	2000	3	100	6.11•10 <sup>-7</sup>	3.68•10 <sup>-4</sup>

<sup>a</sup>) Thickness measured by Dektak profilometer

For PBDPDP-DTP the mobilities are determined to be  $1.33 \cdot 10^{-4}$  cm<sup>2</sup>V<sup>-1</sup>s<sup>-1</sup> and  $1.35 \cdot 10^{-4}$  cm<sup>2</sup>V<sup>-1</sup>s<sup>-1</sup>, for the hole and electrons, respectively. This shows ambipolar properties as both hole and electron are equally mobile, which is favorable for device making, and it is also why the device performs the best. This mobility is slightly greater than the mobility reported by Yue *et al.* where the mobility was in the order of 10<sup>-5</sup>[59]. This difference is most likely due to the morphology, deriving from the use of the different sidechains. So even though the charge carrier mobility of the PBDPDP-DTP is superior to the previously reported, the PCE is much lower, this could therefore be due to decay mechanisms of the exciton. The addition of the additive DIO (3%) facilitates the lowering of the electron mobility, which can be associated with some changes in the film morphology. For the PBDPDP-BDTTT film, the addition of DIO also lowers the mobility for both electrons and holes. Surprisingly enough the lowering of the mobility results in an increase of efficiency going from 0.423 % to 0.682%, this is counter intuitively as a lower mobility results in a higher degree of recombination and internal resistance thus it should afford a lower efficiency. PBDPDP-C and PBDPDP-F both exhibit reasonable mobilities, although there is a large imbalance between the hole and the electron mobility. Generally the hole and electron mobility of the BDPDP based polymers are low compared to the ones reported in literature; Hong *et al.*[57] reported hole mobilities for a

BDPDP bithiophene copolymer reaching  $0.026 \text{ cm}^2\text{V}^{-1}\text{s}^{-1}$  and Cui *et al.*[49] originally reported a hole mobility in the order of  $10^{-3} \text{ cm}^2\text{V}^{-1}\text{s}^{-1}$ .

In order to investigate the scalability of the OPV devices from the synthesized polymers, roll coated devices have been fabricated. The procedure is described in detail in section 2.2.1. The key performance parameters of these devices are shown in Table 4. The general performances of the RC devices are lower than the equivalent spin coated devices. To our interests, PBDPDP-C showed some potential as a polymer based acceptor. This is most likely due to its high electron affinity. But the overall performances of these devices are very low.

Table 4: The roll coating I/V data of the polymers PBDPDP-C and PBDPDP-F, the electrode 5010 and 3L refers to the two type of electrodes presented in section 2.2.4. The active area of the fabricated devices were  $1 \text{ cm}^2$ . All devices were printed using CB as solvent for the active layer matrix.

Sample name	Ratio [D:A]	Electrode	$V_{oc}$ [V]	Jsc [ $\text{mAcm}^{-2}$ ]	FF [%]	PCE [%]
PBDPDP-C	1:1.5	5010	0.692±0.021	-0.0065±0.0001	24.7±0.4	0.0011±0.0000
	1:2	5010	0.525±0.036	-0.007±0.000	29.7±1.9	0.0011±0.0000
	1:2 <sup>a</sup>	5010	0.248±0.040	-0.008±0.001	26.5±0.3	0.0005±0.0001
	<b>1:1<sup>b</sup></b>	<b>3L</b>	<b>0.641±0.023</b>	<b>-0.036±0.008</b>	<b>24.0±1.6</b>	<b>0.0056±0.0016</b>
		5010	0.396±0.104	-0.018±0.000	23.3±0.9	0.0017±0.0004
PBDPDP-F	1:2	3L	0.100±0.017	-0.0024±0.001	24.6±0.6	$5.9 \cdot 10^{-5} \pm 9.7 \cdot 10^{-6}$
		5010	0.445±0.310	-0.0022±0.0000	30.9±0.9	0.0003±0.0002

<sup>a</sup>)Annealed <sup>b</sup>) PBDPDP-C as acceptor against P3HT

## 2.1.4. SUMMARY OF THE BDPDP – POLYMERS

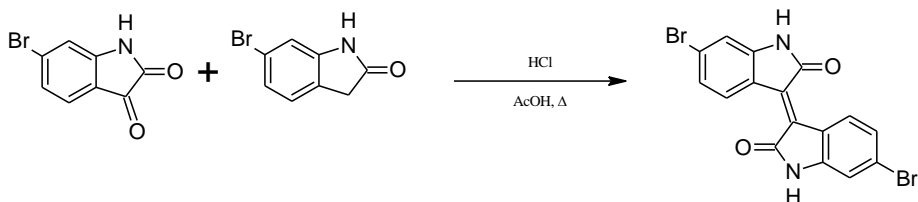
Four polymers containing the acceptor moiety BDPDP have been synthesized via both Stille and Suzuki cross-coupling reaction. The polymers being PBDPDP-DTP consisting of a N-(1-pentylhexyl)dithieno[3,2-b:2',3'-d]-pyrrole polymerized 3,7-bis(phenyl)-1,5-bis(2-octyldecyl)pyrrolo[2,3-f]indole-2,6(1H,5H)-dione, PBDPDP-BDTT consisting of 3,7-bis(4-phenyl)-1,5-bis(2-ethylhexyl)pyrrolo[2,3-f]indole-2,6(1H,5H)-dione and 4,8-bis(5-(2-ethylhexyl)thiophen-2-yl)benzo[1,2-b';4,5-b'']dithiophene, PBDPDP-C 3,7-bis(phenyl)-1,5-bis(2-octyldecyl)pyrrolo[2,3-f]indole-2,6(1H,5H)-dione and 9-(9-heptadecanyl)-9H-carbazole and lastly PBDPDP-F consisting of 3,7-bis(phenyl)-1,5-bis(2-octyldecyl)pyrrolo[2,3-f]indole-2,6(1H,5H)-dione and 9,9-dioctylfluorene. The resulting polymers had bandgap that fell in line with the donor strength of the different donors; the determined bandgaps were the following: 1.46 eV for PBDPDP-DTP, 1.59 eV for the

PBDPDP-BDTHH, 1.85 eV for PBDPDP-C and lastly 1.91 eV for the PBDPDP-F. All the polymers showed ICT interactions with two distinctive low and high wavelength absorbance bands, indicating a strong interaction between the applied donor and BDPDP moieties.

The absorbance spectrum of PBDPDP-BDTHH was slightly different compared to the others, as the absorbance band had a more continuous progression with a relative high absorbance from the onset (780nm) and further. The frontier orbitals (HOMO and LUMO) were determined using cyclic voltammetry, the LUMO levels were found to be ranging from -3.72 to -3.89 eV and the HOMO levels span from -5.22 to -5.69 eV. The synthesized polymers were tested as the donor component in bulk heterojunction OPV devices, using normal geometry in the structure ITO/PEDOT:PSS/active layer/Ca/Al. The active-area of the devices were 0.1 cm<sup>2</sup> and were tested under a sun simulator AM1.5 G. The best achieved PCE were; 0.614% for PBDPDP-DTP, 0.682% for PBDPDP-BDTHH, 0.066% for PBDPDP-C and 0.016% for PBDPDP-F.

## 2.2. ISOINDIGO-BASED LOW BANDGAP POLYMERS

Isoindigo (*i-ID*) is an interesting electron deficient monomer, due to an appropriate LUMO level alignment with fullerene based acceptor components (such as state-of-the-art PC<sub>61</sub>BM and PC<sub>71</sub>BM). Isoindigo is an isomeric derivative of blue dye indigo, which is normally used for coloring jeans. The interest in this moiety was originally fueled by Reynolds *et al.*[62] in 2010 who showed an *i-ID* oligothiophene as the donor component (p-type) in an OPV the resulting device exhibited a PCE of 1.76 % with a V<sub>oc</sub> of 0.74 V, J<sub>sc</sub> of 6.3 mAcm<sup>-2</sup>, and a FF of 38%. *i-ID* is interesting as it is a relative efficient electron acceptor (withdrawing), optical transition dipole, and ease of synthetic procedure. The electron withdrawing properties derive from the lactam units in the central part of the molecule, as shown in Scheme 7.



Scheme 7: The molecular structure and the general synthetic path of the dibromo derivative of Isoindigo (*i-ID*).

Shortly after Reynolds and coworkers initial report; it sparked an array of reports by Zhang *et al.*[63], Liu *et al.*[64] and Wang *et al.*[65] with efficiencies ranging from 1 to 3% for different combination of *i-ID* and donor-moieties. Wang *et al.*[66] in 2011 already showed the great potential of the *i-ID* with a polymer of *i-ID* together with a donor consisting of a dithiophene spaced 4,8-bisalkoxy-benzo[1,2-*b*:4,5-*b'*]dithiophene for a PCE of 7.31%, with a V<sub>oc</sub> of 0.72 V and a J<sub>sc</sub> of 14.96 mA cm<sup>-2</sup>. This was the highest reported PCE until Deng *et al.*[67] in 2014 published a report on an *i-ID* based polymer with a PCE of 8.2% with an impressive J<sub>sc</sub> of 15.2 mAcm<sup>-2</sup>. A common feature of these *i-ID* polymers is that the LUMO levels align very well with that of commonly used PCBM derivatives [68]–[70]. There has been conducted with numerous experiments on the OPV characteristics of the polymers. Despite the many merits of the *i-ID*, little work has been done on the large area devices, therefore in this study two different materials are going to be synthesized. The interesting LUMO characteristics of the *i-*

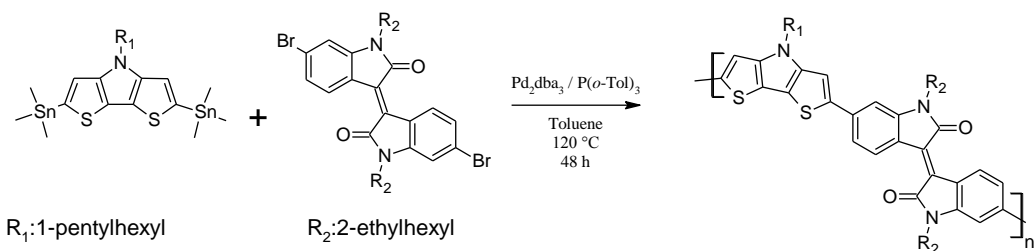
ID are going to be combined with two donor moieties of varying donor strength. The DTP moiety as presented in the previous section has high donor strength while the DTF moiety is slightly less donating. This is done to improve the depth of the HOMO in order to ensure a high  $V_{oc}$  and stable polymer.

## 2.2.1. MATERIALS AND METHODS

### 2.2.1.1 Materials

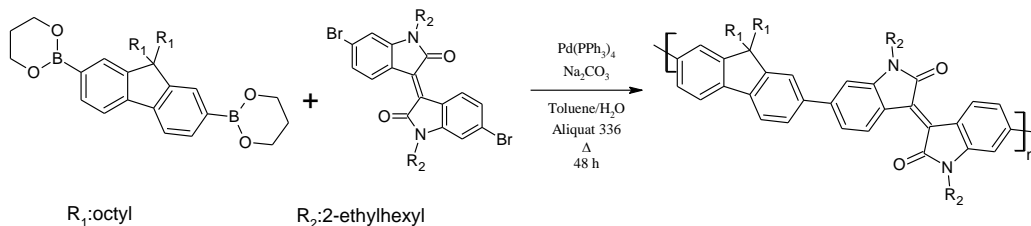
The *i*-ID and donor candidates were synthesized using the procedure reported in literature [62], [71]. The chemicals were commercially available and used without further purification if not stated otherwise.

### 2.2.1.2 Syntheses



Scheme 8: Synthetic path for PDTPI, via the Stille coupling of 2,6-di(trimethyltin)-*N*-(1-pentylhexyl)dithieno [3,2-*b*:2',3'-*d*]-pyrrole and 6,6'-dibromodi(2-ethylhexyl)isoindigo.

**PDTPI.** As seen in Scheme 8 and reported in [72], a mixture of 2,6-di(trimethyltin)-*N*-(1-pentylhexyl)dithieno [3,2-*b*:2',3'-*d*]-pyrrole (104.30 mg, 0.158 mmol), 6,6'-dibromodi(2-ethylhexyl)isoindigo (100.00 mg, 0.155 mmol), tris(dibenzylideneacetone)dipalladium ( $\text{Pd}_2(\text{dba})_3$ , 2.84 mg, 3.10 mmol), and tri-*o*-tolylphosphine ( $\text{P}(o\text{-Tol})_3$ , 7.55 mg, 24.8 mmol) was preliminarily degassed with  $\text{N}_2$ , and then toluene (16 mL) was added. The mixture was further purged with  $\text{N}_2$  for 20 min and heated to 120°C for 48 h. Subsequently the reaction was cooled to room temperature and the solution was precipitated in methanol. The crude polymer was collected by filtration and then purified on a Soxhlet extractor using acetone and hexane in succession. The polymer was extracted with chloroform and obtained by precipitating the chloroform solution in methanol, yielding 105 mg (55%) solid dark polymer. GPC,  $M_n$ : 8860 Da; PDI 1.52.  $^1\text{H}$  NMR (600 MHz,  $\text{CDCl}_3$ , d, ppm): 9.11 (d, 2H), 6.65–7.31 (m, 6H), 4.39 (s, br, 1H), 3.75 (s, br, 4H), 0.95–2.27 (m, br, 52H).



Scheme 9: Synthetic path for PFI via the Suzuki polymerization of 6,6'-dibromodi(2-ethylhexyl) and 9,9-dioctylfluorene-2,7-diboronic acid bis(1,3-propanediol) ester.

**PFI.** A mixture of 6,6'-dibromodi(2-ethylhexyl)isoindigo (100.00 mg, 0.155 mmol), 9,9-dioctylfluorene-2,7-diboronic acid bis(1,3-propanediol) ester (86 mg, 0.155 mmol), Pd(PPh<sub>3</sub>)<sub>4</sub> (2.40 mg, 2.09 · 10<sup>-3</sup> mmol), Na<sub>2</sub>CO<sub>3</sub> (530 mg, 5 mmol) and a drop of Aliquat 336 was degassed with nitrogen, then toluene (7.5 mL) and oxygen-free H<sub>2</sub>O (2.5 mL) were added. The resulting mixture was kept at 90 °C for 24 h. Subsequently cooled to ambient temperature, the mixture was then precipitated in methanol. The crude polymer was collected by filtration and then extracted on a Soxhlet's extractor with acetone, hexane and chloroform in succession. The final polymer was obtained by precipitating the chloroform solution in methanol. <sup>1</sup>H NMR (600 MHz, CDCl<sub>3</sub>, d, ppm): 9.33 (d, 2H), 7.88 (m, 2H), 7.4–7.8 (m, 6H), 7.13 (s, br, 2H), 3.8 m, br, 4H), 0.95–1.27 (m, br, 58H)

### 2.2.1.3 Methods

The UV-vis spectrum, CV, <sup>1</sup>H NMR (both PDFI and PDTPI) and the BHJ OPV devices of PDFI was made according to the procedure described in 2.1.2. Transmission electron microscope (TEM) images were recorded on a Hitachi H-7650 transmission electron microscope at an accelerating voltage of 100 kV. The external quantum efficiency (EQE) was determined using a QEX10 system (PV Measurements).

The CV of PDTPI was conducted on a different setup, being a CHI660B electrochemical analyzer (CH Instruments) using a three-electrode cell set-up with 0.1 M TATBF<sub>4</sub> in acetonitrile as the electrolyte at a scan rate of 1 V s<sup>-1</sup>. A glassy carbon working electrode with a diameter of 1 mm, a platinum counter electrode, and an Ag/Ag<sup>+</sup> pseudo reference electrode were applied. The material DTPI was tested against PC<sub>61</sub>BM as the acceptor. The PDTPI devices where tested Solar cells were measured with a Keithley 2400 source meter under a KHS 575 solar simulator with an AM1.5G 1000 Wm<sup>-2</sup> intensity.

**Spin-coated single junction OPV:** All the devices with PDTPI was coated on a poly(ethylene terephthalate) (PET) substrate, with a conductive PEDOT:PSS (Heraeus Clevious PH1000) was applied as charge collector, an electron transport layer (ETL) was deposited by spin coating of a solution of Al doped ZnO nanoparticles (dissolved in acetone, 49 mg mL<sup>-1</sup>) at 1000 rpm, upon the ETL the active layer (AL) was spin coated from a DCB solution of the PDTPI:PC<sub>61</sub>BM with the weight ratio 1:2 (20 mg mL<sup>-1</sup>) at 600 rpm. A hole transport later (HTL) consisting of PEDOT:PSS (Agfa EL-P-5010 : isopropanol 2 : 1 w/w) was spin-coated at 3000rpm, and finally Ag was vacuum deposited as the back electrode. The active area of the device was 0.25 cm<sup>2</sup>.

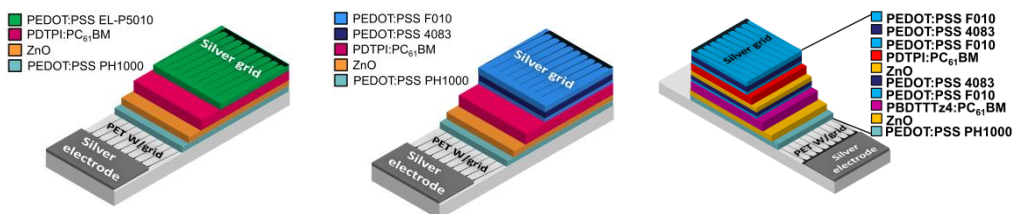


Figure 23: A schematic illustration of the 3 different devices used for testing PDTPI. The left one being the spin-coated device structure, middle one for the roll-coated single junction structure and the right one is the devices structure of a rollcoated tandem device as reported in literature[72], [73].

**Roll-coated single junction OPV:** The roll coated devices were slot-die coated on a substrate known as Flextrode, consisting of the highly conductive PEDOT:PSS (Heraeus Clevious PH1000) as the charge collector and ZnO nanoparticles on a barrier material (flexible substrate) with a large scale roll-to-roll flexographic printed silver electrodes. As before, the active layer comprised of PDTPI:PC<sub>61</sub>BM (1:X, weight ratio, 20 mg mL<sup>-1</sup>) and a HTL PEDOT:PSS (Clevious P VP Al 4083 and Clevious F-010) was slot-die coated on top. The method used has been reported by Andersen *et al.*[73] and Angmo *et al.*[74]. The back Ag electrode was applied by flexographic printing of a heat curable silver paste (PV410, Dupont)[73]. The active areas of these devices were all 1 cm<sup>2</sup>.

**Roll-coated tandem OPV:** The tandem OPVs were fabricated similarly to the single junction roll-coated device as previously described. The layer composition is shown in Figure 23, firstly the front (relative) high-bandgap polymer was (either PBDTTTz-4 or P3HT) was coated in a ratio 1:1 with PC<sub>61</sub>BM and then secondly the low-bandgap polymer PDTPI was coated in a ratio 1:2 with PC<sub>61</sub>BM. The two active layers were separated by PEDOT:PSS F010 (Clevious F-010), PEDOT:PSS Al 4083 (Clevious P VP Al 4083) and ZnO. Detailed descriptions of the printing methodology have been reported by Andersen *et al.*[73].

## 2.2.2. MATERIALS CHARACTERIZATION

All below shown figures are either unpublished data or adaptations of figures published in paper I [72]. The <sup>1</sup>H NMR data and molecular weight ( $M_n$ ) of the synthesized polymers are all shown in the materials and methods section 2.2.1. An essential parameter for the successful polymeric material in the OPV context is the absorbance spectrum. For the materials of PDTPI and PFI, the spectra are shown in Figure 24 and Figure 25, respectively.

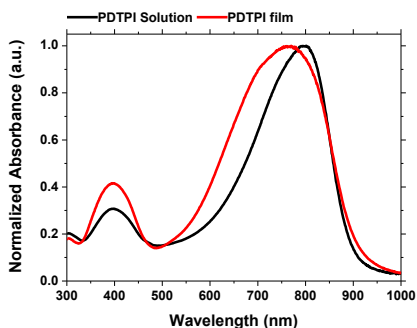


Figure 24: Absorbance spectrum of PDTPI in a  $\text{CHCl}_3$  solution (**black**) and in film (**red**).

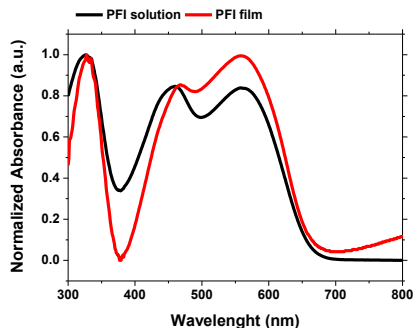


Figure 25: Absorbance spectrum of PFI in a  $\text{CHCl}_3$  solution (**black**) and in film (**red**).

When looking at the absorbance spectra, the first thing that stands out is the large difference between the onset of the absorbance between PDTPI and PFI, being approximately 900 nm for the PDTPI and 660 nm for PFI. This clearly emphasizes the difference between the two donor monomers DTP and Flourene (F). For PDTPI, it is found  $\pi$ - $\pi^*$  transition at 390 nm combined with the large broad peak with a maximum at approximately 790 nm, deriving from the ICT between the DTP donor moiety and *i*-ID. The film absorption of PFI has a maximum at 560 nm, combined with two lower laying maxima at 465 nm and 328 nm. The  $\pi$ - $\pi^*$  transition peaks with the two low laying maxima (at 465 nm and 328 nm) and while the local maxima at 328 nm is located at the same wavelength for both the film and solution, the maxima at 465 nm is red-shifting slightly (5 nm) when going from solution to film. This could indicate that the lowest laying maximum derive from a molecular confirmation that does not interact more with the surrounding molecules when becoming solid. Therefore to assume the peak derives from the F moiety might be reasonable as the quaternary substituted carbon of the F moiety that somehow will counter act the intermolecular interaction. Li *et al.*[75] showed that the peak at approximately 450 nm (in solution) derives from the *i*-ID  $\pi$ - $\pi^*$  transition, an interesting absorbance characteristics is that native *i*-ID also shows a slightly D-A characteristics with two maxima. The absorbance of the PFI molecule has a very similar progression to a polymer also consisting of *i*-ID and 9,9-di-*n*-octyl-9H-fluorene[68], with a maximum absorbance at approximately 560 nm. The absorbance onset of PFI is low compared to that of PDTPI, this derives from the lower donor strength of the F moiety and also from the absorbance spectrum indicating a low interaction between the D-A components of the given polymer. An interesting characteristic of both PDTPI and PFI is that, going from solution to film, a blue shift occurs. This blue shift may originate from two aspects:

1. Aggregation of the macromolecules are formed in solution (such as entanglement of the polymer chains)
2. Interaction between the alkyl chains retarding the intermolecular  $\pi$ - $\pi$  interactions.

For the first point, the molecular aggregation has been illustrated by Yue *et al.*[76] where it was found that an array of planar D-A LGB polymers showed a blue-shift when going from solution to solid of 5-19 nm. The reported polymers comprised of DTP as donor and the acceptor moieties were phthalimide or thieno[3,5-*c*]pyrrolo-4,6-dione. It was observed that a blue shift of 5-13 nm could be introduced in a solution of CB when the temperature was increased from 25 to 70°C. This blue shift has been attributed to the breakup of inter-chain

aggregates at the higher temperatures, has been shown in multiple cases[59], [77], [78]. For the second aspect listed, Ho *et al.*[79] demonstrated that the alkyl sidechains can reduce, or even counter the  $\pi$ - $\pi$  stacking of the polymers containing *i*-ID. The polymer system that Ho *et al.* investigated was poly(cyclopentadithiophene-*alt*-isoindigo), where the cyclopentadithiophene (CPT) was alkylated with various branched or linear alkyl chains. They showed that sidechains can prevent a red shift, counter intuitively the linear n-octyl side chain in that study, showed a larger effect on the torsion of the polymer backbone. Torsion promotes the misalignment of the  $\pi$ -orbitals, which in turn will have a lower conjugation length e.g. blue shift. This behavior has also been reported by Stalder *et al.*[48] that showed a similar trend for copolymers consisting of *i*-ID and dithieno[3,2-b:2',3'-d]silole copolymer. Taking this into account one would expect a system like the PFI to exhibit a blue shift, but this is very limited. The broadening of the absorbance seen in PDTPI indicates, despite all, a larger degree of  $\pi$ - $\pi$  interactions. While the film of PFI does not show a similar trend, this could be due to the large degree of spatial interactions of the F donor moiety, which counteracts the  $\pi$ - $\pi$  stacking due to its bulkiness. The broadening of absorbance can be attributed to such  $\pi$ - $\pi$  interactions as well. Using Equation 2-1, the band gaps of molecules where; for PDTPI 1.38 eV (898 nm) and for PFI 1.8 eV (665 nm). Besides the optical properties, the energy levels of the orbitals are essential for the device performance.

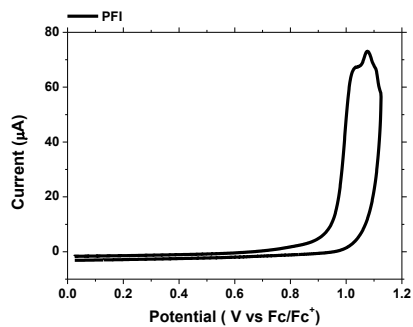
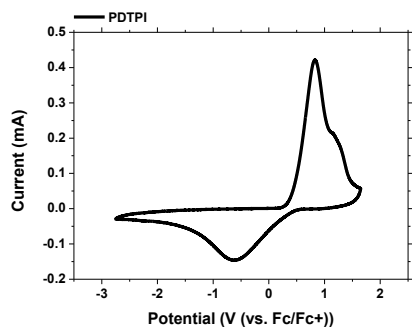


Figure 26: Cyclic voltammetry of the polymer PDPTI. Figure 27: Cyclic voltammetry of the polymer PFI.

The frontier orbitals are determined by CV, the results of the CV is shown in Figure 26 and Figure 27. The first thing to notice when comparing the two CV diagrams is that while the PDTPI is reversible PFI is not, on Figure 27 only the oxidation onset is shown. As discussed previously the lack of reversibility can derive from an electrochemical facilitate reaction occurring. It should be noted that the measurements were conducted on two different setups. But the experimental conditions are comparable, as both CV measurements are conducted on drop-casted neat polymeric films without a controlled thickness. The HOMO levels of the polymeric films are determined using Equation 2-2; combined with the  $E_g$  the LUMO levels of the polymers are calculated.

According to Deng and Zhang the general HOMO level of the *i*-ID polymers are in the range of -5.20 eV to -5.49 eV against vacuum. The relative low lying HOMO levels will potentially afford a high  $V_{oc}$  when used in the devices. The HOMO level of the PFI polymer is lower than the expected, with a value of -5.75 eV.

Table 5: Photo-physical properties of the two conjugated polymers, the LUMO energy level is for PDTPI and PFI was found by combining absorbance onset and the ionization potential found via CV.

Sample name	$\lambda_{\text{onset}}$ [nm]	$E_g$ [eV]	$E_{\text{ox onset}}$ [V]	$E_{\text{HOMO}}$ [eV]	$E_{\text{LUMO}}$ [eV]
PFI	665	1.86	0.95	-5.75	-3.89
PDTPI	898	1.38	0.44	-5.23	-3.85

The HOMO of the two polymers differs a bit, as the two donor moieties of the two polymers exhibit very different donating strengths. That is also why the band gaps of the polymers are different. The LUMO, which is directed by the *i*-ID moiety of the polymers, are nearly identically. The issue regarding the LUMO level is that PC<sub>61</sub>BM has a LUMO i between 4.02 to 3.7 eV, depending on the determination method. Therefore the driving force for the charge separation is not optimal; this could end up being a problem. But looking in the literature, the LUMO levels falls very much in line with the reported LUMO levels shown in the review by Stalder *et al.* [69], where the LUMO levels of the reported polymers are ranging from -3.54 to -4 eV. The devices have been made at two different device testing facilities; therefore PFI is tested in a normal geometry device setup (small area 0.1 cm<sup>2</sup>) and PDTPI is tested in large area (~0.8 cm<sup>2</sup>) inverted cell geometry.

### 2.2.3. PFI DEVICES

The PFI polymer was tested both in regards to acceptor concentration and with regards to addition of additives. The donor (polymer) and acceptor (fullerene) content varied using different spin coating speeds. In Figure 28 and Figure 29 the devices of polymer PFI is shown, it can be seen that the highest voltage is obtained at the lowest spin speed for both ratios.

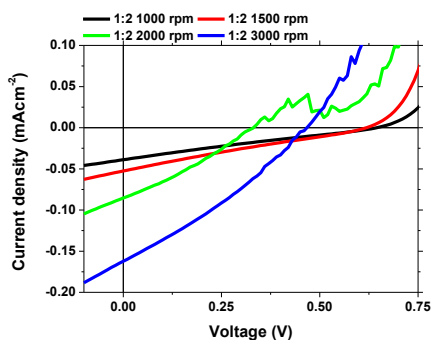


Figure 28: I/V characteristics of the best performing OPV devices of the donor PFI polymer with the acceptor PC<sub>71</sub>BM, the ratio was 1:2 (donor:acceptor). At different spin speeds 1000 rpm (black), 1500 rpm (red), 2000 rpm (green) and 3000 rpm (blue).

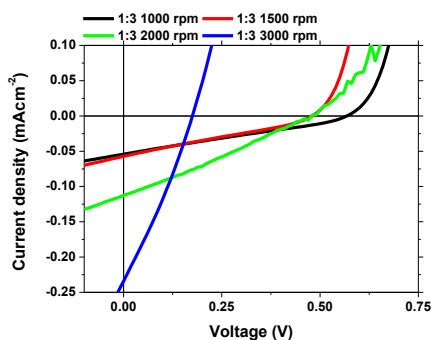


Figure 29: I/V characteristics of the best performing OPV devices of the donor PFI polymer with the acceptor PC<sub>71</sub>BM, the ratio was 1:3 (donor:acceptor). At different spin speeds 1000 rpm (black), 1500 rpm (red), 2000 rpm (green) and 3000 rpm (blue).

While the highest photo induced current is from the highest spin speeds, this indicates that a thin active layer exhibits a higher photocurrent, due to the smaller distance that the charge carriers has to travel. The correlation between thickness and spin speed has not directly been investigated; but the thickness of the active layer in the devices at 3000 rpm was determined by Dektak profilometer to be approximately 90 nm, while that of the devices at 1000 rpm was determined to be around 120 nm.

*Table 6: Device performance of the organic photovoltaics, using the four polymers PFI as the donor against the acceptor PC<sub>71</sub>BM; in various weight ratios. The polymer:fullerene films was spin coated from ortho-dichlorobenzene with a dry content of 30 mg mL<sup>-1</sup>. The values shown are the average of at least 4 devices.*

Ratio (D:A)	Spin speed [rpm]	V <sub>oc</sub> [V]	J <sub>sc</sub> [mAcm <sup>-2</sup> ]	FF[%]	PCE <sub>average</sub> [%]	PCE <sub>best</sub> [%]
1:2	1000	0.53±0.18	0.039±0.001	23.1±4.6	0.005±0.002	0.006
	1500	0.48±0.16	0.053±0.002	22.9±6.5	0.005±0.002	0.008
	2000	0.21±0.12	0.085±0.000	28.5±1.5	0.005±0.003	0.008
	3000	0.28±0.08	0.175±0.007	26.3±5.0	<b>0.016±0.005</b>	<b>0.023</b>
1:3	1000	0.57±0.01	0.055±0.001	26.4±0.4	0.0082±0.0001	0.008
	1500	0.33±0.11	0.060±0.002	25.5±1.4	0.0050±0.0017	0.008
	2000	0.27±0.15	0.106±0.005	23.4±6.3	0.0070±0.0052	<b>0.014</b>
	3000 <sup>a</sup>	0.12±0.06	0.234±0.000	27.0±1.7	<b>0.0077±0.0040</b>	0.011

<sup>a</sup>) average of 2 devices due to bad film formation

This 30 nm difference can facilitate this relative large difference in regards to J<sub>sc</sub> and V<sub>oc</sub>. The summarized device data is shown in Table 6, where it can be seen that there is a large difference in both the average V<sub>oc</sub> and the average J<sub>sc</sub> as shown for the best devices illustrated in Figure 28 and Figure 29.

The efficiency of the devices with the D:A ratio of 1:2, spun at 3000 rpm, was the best performing, showing a PCE of 0.016±0.005 % and a maximum efficiency of 0.023%. Despite the highest PCE, the devices has a V<sub>oc</sub> of 0.28V which is very low compared to that to state-of-art solar cells with reasonable PCE's. The increase in the current as function of the increase speed (invers proportional with thickness) indicates that there must be a high resistance and therefore a high degree of recombination. This could be due to low charge mobility. If the mobility is low, then recombination will be counter acting the efficiency of the device. But the low voltage of the device for the thin devices could be an indication of incomplete coverage that lowers the V<sub>oc</sub> of the device via shunting.

To investigate the reason behind the poor performance further, the charge carrier mobility has to be investigated. The mobilities have been determined via the space charge limited current (SCLC) method on hole only and electron only device, respectively.

Table 7: Hole and electron mobility determined by SCLC measurements on hole and electron only devices of the polymer PFI and the acceptor PC<sub>71</sub>BM..

Ratio [D:A]	Spin speed [rpm]	Thickness [nm]	Electron mobility [cm <sup>2</sup> V <sup>-1</sup> s <sup>-1</sup> ]	Hole mobility [cm <sup>2</sup> V <sup>-1</sup> s <sup>-1</sup> ]
1:2	1000	125	3.431•10 <sup>-4</sup>	5.154 • 10 <sup>-6</sup>
	3000	93	1.934•10 <sup>-4</sup>	- <sup>a</sup>
1:3	1000	129	6.871•10 <sup>-4</sup>	1.926 • 10 <sup>-7</sup>
	3000	87	6.850•10 <sup>-4</sup>	1.150 • 10 <sup>-4</sup>

<sup>a</sup>) not available

The charge carriers mobilities are shown in Table 7 and while the electron mobility are in the same order of magnitude, the hole mobility varies with multiple orders of magnitudes. For the 1:3 ratio devices, the electron mobilities are nearly identical as result of the high content of the highly conducting PC<sub>71</sub>BM. The difference between the electron mobility of the 1:2 ratio devices are slightly larger but still they show the same order of magnitude, the difference in mobility is that the increasing thicknesses also increase the mobility.

The hole mobility is much more varying for the different ratios and different spin speeds. It is normally associated with the p-type material (donor polymer) which might be the reason for the low overall efficiency of the presented devices. According to the results, the poor performance can be ascribed to the low mobility.

For the devices with the D/A ratio 1:3 casted at 3000 rpm, the relatively balance (compared to the other devices tested) between hole and electron mobility, might be why it performs superior to the others. Unfortunately the hole mobility of the devices with the D/A ratio of 1:2 casted at 3000 rpm could not be determined, therefore it cannot be stated certainty whether or not it exhibited the same balance, as indicated by the relative (to the other devices) good performance.

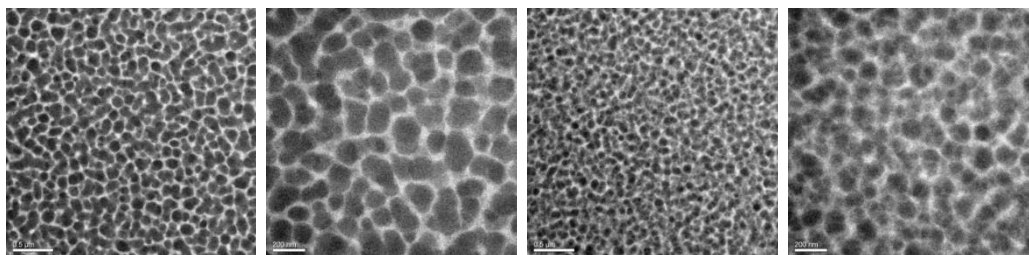


Figure 30: TEM picture of the active layer film ( $PFI:PC_{71}BM = 1:2$ ) casted at 3000rpm. The left image has the scale bar of  $0.5 \mu\text{m}$  and the right image has a scale bar of 200 nm.

Figure 31: TEM picture of the active layer film ( $PFI:PC_{71}BM = 1:3$ ) casted at 3000rpm. The left image has the scale bar of  $0.5 \mu\text{m}$  and the right image has a scale bar of 200 nm.

TEM images were made for the for the active layer film with two different ratios between PFI and  $PC_{71}BM$ , but at the cast at the same spin speed. It is clear that the morphologies show a tendency to form large domains of nearly 100 nm size. The TEM method does not account for the different materials of these domains but only represent different electron densities around the matrix. This difference could therefore indicate the formation of domains that are not favorable for the device performance. Therefore the low performance of the devices is possible partly ascribed to both the large imbalance of the charge carrier mobility and the presence of unfavorable domains sizes in the film.

#### 2.2.4. PDTPI DEVICES

The PDTPI polymer was used in another type of OPV device, as this material has been tested in a more scalable setup using both vacuum free processing and ITO free substrates. The PDTPI was tested in inverted devices geometry. The device geometry was chosen as this method has been shown to be readily scalable [80]. In Figure 32 the photovoltaic performance of both the roll coated and the spin coated devices are shown. In can be seen that despite the active area of the spin coated device is only  $0.25 \text{ cm}^2$  compared to the  $1 \text{ cm}^2$  area of the roll coated one, an increase in  $J_{sc}$  is observed with increased active area, which is opposite to what is normally expected.

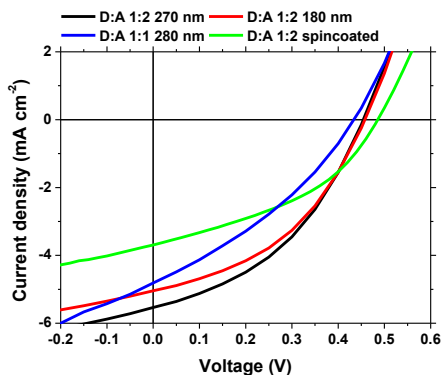


Figure 32: The photovoltaic performance of the roll-coated and the spin coated single junction solar cells with different PDTPI: PC<sub>61</sub>BM ratios and film thicknesses. D:A ratio of 1:2 two thickness is presented; 270 nm (**black**) and 180 nm (**red**). For the D:A ratio of 1:1 one thickness is presented; 280 nm (**blue**). The thickness of the active layer of the spin coated cells were estimated to be 160-200nm and the D:A ratio was 1:2 (**green**). Adapted from paper **I** [72].

The photovoltaic I/V performance of the devices are shown in Table 8. The increase in efficiency could be due to the utilization of different PEDOT:PSS based top-electrodes. The top electrode of the spin coated device was the Agfa EL-P5010 whilst the roll-coated devices utilized a 3 layer PEDOT-PSS electrode as shown in Figure 23. The different electrodes will account for some of the different performances of the devices, deriving from the production method. The two production method must result in different morphologies as the different evaporation rate will have a strong impact on the morphology, influencing the  $J_{sc}$ , as is observed: an increase for the device going from a spin coated device to a roll-coated device. But the morphology will not be investigated further in this study.

Table 8: Summarized I/V-performance of both the spin coated and roll coated devices, with the donor (D) PDTPI and acceptor (A) PC<sub>61</sub>BM. Adapted from paper **I**.

D:A ratio	Thickness[nm]	V <sub>oc</sub> [V]	J <sub>sc</sub> [mA cm <sup>-2</sup> ]	FF [%]	PCE [%]
1:1	280	0.42±0.01	-4.6±0.2	32.2±0.6	0.62±0.05
1:2 <sup>a</sup>	160-200 <sup>b</sup>	0.49	-3.69	40.3	0.72
1:2	180	0.45±0.04	-4.95±0.18	40.9±1.1	0.92±0.05
1:2	270	0.46±0.04	-5.25±0.28	41.3±1.4	0.99±0.08

<sup>a</sup>) Spin coated sample <sup>b</sup>) Estimated thickness

An increase in FF is observed when comparing the spin coating technique with the roll coating one; this difference might also be partly ascribed to the improved interface of the 3 layer electrode design, compared to the single layer design via spin-coating. This increase could also be ascribed to the increase in charge carrier transport in the active layer; both reasons will improve the collection of free charge carriers leading to the observed increment of the  $J_{sc}$ , as

the unfavorable recombination of the free charge carriers are reduced. Two different film thickness have been shown, and it can be seen that increasing the thickness slightly increases the efficiency, the decreased PCE of the thinner film device is mainly associated with the decrease of the  $J_{sc}$  which most likely is from the lower absorbance, as the other device parameters are unaffected by the changed thickness. The best performing device setup was that with the 1:2 weight ratio of PDTPI:PC<sub>61</sub>BM, with an active layer thickness of 280 nm. The device achieved a PCE of 0.99%,  $V_{oc}$  of 0.46 V and a  $J_{sc}$  of 5.25 mA cm<sup>-2</sup>. It should be noted that the Flextrode has a decreased transmission from 60% to 35% in the wavelength interval of 600-900nm [81], where the PDTPI has the highest absorbance and therefore highest EQE (see Figure 33).

As shown in Figure 24, the absorbance of PDTPI is primarily located in the long wavelength area (from 600-900 nm). This discontinuous nature of PDTPI might have an impact on the performance of the devices, as light that is not absorbed cannot be converted into electricity. Therefore an EQE measurement has been conducted and the results are shown in Figure 33.

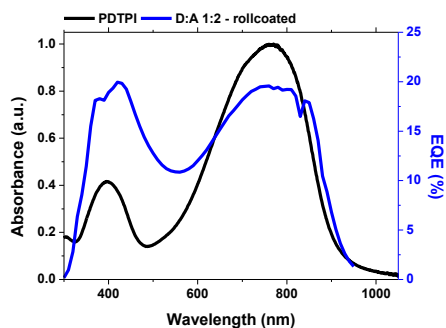


Figure 33: External quantum efficiency measurement of the PDTPI:PC<sub>61</sub>BM (1:2) device (blue) combined with the absorbance spectrum of PDTPI (black).

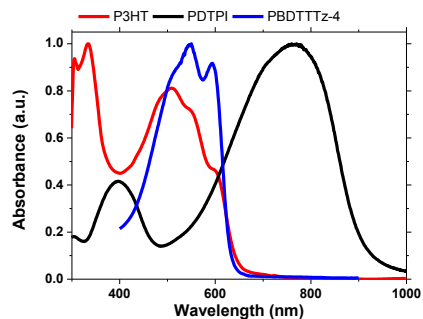


Figure 34: Absorbance spectra of P3HT (red), PDTPI (black) and PBDTTTz-4 (blue). Adapted from paper I.

The EQE has, as shown in Figure 33, the same overall progression as the absorbance of the PDTPI polymer. The EQE has local maxima at 450 nm and 790 nm, with an EQE approaching 20%. And in between these, a local minimum of the EQE (12.5%) are found, in the region of 400-600 nm. This makes PDTPI an excellent candidate for a low bandgap polymer, as its absorbance spectrum can readily be compensated by a higher gap polymer in a tandem device. An example of these high bandgap polymers could be; P3HT and PBDTTTz-4 [82]–[84] as these present an ideal compensation in light harvesting on PDTPI, as illustrated in Figure 34.

This lead to the testing of RC tandem photovoltaics as described in 2.2.1 and the I/V characteristics can be seen on Figure 35. It can be seen that the  $J_{sc}$  of the P3HT:PDTPI device is underperforming compared to the devices of PBDTTTz-4:PDTPI.

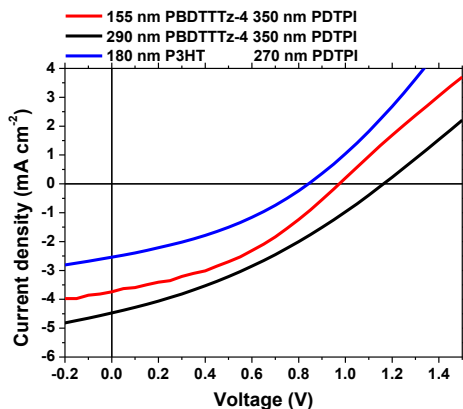


Figure 35: The photovoltaic I/V characteristics of the best performing tandem junction devices of PDTPI as the low-bandgap polymer. The combinations are as following PBDTTz-4 (155 nm):PDTPI (350 nm) (red line), PBDTTz-4 (290 nm):PDTPI (350 nm) (black), and P3HT (180 nm):PDTPI (270 nm) (blue). Adapted from paper I.

The device with P3HT is actually performing worse than the single junction device. The  $V_{oc}$  of the P3HT devices are slightly lower than the theoretical maximum, which can be determined by the sum of the single junctions  $V_{oc}$ 's. This is not the case for the PBDTTz-4 devices, where the total  $V_{oc}$  approaches the sum of the two sub cells. The increments of the  $V_{oc}$  between the two devices are a result of the increased thickness of the front electrode derives from the uneven surface of the flextrode; where silver spikes will result in shunting that lowers the  $V_{oc}$  of the device[73], [85].

Table 9: Summarized I/V-performance of the roll coated tandem devices. Utilizing PDTPI as the low-bandgap polymer combined with either P3HT or PBDTTz-4, as the high bandgap polymer. Adapted from paper I.

Sample name (thickness)	Voc [V]	Jsc[mAcm <sup>-2</sup> ]	FF[%]	PCE[%]	PCE[%]
PBDTTz-4 (155 nm) PDTPI (350 nm)	0.95±0.01	-2.83±0.98	33.9±3.8	1.12±0.23	1.40
PBDTTz-4 (290 nm) PDTPI (350 nm)	1.08±0.09	-4.60±0.32	32.9±0.52	1.63±0.05	<b>1.73</b>
P3HT (180 nm) PDTPI (270 nm)	0.85±0.01	-2.49±0.07	35.2±0.1	0.74±0.01	0.75

In Table 9 the key parameters of the photovoltaic performance is noted, where it can be seen that the best performing tandem device was the device consisting of a front layer consisting of 290 nm PBDTTz-4 a back layer consisting of 350 nm PDTPI with a PCE of 1.73%

## 2.2.5. SUMMARY OF THE ISOINDIGO CONTAINING OPV DEVICES

The two different *i*-ID containing materials were synthesized and characterized; the first being a relative high-bandgap copolymer PFI, consisting of alternating 9,9-dioctylfluorene and di(2-ethylhexyl)isoindigo which was polymerized via a Suzuki coupling reaction; the second polymer was a low-band gap polymer consisting of alternating di(2-ethylhexyl)isoindigo and N-(1-pentylhexyl)dithieno[3,2-b:20,30-d]-pyrrole moieties which was polymerized via Stille coupling reaction. The polymers showed different absorbance onset, for PFI the onset was 665 nm affording a bandgap of 1.85 eV and for PDTPI the onset was 898 nm resulting in a bandgap of 1.38 eV. The two different bandgaps are a result of very different HOMO energies being -5.75 eV and -5.23 eV for PFI and PDTPI, respectively. This is assumed to derive from the different donor units of the two copolymers which have relatively different donor strengths. The LUMO levels are as expected, rather similar being -3.89 eV and -3.85 eV for PFI and PDTPI, respectively.

In regards to the device performance, the two polymers showed remarkable different traits. For the PFI polymer small area devices ( $0.1 \text{ cm}^2$ ) were fabricated using a normal device geometry ITO/PEDOT:PSS/active layer/Ca/Al and through optimization an efficiency of only 0.016% with a low  $V_{oc}$  of 0.28 V and a  $J_{sc}$  of  $0.175 \text{ mA cm}^{-2}$ . The best performance was obtained for a device with the active layer consisting of 1:2 weight ratio between PFI and PC<sub>71</sub>BM and a layer thickness of approximately 90 nm (Figure 28). The low performance was contributed primarily to both the low electron mobility, being  $1.93 \cdot 10^{-4} \text{ cm}^2 \text{V}^{-1} \text{s}^{-1}$  and TEM images (Figure 30) also showed a large inhomogeneous nature of the prepared films, which could indicate a large phase separation thus resulting in a low exciton dissociation that will lower the photo induced current.

The PDTPI polymer was tested in inverted device geometry and tested both as a small area ( $0.25 \text{ cm}^2$ ) spin coated device and large area ( $1 \text{ cm}^2$ ) roll-coated device. The devices fabricated using PDTPI were all ITO-free and non-vacuum techniques applied. The small area devices afforded a efficiency of 0.72%, with a  $V_{oc}$  of 0.49 V and a  $J_{sc}$  of  $-3.69 \text{ mA cm}^{-2}$ , thus showing a much higher potential than the other *i*-ID based polymer. The medium area device showed a maximum efficiency of 0.99% with a  $V_{oc}$  of 0.46 V,  $J_{sc}$  of  $-5.25 \text{ mA cm}^{-2}$  and FF of 41.3 %. Due to the absorbance characteristics of PDTPI and the resulting EQE of the devices, this polymer was tested in a tandem OPV stack with the relative high-bandgap polymer of PDBTTTz-4 to afford a tandem device with a PCE of 1.73 and a  $V_{oc}$  of 1.08 V.

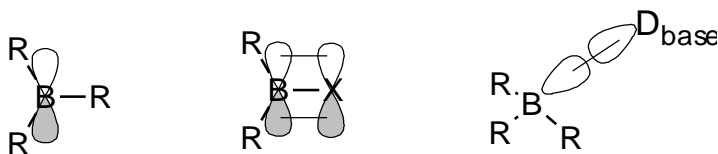
This study clearly emphasizes the structural dependency of donor moiety on HOMO level of the D/A polymer, while the LUMO level is clearly controllable via the acceptor moiety.



# CHAPTER 3. NOVEL N-BORYLATED CARBAZOLE FOR HIGH PERFORMANCE OPVS

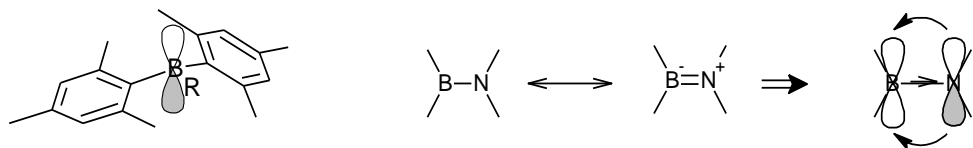
## 3.1. MOTIVATION

As described in Chapter 2, there has been a large focus on developing electron-deficient moieties, an attractive one is the three-coordinated boron (B) atom due to its vacant  $\pi$  orbital making it a relative strong acceptor [86].



*Scheme 10: Illustration of the orbital configuration of three coordinated boron through  $\pi$ -interactions or complexation between Lewis base and Lewis acid. Inspired by Jäkle [86]*

In Scheme 10, the orbital structure of the boron containing system is illustrated, presenting how boron can obtain the octet configuration either via  $\pi$ -overlap with an appropriate substituent (X in Scheme 10) or via Lewis-acid and Lewis-base interaction ( $D_{\text{base}}$  is the Lewis base). These interactions have drawn attention, as they pose a change to the placement of the frontier orbitals, which affects their photo physical properties. The boron atom poses another interesting characteristic, as it is more electro positive than carbon, which in turn makes it an  $\sigma$ -donor[87], [88]. The stability of the boron is the largest concern in regards to utilizing the interesting electron properties, as it can readily undergo hydrolysis reactions with moisture via a nucleophilic attack in ambient atmosphere, by e.g.  $\text{H}_2\text{O}$  [87]. However, this can be prevented by introduction of a bulky functionality that affords a steric/kinetic hindrance of reaction. The protective group applied in this work is a mesitylene group (Mes, 2,4,6-trimethylphenyl) that forms a cage of electron clouds around the vacant  $\pi$ -orbital preventing unfavorable reactions (see the left figure in Scheme 11).



*Scheme 11: Stability improvement on boron: Left: an illustration of the sterically hindrance of the  $\pi$ -orbitals of the boron by functionalizing with 2,4,6-trimethylphenyl (Mes); Right: the molecular interactions of a direct N-B bond and the interactions of these. Inspired by Entwistle et al.[89].*

Many interesting molecular properties have been shown in numerous applications in literature[86], [90], [91]. Beside small molecule applications[88], [92]–[94], polymeric materials where B is introduced into the system have been performed via different approaches.

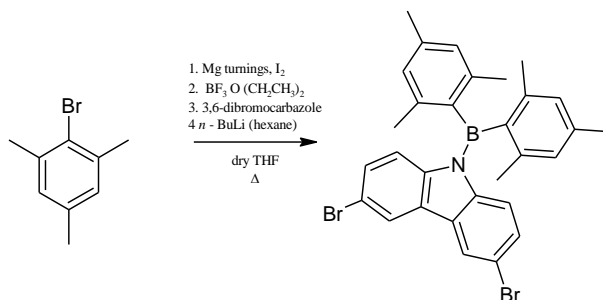
Firstly, by direct introduction into back-bone, which was sparked by Matsumi *et al.*[95] reporting a synthesis of a  $\pi$ -conjugated system via poly-addition using a hydroboration reaction between an array of diethynyl-aromatic compounds, such as 2,7-diethynyl-flourene and 1,4-diethynyl-phenyl. This afforded analogs to the known polymer poly(phenylvinylene) (PPV), differing only with the introduction of a boron as a  $\pi$ -linkage. Then series of reports have followed, e.g., Sundararaman *et al.* [96] revealed the incorporation of boron into the backbone of polythiophene, which was protected kinetically by different protective groups. It was found that these groups, being types of an aromatic, had a large effect on the absorbance and emission characteristics of the polymers. This was taken as proof of the large  $\pi$ -interaction of the back-bone. Secondly, two similar approaches can be taken to implement pendant side-functionalization of boron: 1.) Directly grafting the appropriately protected boron-group onto a functional monomer, then polymerized the monomer forming a conjugated back-bone, as illustrated by Zhao *et al.*[97]. They synthesized and characterized a relative versatile 1,2-diboryl-1,4-phenylene monomer for polymerization via the triple bond resulting poly(aryleneethynylene) [97]. The borylated monomer presented stability towards Sonogashira reactions using Pd(0), and resulted in highly emissive polymers both in solution and more importantly in solid. It has been argued by Yuan *et al.*[98]; that the acceptor strength of the B atom is comparable to moieties such as  $-\text{NO}_2$  and  $-\text{CN}$ ; 2.) Post modification on the polymer backbone with a boron containing reactant, where the boron was directly grafted to the polythiophene backbone, this modification afforded a significant red shift on its absorbance, thus lowering the  $E_g$  compared to an equivalent silylated polythiophene polymer, which supports the notion that the boron functionality is an acceptor type. Thirdly, a similar approach that could be called “pendant with aromatic spacer” as illustrated by Reitzenstein *et al.*[99] with an array of N-*p*-(diarylboryl)phenyl substituted 2,7 or 3,6 linked polycarbazoles. They found that borylation on 2,7 linked polycarbazole did not change absorbance or emission spectrum when comparing to its controlled reference polymer, while borylation on the 3,6 linked carbazole resulted in pronounced influence on the optical properties (enhanced fluorescence quantum yield). This was ascribed to the difference in the conjugation along the polymer backbone between the 2,7 and 3,6, where the latter is interrupted by the presence of N atom making it more susceptible for changes in the pendant side chain. The 3,6-linked N-*p*-(diarylboryl)phenyl substituted polycarbazol was considered a viable candidate for the OLEDs. The changes in the molecular dynamics are ascribed to the introduction of boron due to charge transfer between the electron rich carbazole moiety and the electron poor - $\text{BMes}_2$ . This derives from the process of charge stabilization; therefore such system can stabilize both formed cations and anions[93], [94]. One way circumventing the spatial dimension is to directly attach boron to nitrogen, whose bonding is comparable to the isoelectronic C=C bond. It has been shown in literature to afford less  $\pi$ -electron delocalization than a similar “aromatic” benzene derivative[100]. This N-B bond can support a nonaromatic quinonoid from, with a partial positive charge on the N atom and partial negative charge on the boron atom (shown in Scheme 11); although it should be noted that such a polarization does not result in a net charge polarization[89]. Despite the growing interest in borylated carbazole polymer, only little work has been done in investigating these polymers performance in the field of organic photovoltaics, which is the scope of this work[101]. Therefore, on the basis of Taniguchi *et al.*[102], been designed, synthesized, and investigated the photo physical properties of a 9- $\text{BMes}_2$  modified 3,6-dibromocarbazole as a monomer, and polymerize it into conjugated polymers for OPVs.

## 3.2. MATERIALS AND METHODS

### 3.2.1.1 Materials

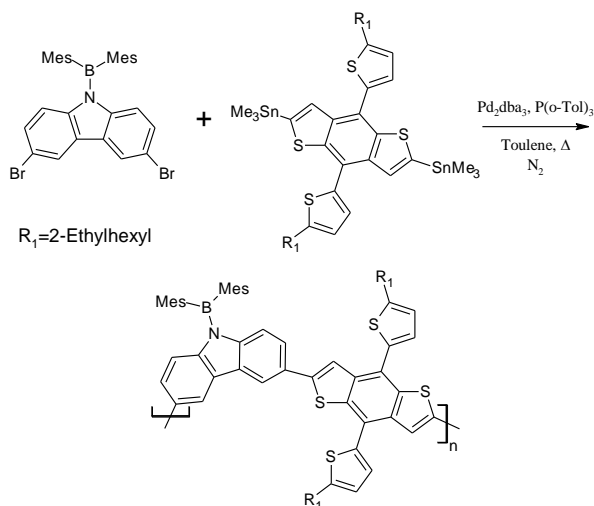
All materials were synthesized according to literature procedure as introduced in the details below. Chemicals taken were of commercial grade, and used without further purification, if not stated otherwise.

### 3.2.1.2 Syntheses



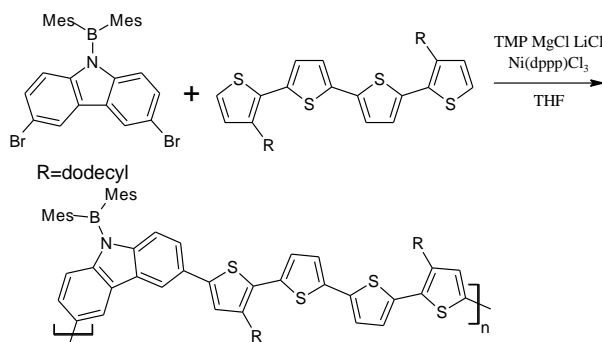
Scheme 12: The synthesis of 3,6-dibromo-N-(dimesitylboryl)carbazole (borylated carbazole (BC)).

**3,6-dibromo-N-(dimesitylboryl)carbazole (BC).** As fully described by Sveegaard [103], 1.38 g of magnesium turnings (56.7 mmol, 2.84 eq.) activated by a iodine crystal that was fed into a dry two-necked flask. 50.0 mL of dried THF was added, then followed by the addition of 8.50 mL of 2-bromomesitylene (11.1 g, 55.5 mmol, 2.78 eq.) in one portion, all under inert atmosphere. Once mesitylene Grignard reagent was initiated by heating, gentle reflux was maintained using an icebath to avoid violent boiling. When the frothing stopped, the solution was heated to reflux, until all the magnesium turnings were dissolved (1.5-2 hours). 2.80 mL boron trifluoride diethyl etherate (3.22 g, 22.7 mmol, 1.14 eq.) was dropwise added and the solution was refluxed for another three hours, followed by cooling to ambient temperature, yielding a white precipitate and a yellow-orange solution. Then 6.51 g of 3,6-dibromocarbazole (20.0 mmol, 1.00 eq.) was dissolved in 50.0 mL of dry THF in a dry one-necked flask under argon atmosphere and cooled to  $-78^{\circ}\text{C}$ . 8.50 mL 2.50 M *n*-BuLi in hexane (21.3 mmol, 1.06 eq.) was added dropwise to the carbazole under violent stirring and stirred for 2.5 hours. The liquid from the dimesitylboron fluoride-flask was transferred to the carbazole-flask at  $-78^{\circ}\text{C}$  under vigorous stirring, taken to room temperature and then the solvent was immediately removed *in vacuo* at room temperature. The solids were extracted with pentane and the pentane phase was dried *in vacuo*. The solid was recrystallized from ethyl acetate. Yield: 5.58 g (9.73 mmol, 48.7 %) as snow white, glinting crystals.  $^1\text{H}$  NMR ( $\text{CDCl}_3$ ,  $\delta$ , ppm); 8.06 (s, 2H), 7.22(d, 2H), 6.84 (s, 4H), 6.77 (d, 2H), 2.35 (s, 6H), 2.01 (s, 12H).  $^{13}\text{C}$  NMR ( $\text{CDCl}_3$ ,  $\delta$ , ppm): 142.41, 141.14, 139.93, 129.92, 129.10, 128.87, 122.66, 117.15, 116.24, 22.02, 21.47. Carbon atoms coupled to boron atom were invisible due to the rapid quadrupolar relaxation.  $^{11}\text{B}$  NMR ( $\text{CDCl}_3$ ):  $\delta=58.80$ . FT-IR: 3049-2829, 1604, 1468, 1431, 1294, 1285, 1275, 845  $\text{cm}^{-1}$  (No N-H stretching found). Melting point: 245-255  $^{\circ}\text{C}$ .



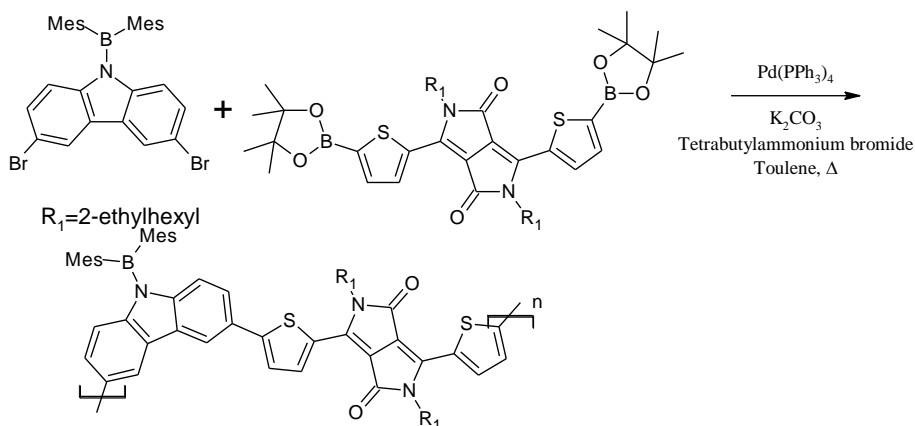
*Scheme 13: The synthesis of the borylated polymer PBCBDTTT via Stille cross-coupling between 3,6-dibromo-N-(dimesitylboryl)carbazole and 2,6-bis(trimethyltin)-4,8-di(5-(2-ethylhexyl)thiophene-2-yl)benzo[1,2-b:4,5-b']dithiophene.*

**PBCBDTTT.** A mixture of 3,6-dibromo-N-(dimesitylboryl)carbazole (50 mg, 87  $\mu\text{mol}$ , 1.00 eq), 2,6-bis(trimethyltin)-4,8-di(5-(2-ethylhexyl)thiophene-2-yl)benzo[1,2-b:4,5-b']dithiophene (79 mg, 87  $\mu\text{mol}$ , 1.00 eq), tris(dibenzylideneacetone)dipalladium ( $\text{Pd}_2\text{dba}_3$ , 2 mg, 1.75  $\mu\text{mol}$ , 2 mol%), and tri-*o*-tolylphosphine ( $\text{P}(\text{o-Tol})_3$ , 14 mg, 13  $\mu\text{mol}$ , 14 mol%) was degassed twice via vacuum, followed by nitrogen purging. They were then dissolved in toluene (15 mL) and the degassed via three freeze-pump-thaw cycles. The solution was kept under an inert nitrogen atmosphere and heated to 120°C for 48 h. The product was then precipitated in methanol. The obtained polymer was further purified via two consecutive precipitations from chloroform. The obtained product PBCBDTTT was a yellow solid (70 mg). (also see in article **III** in the Appendix).  $^1\text{H NMR}$  ( $\text{CDCl}_3$ ,  $\delta$ , ppm) 7.90-8.05 (s, 2H), 7.62-7.75 (m, 4H), 7.34 (d, 2H), 7.17 (s, 2H), 7.07 (s, 2H), 7.00 (s, 2H), 6.77-6.83 (m, 2H), 2.96-3.02 (d, 4H), 2.15-2.50 (m, 16H), 1.60-1.81 (m, 2H), 1.30-1.50 (m, 18H), 0.96-1.05 (m, 12H).



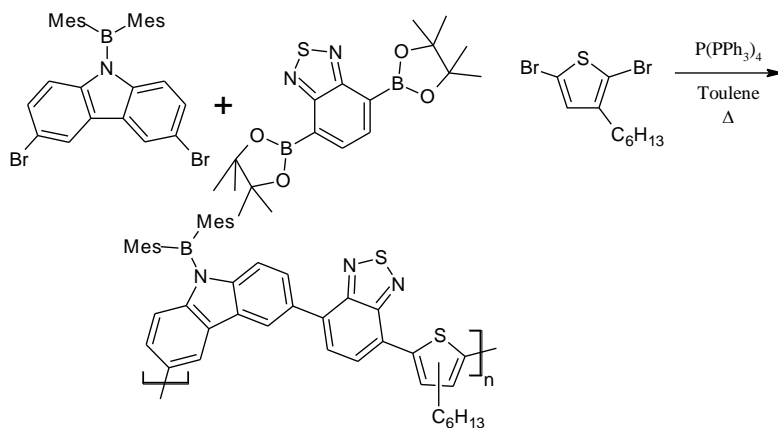
*Scheme 14: The synthesis of the polymer PBCQT from a direct arylation polymerization between 3,6-dibromo-N-(dimesitylboryl)carbazole and 3,3''-didodecyl-2,2':5',2'':5'',2''-quaterthiophene.*

**PBCQT.** 3,3'''-didodecyl-2,2':5',2'':5'',2'''-quaterthiophene (300.1 mg, 0.450 mmol, 1.00 eq.), 3,6-dibromo-*N*-(dimesitylboryl)carbazole (57.7 mg, 0.450 mmol, 1.00 eq.), Ni(dppp)Cl<sub>2</sub> (2.50 mg, 4.61 μmol, 1 mol%), and dry THF (20.0 mL) was added into a dry two-necked flask under argon atmosphere. TMPMgCl · LiCl (1.10 mL, 0.9 M, 0.990 mmol, 2.20 eq.) was added dropwise and the solution was refluxed for 48 hours. The solution was poured into 100 mL methanol and the precipitated red solid was filtered and washed with methanol. The solid was dried *in vacuo* at 50 °C. The obtained product PBCQT was a deep red solid (169 mg). (also see in article **III** in the Appendix) <sup>1</sup>H NMR (CDCl<sub>3</sub>, δ, ppm) 7.82-7.91 (m, 2H), 7.39-7.51 (m, 2H), 7.10-7.22 (m, 4H), 7.06 (s, 2H), 6.91-6.99 (m, 4H), 6.71 (s, 2H), 2.11-2.85 (m, 18H), 1.28-1.68 (m, 44H), 0.91 (t, 6H).



*Scheme 15: The synthesis of the polymer PBCDPP via a Suzuki cross-coupling polymerization between 3,6-dibromo-*N*-(dimesitylboryl)carbazole and 3,6-bis(5-boronic acid pinacol ester)thiophen-2-yl)-2,5-bis(2-ethylhexyl)-6-(thiophen-2-yl)pyrrolo[3,4-*c*]pyrrole-1,4(2H,5H)-dion.*

**PBCDPP.** 3,6-bis(5-(boronic acid pinacol ester)thiophen-2-yl)-2,5-bis(2-ethylhexyl)-6-(thiophen-2-yl)pyrrolo[3,4-*c*]pyrrole-1,4(2H,5H)-dion (0.077 g, 0.135 mmol), 3,6-dibromo-*N*-(dimesitylboryl)carbazole (0.1 g, 0.13 mmol), and 7 mg (3 mol %) of tetrakis(triphenylphosphino)palladium(0) were dissolved in 5 mL of toluene, degassed twice and stirred at room temperature for 30 min. Subsequently potassium carbonate (0.141 g, 1.02 mmol) and tetrabutylammonium bromide (10 mg) were dissolved in 2 mL of water and added to the reaction mixture in a nitrogen atmosphere. Then the reaction mixture was heated and refluxed under nitrogen for 72 h. After cooling, 100 mL of acetone was added. The precipitate was filtered and washed with acetone, 2 M hydrochloric acid, and acetone, successively. The polymer was collected as dark blue powders and dried under vacuum for 24 h. <sup>1</sup>H NMR(CDCl<sub>3</sub>, δ, ppm) 8.91-9.05 (m, 2H), 8.25-8.37 (d, 2H), 7.64-7.78 (m, 2H), 7.40-7.52 (m, 4H), 7.02-7.28 (m, 4H), 2.38-2.41 (m, 2H), 1.44-1.64 (m, 16H), 1.28-1.42 (18H), 0.90-0.96 (m, 12H).



Scheme 16: The synthesis of the polymer P3HTBCBT from a random Suzuki cross-coupling polymerization between 3,6-dibromo-*N*-(dimesitylboryl)carbazole and 2,5-dibromo-3-hexylthiophene and 2,1,3-Benzothiadiazole-4,7-bis(boronic acid pinacol ester).

**P3HTBCBT.** A flask was charged with 3,6-dibromo-*N*-(dimesitylboryl)carbazole (250.0 mg, 0.43 mmol), 2,1,3-Benzothiadiazole-4,7-bis(boronic acid pinacol ester) (356.5 mg, 0.91 mmol) and 2,5-dibromo-3-hexylthiophene (97  $\mu$ L, 0.45 mmol). The solids were dissolved in 25 mL toluene. A catalytic amount of tetrakis(triphenylphosphino)-palladium(0) was added together with aqueous potassium carbonate (2M, 2mL). The mixture was degassed utilizing 10 consecutive pump-purge (with  $N_2$ ) procedures. The mixture was heated to 90°C and kept under inert atmosphere for 72 h until changing to deep red from colorless with green fluorescents. The polymer was obtained by precipitation in acetone, resulting deep red solid. Due to the complexity of the  $^1H$ NMR data of this random copolymer, the acquired  $^1H$ -NMR data was not presentable.

### 3.2.1.3 Methods

The CV, NMR ( $^1H$ ,  $^{11}B$  and  $^{13}C$ ) UV-vis, SCLC and OPV devices were all obtained using the methods described in section 2.1.1.3. The FTIR data was obtained on a Varian 610-IR with an ATR diamond crystal as sample holder.

**Molecular simulations** it was conducted at the B3LYP level with the basis set 6-31G(d,p) using Gaussian 9, and visualized by Gaussian Viewer 5 (GW5). The alkyl side functionalities have been reduced to methyl groups to reduce the calculation load of the simulations.

## 3.3. MATERIALS CHARACTERIZATION

**3,6-dibromo-*N*-(dimesitylboryl)carbazole: molecular simulations:** To confirm the synthesis of the BC monomer, a computational analysis was conducted and then compared with the experimental FTIR data.

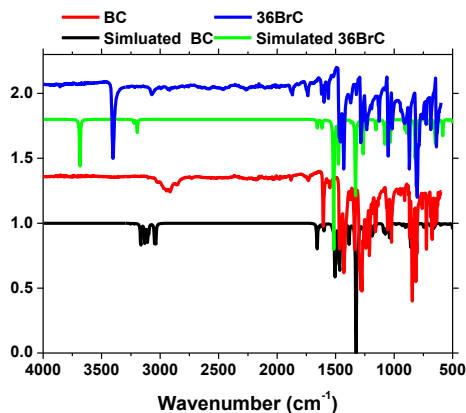


Figure 36: Comparison between the computational (BC (black) and 36BrC (green)) and the experimentally obtained vibrational data (BC (red) and 36BrC (blue)).

In Figure 36, both simulations and the experimentally acquired frequencies are presented. Notable mismatch of the signals over  $3250\text{ cm}^{-1}$  between calculated and experimental data was found for 3,6-dibromocarbazole (36BrC) (blue and green, respectively). The mismatch is approximately  $284\text{ cm}^{-1}$ , as simulated 36BrC shows a signal at  $3684\text{ cm}^{-1}$  whilst the experimental data shows a signal at  $3400\text{ cm}^{-1}$ . Using table values and GaussianViewer (GW) this signal is determined to derive from stretching of the proton nitrogen bond in the secondary amine of the carbazole (see Scheme 12). The peaks from  $1600$  to  $1000\text{ cm}^{-1}$  derives from the carbon-carbon stretch of the aromatic rings in the carbazole. While the peak at approximately  $890\text{ cm}^{-1}$  derives from the symmetric stretching of the two carbon-bromo bonds, these are presented in both 36BrC and BC. Therefore it can be concluded that bromo functionality of the 3,6-dibromocarbazole is not modified under the synthesis of the N-B bond, which could occur under the application of the *n*-BuLi. It is expected that the large experimental mismatch between the modelled and the experimental data (mainly on the determined N-H stretch) derives from an inherent difference between the two systems, as the calculated data was based on the single molecular behavior in vacuum while the experimentally acquired data is from solid phase. Therefore the frequencies might be affected by the intermolecular hydrogen bonding occurring in the solid phase and this is not taken into account in the single molecule in vacuum simulations. The lack of N-H stretch in compound BC is ascribed to the removal of the hydrogen and the presence of the newly formed N-B bond. This is also supported by the relative strong signal in the area of  $1350\text{ cm}^{-1}$ , using GW's vibration function this large signal is ascribed to the N-B stretch. Using the modelled data and combining the emerging of a signal in this area after the borylation advocates the formation of the N-B bond. This is furthermore evidenced by the increased signals in the region of  $2750$  to  $3250\text{ cm}^{-1}$ , i.e., the stretching of the aromatic C-H bond and the C-H stretch of the methyl groups on the mesitylene groups attached to boron. So a successfully synthesized BC material had been also agreed by  $^1\text{H}$ - and  $^{11}\text{B}$ -NMR studies.

### 3.3.1. MOLECULAR SIMULATIONS OF BORYLATED COMPOUNDS

As mentioned above, the molecular simulations were conducted to investigate both the molecular geometric configuration and the electron distribution as a result of the introduction of the boron atom.

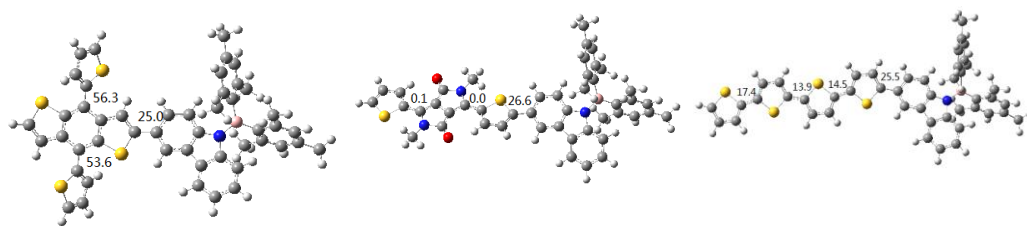


Figure 37: The geometrically optimized structure of PBCBDTTT (left), PBCDPP (middle) and PBCQT (right)

The geometrically optimized polymers PBCBDTTT, PBCDPP and PBCQT are exhibited in Figure 37 the P3HTBCBT has been ignored for calculations due to its complexed random copolymer structure. It should be noted that the dodecyl segments on the  $\beta$ -position carbon of the thiophene moiety directly bonded to carbazole unit (shown in Scheme 14) has been omitted in the simulation of PBCQT. For the PBCBDTTT the 2-ethylhexyl of the pendant thiophenes has been completely omitted, as it is assumed that it does not influence the electron density of the moiety nor the dihedral angle. For the DPP moiety the amine alkyl modification, 2-ethylhexyl is reduced to a methyl as a thorough omission might influence both the electron density and the dihedral angle. The dihedral angle between the BC moieties and the respective donor moieties are ranging from 25.0 to 26.6°. These angles are comparable with those between carbazole and DTBT moieties in the copolymer of (4-hexyl-2-thienyl)-2,1,3-benzothiadiazole (d3HTBT) and 3,6 linked N-alkylcarbazole with its dihedral angle of 37°, reported by Fu *et al.* [104], while the none-alkylated thiophene derivative (2-thienyl)-2,1,3-benzothiadiazole (dTBT) also polymerized via the 3,6 position of the N-alkylcarbazole had a torsion of 14°.

Fu *et al.* [104] explored that the functionalization of the  $\beta$ -position carbon facing the carbazole rings will result in a larger torsion than a unsubstituted carbon. Comparing this situation with the modelled compounds of this study, it would be expected that the angle was slightly lower due to lack of steric interference from the thiophene units. This torsion could therefore derive from the introduced dimesityl-boryl groups on the carbazole. Berton *et al.*[105] modelled a similar system to Fu *et al.*[104], although using a slightly different basis set 6-31G\* compared to the 6-311+G\* (both B3LYP), determined a similar angle of 26° for a unsubstituted  $\beta$ -position carbon facing the carbazole rings. This could therefore indicate that the dimesityl-boryl modification of the carbazole does not have an impact on the dihedral angle between the carbazole and the adjacent moiety. Although the conducted simulations at the B3LYP/6-31G(d,p) level have been done in vacuum and only for one set of components, this will influence the dihedral angle and also the packing, e.g., spatial interactions of the moiety will not be considered during the simulations. One would expect the rather sterically hindered dimesitylene groups having a negative influence on  $\pi$ - $\pi$  stacking of the polymers. The simulations can also give an indication of the distribution of electrons, i.e., the frontier orbitals being the HOMO and the virtual LUMO.

As for the optimized structures, the frontier orbitals are also determined at B3LYP/6-31G(d,p) and can be seen in Figure 38. The HOMO orbitals are found being distributed all along the backbone, even though the aromatic ring of BC facing away from the adjacent moiety in these simulation does not seem to be inter-connected. This disconnection across the carbazole moiety has been discussed by Fu *et al.*[106] arguing that a 3,6-carbazole breaks the

conjugation in the 5 membered pyrrole ring of the carbazole. This conjugation break could therefore explain that the ring facing away from the adjacent moiety seemingly does not interact with the connected moiety. This isolation is also seen by Azazi *et al.*[107], they observed that the HOMO orbital of a coupled 3,6-carbazole with a DTBT moiety are distributed along the DTBT moiety and only half of the 3,6-carbazole unit. When discussing the interactions between BC and the different moieties, it becomes apparent that majority of the orbitals are arranged around other moieties rather than BC.

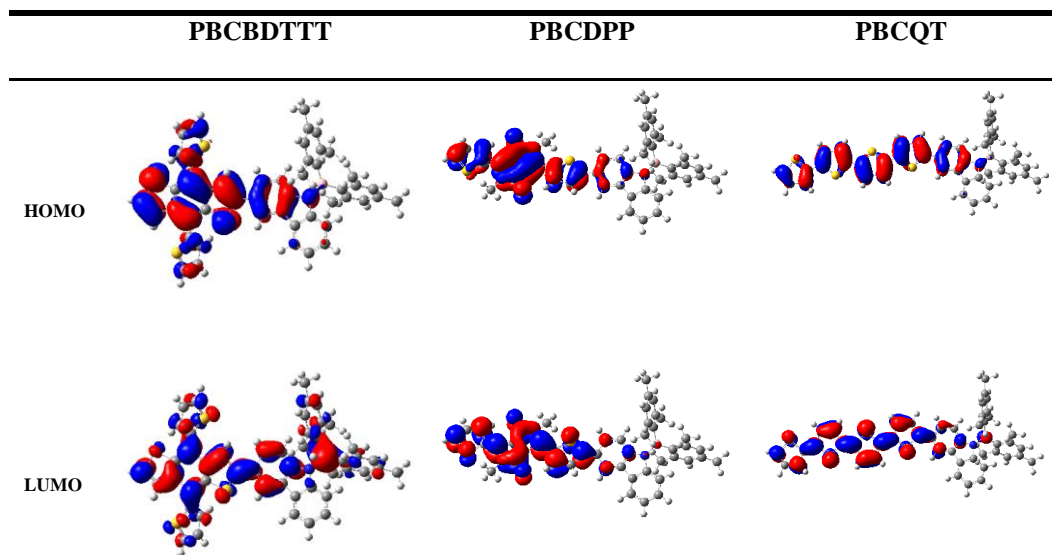


Figure 38: The frontier orbitals (top, HOMO) and (bottom, LUMO) for the optimized structure at the B3LYP/6-31G(d,p) level of PBCBDTTT (left), PBCDPP (middle), and PBCQT (right).

As expected, the HOMO of PBCBDTTT is distributed all along the backbone but mainly located on BDTTT, meaning that the HOMO electron density in BDTTT region is much higher than in the BC moiety. It also becomes interesting when observing the LUMO level, as a large fraction of it, is distributed on the boron atom of the dimesitylene boryl side group of the BC moiety, exhibiting a connection between the medium strength donor BDTTT and the boron atom of the BC [44]. This strengthens the idea that the  $\pi^*$  of the boron atom can act as a pseudo acceptor, which could result in a quasi D-A structure of PBCBDTTT despite BDTTT being a donor and native carbazole also exhibit an electron donating property. For PBCQT, the HOMO orbitals show the same characteristics as in PBCBDTTT where the HOMO orbitals are located all along the back bone. The same pseudo acceptor characteristics are also apparent on the PBCQT where the boron atom also has a fraction of the LUMO orbitals, but it should be noted that this fraction is much lower for the boron atom in PBCQT than that in the modelled PBCBDTTT. In general, such partial LUMO distribution on B atom in carbazole unit linked with either BDTTT or QT still presents the pseudo acceptor characteristics. The narrative is slightly different when considering PBCDPP being a strong electron acceptor; the HOMO orbitals are also located all along the back bone, while the LUMO is distributed on the DPP moieties and only slightly on boron atom. This is assumed to derive from the stronger

electron withdrawing capabilities of the DPP moiety compared to that of the boron atom. Using the modelling data, we estimate the HOMO and LUMO levels and thereby band gap of the materials, as can be seen in Table 10.

Table 10: The theoretically obtained HOMO and LUMO values for the polymers PBCBDTTT, PBCDPP and PBCQT determined at the B3LYP/6-31G(d,p) level.

Compound	HOMO [eV]	LUMO [eV]	$E_g$ [eV]
PBCBDTTT	-5.08	-1.60	3.48
PBCDPP	-4.78	-2.46	2.31
PBCQT	-4.83	-1.92	2.92

In Table 10, the energy levels are given, and it becomes quite clear that the  $E_g$  of these polymers are high, the polymer PBCBDTTT would, if these calculations were accurate, be considered as an insulator rather than a semiconductor. As the modelled data represents the estimated values for a dimer in vacuum, many effects are not considered especially the intermolecular dynamics of polymers which facilitates the lowering of the band gap. But also the relative short length of conjugation will have an impact on the theoretically calculated  $E_g$ , Azazi *et al.*[107] pronounced that increasing the modelled simulation length from 1 to 4 monomers, would lower the band gap obtained at the B3LYP/6-31G\* level from 3.09 eV to 2.61 eV on the previously mentioned model system, showing a clear correlation between the conjugation length and the band gap, as expected. This is also why the frontier orbitals acquired via this dimer estimation are considered to be associated with a certain degree of error. But the trends of the polymers might still be valid, such as the LUMO level of the PBCDPP appeared the deepest while the HOMO level could be the lowest lying.

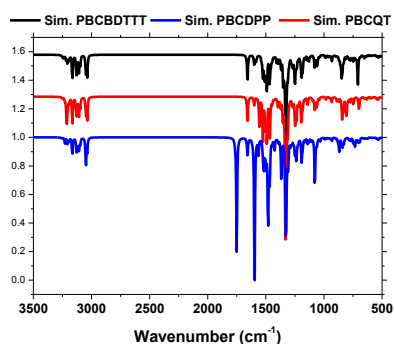


Figure 39: The simulated vibrational data of three compounds PBCBDTTT (black), PBCDPP (blue) and PBCQT (red) obtained by geometrically optimized at the B3LYP/6-31G(d,p) level.

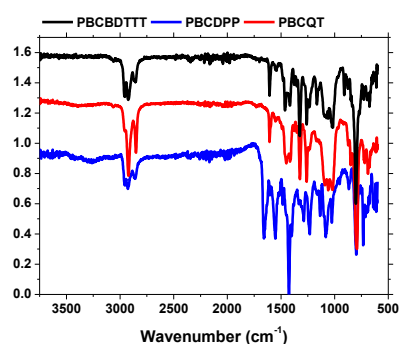


Figure 40: The experimentally vibrational data of three compounds PBCBDTTT (black), PBCDPP (blue) and PBCQT (red) obtained via FTIR.

The molecular simulation also offers an insight into molecular vibrational patterns of the given molecules (Figure 39), and these patterns can be compared with the experimentally obtained vibrational patterns acquired by FTIR (Figure 40). It can be noticed that the progression on three simulated dimers are comparable to the experimentally acquired data. But there is although a mismatch of circa  $50\text{ cm}^{-1}$ , that is assumed to derive from the inherent difference between the gas phase vibration where there is no interaction and to the solid phase interactions where intermolecular interactions can occur. The two largest differences between the experimental data and the modelled ones are the large signal at approximately  $750\text{ cm}^{-1}$  and the signals in the interval of  $1000\text{-}1200\text{ cm}^{-1}$ . All the mentioned signals are assigned to derive from the aliphatic sidechains which is excluded from the molecular modelling. The largest concern regarding the polymerization of the BC monomer, is the stability of the N-B bond, but the presences of the N-B at  $1350\text{ cm}^{-1}$  and the lack of the N-H stretch proved that this bond has survived the cross-coupling reactions of the polymerizations, thus it is concluded that the polymerization has occurred and that the desired BC moiety keeps intact in the structure.

### 3.3.2. PHOTOPHYSICAL PROPERTIES

The absorbances spectra of the four synthesized polymers are shown in Figure 41, for each polymer both solution and film absorbance spectra are depicted.

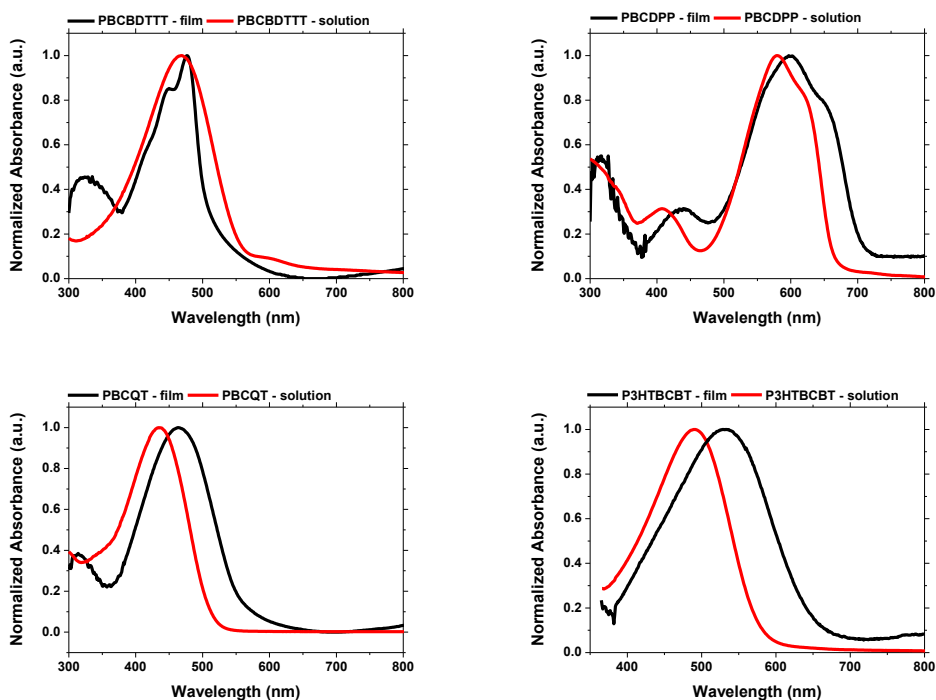


Figure 41: UV-vis absorption of BC polymers in both film (**black**) and solution (**red**) in  $\text{CHCl}_3$ ; for the four polymers PBCBDTTT (upper left), PBCDPP (upper right), PBCQT (lower left) and P3HTBCBT (lower right).

The absorption of PBCBDTTT (both film solution) is rather different compared to the other materials, as the absorbance spectra narrows slightly, while the absorbance maxima increase from 468 nm to 477 nm, going from solution to film. The onset absorbance of the PBCBDTTT is nearly 600 nm which affords a relative high bandgap of 2.07 eV. The lack of broadening can be ascribed to the spatial dimension of both BDTTT and BC, where the pendant thiophene of BDTTT has a dihedral angle exceeding 50° compared to the planar center of the molecule (Figure 37). When combined with the dimesityl boryl of BC unit, spatial interactions could be expected to have a negative influence on  $\pi$ - $\pi^*$  transition of this polymer, which is revealed by the peak absorption at 324 nm. The pseudo-acceptor nature is indicated by the ICT between the pseudo-acceptor BC to the BDTTT moiety, as shown peak absorbance at around 470 nm corresponds to that found by Mirsa *et al.*[108] and Entwistle *et al.*[88] for trimesityl borane containing small-molecules as well. PBCDPP exhibits a broad absorption of approximately 40 nm, which is ascribed to the more planar structure of DPP than that of BC, it has a maximum absorbance at 578 nm in solution and at 597 nm in film, pronouncing the pseudo-accepting characteristic through ICT. The film absorbance onset of this polymer is 700 nm which results in an  $E_g$  of 1.77 eV. The  $\pi$ - $\pi^*$  stacking is also apparent in this molecule, as there are two local maxima in the low wavelength region, the first one at 438 nm is ascribed to the DPP moiety while the one at 320 nm is expected to derive from the BC moiety. This corresponds to the findings of Jo *et al.*[109], which showed a carbazole polymerized at the 2,7 position with DPP, exhibiting a slightly lower band gap with an onset absorption of 750 nm. The copolymer with 2,7-carbazole and DPP also showed an ICT peak at approximately 440 nm. The polymer with the second largest red shift on its absorption from solution to film is PBCQT going from 435 to 465 nm, while exhibiting a broadening of approximately 50 nm. The absorption onset is 557 nm affording an  $E_g$  of 2.23eV. The redshift of the absorbance maximum from solution to film is ascribed to the QT moiety for its higher degree of aggregation in solid states associated with the QT structure, as shown by Lim *et al.*[110] and Ong *et al.*[111]. Also this molecule exhibits the same donor-pseudo acceptor ICT with its absorbance at 435 nm in solutions and at 465 nm in film. P3HTBCBT as the only three components random co-polymer containing both a native donor 3-hexylthiophene (3HT) and BT, it would be expected that this compound would not only exhibit a ICT peak but also a low band gap as a result of having both 3HT and BT. Witker *et al.*[112] presented a native carbazole-BT polymer with an absorbance maximum at 460 nm, which is lower than P3HTBCBT with its maximum at 534 nm for film absorbance. The P3HTBCBT polymer showed an absorbance onset at 647 nm affording a band gap of 1.92 eV. Generally the different polymers all presented (excluding PBCDPP) pronounced a relative high bandgap. These high band gaps are assumed to derive from the relative low acceptor strength of the BC monomer for pulling electrons, even though the molecular simulations indicate this D/quasi-A structure. By combining the interesting electron properties presented in section 3.3.1, the frontier levels of these polymers can be determined.

In Table 11, the electrochemical and photophysical properties are summarized. Through CV measurements, the HOMO levels were determined and LUMO levels were calculated. All the calculated LUMO levels are sufficient to afford the necessary driving force (0.3 eV higher than the LUMO of PC<sub>71</sub>BM) to facilitate proper charge dissociation and are assumed to afford a relative efficient photo induced current[113]. Generally all the relative deep HOMOs, of approximately -5.5 eV, are expected to afford high  $V_{oc}$ .

PBCQT has high structural resemblance to the polymers reported by Lim *et al.*[110] that showed a *n*-alkyl carbazole polymerized with QT affording a HOMO of -5.13 eV and a LUMO of -2.94 eV ( $E_g = 2.19$  eV).

Table 11: The electrochemical and photophysical parameters of the BC based polymer, adapted from paper III. The mobilities ( $\mu_{\text{Electron}}$  and  $\mu_{\text{Hole}}$ ) is determined via the previously described SCLC method (see section 2.1.2) on hole only and electron only devices, the mobilities are measured on polymer:PC<sub>71</sub>BM films at the optimized ratio (see Figure 42)

Polymer sample	Thickness [nm]	$\lambda_{\text{onset}}$ [nm]	$E_g$ [eV] <sup>a</sup>	$E_{\text{oxonset}}$ [eV]	$E_{\text{HOMO}}$ [eV]	$E_{\text{LUMO}}$ [eV] <sup>b</sup>	$\mu_{\text{Electron}}$ [cm <sup>2</sup> V <sup>-1</sup> s <sup>-1</sup> ]	$\mu_{\text{Hole}}$ [cm <sup>2</sup> V <sup>-1</sup> s <sup>-1</sup> ]
<b>PBCBDTTT</b>	100	600	2.07	0.72	-5.52	-3.45	$1.54 \times 10^{-4}$	$5.33 \times 10^{-4}$
<b>PBCQT</b>	85	557	2.23	0.76	-5.56	-3.33	$1.72 \times 10^{-4}$	$1.79 \times 10^{-6}$
<b>PBCDPP</b>	85	700	1.77	0.34	-5.14	-3.37	$3.33 \times 10^{-4}$	$2.77 \times 10^{-4}$
<b>P3HTBCBT</b>	110	647	1.92	0.80	-5.60	-3.68	$5.58 \times 10^{-4}$	$2.95 \times 10^{-4}$

<sup>a</sup>)  $E_{\text{bg}} = 1240/\lambda_{\text{onset}}$  <sup>b</sup>)  $E_{\text{LUMO}} = E_{\text{HOMO}} + E_g$

The effect of the dimesityl boryl modification of the carbazole becomes apparent as both LUMO and HOMO are lowered with 0.39 eV and 0.43 eV respectively, in contrast to native carbazole D-A polymers, which aligns the LUMO better with PC<sub>71</sub>BM and the HOMO to facilitate a high  $V_{\text{oc}}$ . Such an effect on both the HOMO and the LUMO level indicates an ambipolar interaction of the BC moiety, as the HOMO normally is associated with the D and LUMO directing the A (as shown in Chapter 2), while the presence of BC lower both of frontier orbitals. Rietzenstein *et al.*[99] synthesized a polymer consisting of a 3,6 linked carbazole, which were substituted at the N-position with a *p*-(diarylboryl)phenyl, which has some structural resemblance with the polymers synthesized in this study. The polymer presented by Rietzenstein *et al.*[99] had a slightly high HOMO at -5.04 eV, while more comparably low HOMO level, ranging from -5.49 eV to -5.78 eV depending on composition, were obtained by Chen *et al.*[114] on a copolymer between a 2,7 linked flourene and a 3,6 linked carbazole which were substituted at the N-position with a *p*-(diarylboryl)phenyl or 2-(diarylboryl)thiopenyl. They ascribed such deep HOMO levels to the high electron density of the backbone. However, in these two reports, the absence of N-B linkage and resulted orbital mixing must be taken into account when considering their apparent structural resemblance. This is despite that, as reported by both Bai *et al.*[115] and Entwistle *et al.*[88], the orbital interaction can occur through space or via  $\pi$ -orbital interactions. All these further support the notion that the N-borylated carbazole will work as a hybrid between a donor and an acceptor i.e., pseudo-acceptor. For PBCDPP, when comparing its HOMO of -5.14 eV and LUMO of -3.37 eV to the reported -5.4 eV (HOMO) and -3.9 eV (LUMO) of the carbazole-DPP polymer via the 2,7 linkage by Jo *et al.*[109], they are about 0.4-0.5 eV higher while the higher HOMO will most likely lead to a lower  $V_{\text{oc}}$  than for example PBCBDTTT. The reason that both HOMO and LUMO of PBCDPP is not lowered in contrast to those of PBCBDTTT and PQTBC, could be that the pseudo-acceptor nature of BC, in the PBCDPP, reduced the electron push-pull effects which would be competing with the strong acceptor DPP.

Meanwhile the more linear and therefore more planar 2,7 linked carbazole-DPP moiety will have an effect on the frontier orbitals. For the random copolymer of 3HT, BC and BT, it showed the same low HOMO as PBCQT and PBCBDTTT, but a higher electron affinity (deeper LUMO) is obtained. Kim *et al.*[116] reported a copolymer consisting of 3,6-linked carbazole and DTBT, this polymer showed a HOMO of -5.66 eV and a LUMO of -3.50 which is very close to the values of -5.60 eV and -3.68 eV for P3HTBCBT. This is interesting as P3HTBCBT is a random copolymer, while the polymer reported by Kim *et al.*[116] has clearly defined composition of alternation 3,6-N-alkylcarbazole and DTBT. Due to the similarity of the values, the effect of the BC moiety is limited in regards to the effect on the band gap of this given polymer. The hole and electron mobility of the four polymers are also listed in Table 11, the mobilities are measured via the SCLC method on hole or electron only devices from the optimized polymer:PC<sub>71</sub>BM blend. The mobilities are, all except the hole mobility of PBCQT, relative balanced, at least with in the same order of magnitude (10<sup>-4</sup>). The imbalance in PBCQT could result in a relative poor performance, but the 10<sup>-6</sup> cm<sup>2</sup> V<sup>-1</sup>s<sup>-1</sup> is not so low that necessarily afford a bad performance.

### 3.4. DEVICE PERFORMANCE

The four polymers have been tested as a donor material for OPV devices, with the normal geometry. All the polymers were tested as donors against PC<sub>71</sub>BM as acceptor. In Figure 42 the best performing devices are shown and the optimal D:A compositions are as follows: 1:3 for PBCBDTTT, 1:3 for PBCQT, 1:2 for P3HTBCBT and 1:1 for PBCDPP.

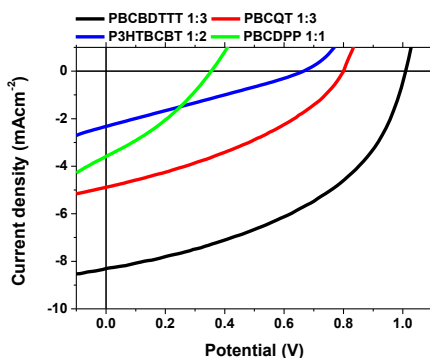


Figure 42: I-V performance of the organic photovoltaic devices using the four materials as donor against PC<sub>71</sub>BM as acceptor with various D:A weight ratios. PBCBDTTT (black) 1:3, PBCQT (red) 1:3, P3HTBCBT (blue) 1:2 and PBCDPP (green) 1:1. All devices are spun from chlorobenzene or *o*-DCB and optimized in regards to spin speed.

The device characteristics of the polymer P3HTBCBT (see Table 12) was slightly different from the reported efficiencies by Berton *et al.*[105] and Fu *et al.*[106]. Berton *et al.* synthesized a polymer with DTBT and 3,6-linked carbazole, affording an efficiency of 0.35%,  $V_{oc}$  of 0.54 V and  $J_{sc}$  of -2.11 mAcm<sup>-2</sup>[105]. The optimal D:A ratio for the reported polymer was found to be 1:3, which is a slightly different compared to the ratio of 1:2 found for P3HTBCBT, but the characteristics  $V_{oc}$  and  $J_{sc}$  are comparable [105]. The device with the D:A ratio of 1:2 and cast at 2000 rpm, showed the average PCE value of 0.27 % whilst maximum performing device within this array of devices possessed a PCE of 0.407 % with a

$V_{oc}$  of 0.66V, a  $J_{sc}$  of 2.32  $\text{mAcm}^{-2}$ , and FF of 26.5%. The devices performance presented by Fu *et al.*[106] is lower than those presented by Berton *et al.* which is mainly due to the low FF[105]. P3HTBCBT also showed a similar low FF as Fu *et al.* reported, the best performing ratio of P3HTBCBT showed the FF of 27.6%, which is the lowest of all devices[106]. As the energy levels dictate the  $V_{oc}$ , it is worth noticing that the  $V_{oc}$  of the two similar polymers are within the same range as P3HTBCBT. The I/V curves for the three ratios are shown in Figure 43. For obtaining higher PCE, additive of DIO where applied and it was found that the introduction of the additive DIO did not afford a more favorable device morphology.

Table 12: I/V characteristics of the polymer P3HTBCBT with PC<sub>71</sub>BM as acceptor. Devices are spin coated from chlorobenzene. The PCE is the average of 4 working cells.

Sample name	Ratio [D:A]	Spin speed [rpm]	DIO [%]	$V_{oc}$ [V]	$J_{sc}$ [ $\text{mAcm}^{-2}$ ]	FF [%]	PCE[%]	PCE <sub>best</sub> [%] <sup>a</sup>
P3HTBCBT	1:1	600	-	0.54	1.09	26.0	0.153	0.244
		1000	-	0.53	1.29	26.7	0.184	0.251
		1500	-	0.51	1.70	27.4	0.197	0.312
		2000	-	0.54	1.29	27.4	0.189	<b>0.453</b>
	1:2	600	-	0.56	1.14	26.6	0.170	0.281
		1500	-	0.56	1.60	26.9	0.239	0.337
		<b>2000</b>	-	<b>0.56</b>	<b>1.72</b>	<b>27.6</b>	<b>0.296</b>	<b>0.407</b>
			1	0.24	0.70	31.1	0.053	0.075
			2	0.48	0.85	28.6	0.141	0.220
			3	0.54	0.90	28.5	0.166	0.269
	1:3	600	-	0.55	0.94	26.4	0.135	0.144
		1000	-	0.57	1.09	26.0	0.190	0.316
		1500	-	0.60	1.49	32.1	0.283	0.373
		2000	-	0.56	1.09	35.2	0.217	0.225

<sup>a</sup>)The best performing cell

As the addition of 1% DIO resulted in a voltage drop of 0.32 V, the voltage increased as the increasing DIO content. With an addition of 3% DIO, the  $V_{oc}$  nearly reached the potential at 0% DIO, level while the  $J_{sc}$  was only 0.90  $\text{mAcm}^{-2}$ . Furthermore it is worth noticing that

despite the efficiency drop, the introduction of the DIO, an increase the FF from 27.6% to 31.1%. This increment is most likely not associated with an improved morphology, but rather a lower strain on the system.

*Table 13: I/V characteristics of the polymer PBCBDTTT with PC<sub>71</sub>BM as acceptor with varying weight ratio. Devices are spin coated from ODCB. Spin coated with 3000 rpm.*

Ratio [D:A]	DIO [%]	V <sub>oc</sub> [V]	J <sub>sc</sub> [mAcm <sup>-2</sup> ]	FF [%]	PCE[%]
1:1	-	0.88	1.06	22.4	0.207
1:2	-	0.91	5.83	36.5	1.93
<b>1:3</b>	-	<b>1.00</b>	<b>8.31</b>	<b>45.7</b>	<b>3.82</b>
	1	1.01	6.65	42.7	2.84
	2	0.99	6.81	40.9	2.75
	3	1.01	6.78	41.2	2.82
1:4	-	0.98	7.76	43.8	3.31

The PBCBDTTT was the best performing polymer, as seen in Table 13, with an efficiency of 3.82%, having a V<sub>oc</sub> 1.00 V, J<sub>sc</sub> of 8.31 mAcm<sup>-2</sup> and a FF of 45.7%. This performance was found when increasing the D:A weight ratio from 1:1 to 1:3, this indicates a poor exciton mobility, as the increasing amount of acceptor increase the available D/A interface, where the charge dissociation occurs. Combined with a better and broader absorbance of the PC<sub>71</sub>BM, is ultimately associated with the high photo current. The relative high voltage is ascribed to both the deep lying HOMO of the polymer and good film formation ability, with a well covering film that lowers the resistance loss etc. As it can be seen in Figure 44, it becomes very clear that when increasing the acceptor amount, the J<sub>sc</sub> is effect dramatically increased from approximately 1 mAcm<sup>-2</sup> to 8.3 mAcm<sup>-2</sup>. This supports the notion that the exciton diffusion length is the key issue, as there is no change in the Voc. The FF of the device also plays an important role in the high efficiency and the FF of these devices is 45.7 %, which is the highest one reported in this work. The relative high photocurrent should be hold against the high bandgap of 2.07 eV, which would only allow the absorbance of around 20-25% of the incident photons. Taken this into consideration, actually this shows the potential of the monomer BC, as this ambi-polar behavior allows the lowering of the HOMO and LUMO, which has a positive effect on the performance as the V<sub>oc</sub> reported here is high, combined with a relative high photocurrent. But as mentioned the bandgap is not as low as the optimal band gap discussed in the introduction (section 1.4); this is of course a down side of the BC monomer.

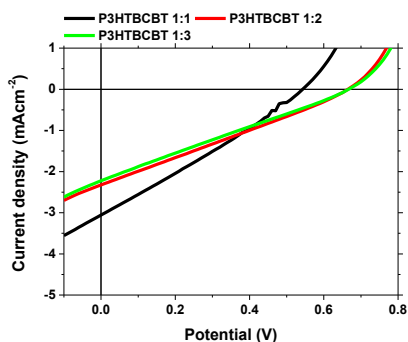


Figure 43: I/V performance of the P3HTBCBT:PC<sub>71</sub>BM with various D:A ratios: 1:1 (black), 1:2 rpm (red) and 1:3 (green). Devices are spin coated from CB, spin coated with 2000 rpm (1:1 and 1:2) and 1500 rpm (1:3).

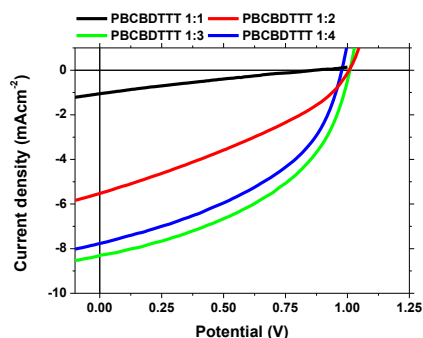


Figure 44: I/V performance of the PBCBDTTT:PC<sub>71</sub>BM with various D:A ratios: 1:1 (black), 1:2 rpm (red), 1:3 (green) and 1:4 (blue). Devices are spin coated from ODCB, spin coated with 3000 rpm. Adapted from paper III

The I/V performance of the other donor-BC polymer PBCQT is presented in Figure 45 and the optimization process and photovoltaic data is presented in Table 14.

The maximum performance obtained is 1.45% with a  $V_{oc}$  of 0.79V,  $J_{sc}$  of 4.88 mAcm<sup>-2</sup>, and FF of 37.2%. The carbazole reference polymer, consisting of a 2,7 linked carbazole with a QT monomer reported by Lim *et al.* only showed a efficiency of 0.40% with a  $V_{oc}$  of 0.66V,  $J_{sc}$  of 2.04 mAcm<sup>-2</sup>, and a FF of 40%. The major improvement going from a native carbazole to the BC monomer is in the lowering of the LUMO to make it better aligning with that of the acceptor (PC<sub>71</sub>BM). This will afford a better charge dissociation and ultimately a higher photocurrent as the photocurrent increases from 2.04 to 4.88 mAcm<sup>-2</sup>. But also the lowering of the HOMO affords an available higher  $V_{oc}$ , as seen as the  $V_{oc}$  increases from 0.66 to 0.79V.

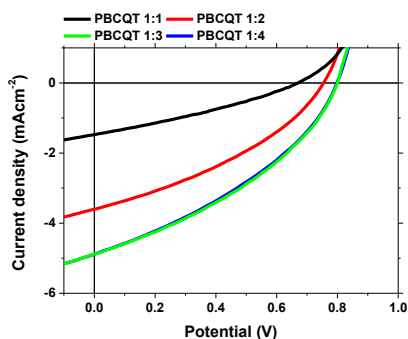


Figure 45: I/V performance of the PBCQT:PC<sub>71</sub>BM with various D:A ratio: 1:1 (black), 1:2 rpm (red), 1:3 (green) and 1:4 (blue). Devices are spin coated from o-DCB, spin coated with 3000. Adapted from paper III

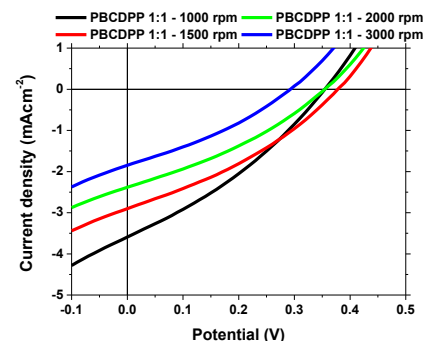


Figure 46: I/V performance of the PBCDPP:PC<sub>71</sub>BM with the D:A ratio 1:1. Devices are spin coated from o-DCB, spin coated with various speeds: 1000 rpm (black), 1500 rpm (red), 2000 rpm (green) and 3000 rpm (blue).

It should though be noted that our PBCQT is linked via the 3,6 position of the carbazole core, this will have an effect on the band gap and also the planarity of the molecule. In this case the pseudo-acceptor BC affords a quasi-A/D structured polymer that outperformance the native carbazole polymer reported by Lim *et al.* [110].

Table 14: *I/V characteristics of the polymer PQTBC with PC<sub>71</sub>BM as acceptor with varying weight ratio. Devices are spin coated from OD<sub>2</sub>C<sub>8</sub>B. Adapted from paper III.*

Ratio [D:A]	Spin speed [rpm]	V <sub>oc</sub> [V]	J <sub>sc</sub> [mAcm <sup>-2</sup> ]	FF [%]	PCE[%]
1:1	1000	0.49	1.25	30.3	0.186
	1500	0.58	1.35	30.2	0.236
	2000	0.67	1.47	30.9	0.304
1:2	1000	0.68	3.23	32.7	0.720
	1500	0.75	3.60	36.2	0.978
	2000	0.62	3.53	34.2	0.747
1:3	1000	0.73	4.53	36.9	1.223
	<b>1500</b>	<b>0.79</b>	<b>4.88</b>	<b>37.2</b>	<b>1.445</b>
	2000	0.63	3.98	34.1	0.864
1:4	1000	0.80	4.88	36.4	1.412

The I/V performance of the acceptor-BC polymer PBCDPP is shown in Figure 46 and the performance data is summarized in Table 15. The best performing device has the ratio D:A of 1:1 (PBCDPP:PC<sub>71</sub>BM weight ratio) spin coated at 1000 rpm without the additive DIO. This device showed an efficiency of 0.410%, with a V<sub>oc</sub> of 0.35V, J<sub>sc</sub> of 3.59 mAcm<sup>-2</sup> and a FF of 32.28%. No experiments were conducted by varying the content of acceptor; as this material showed a very low solubility and was therefore had to be dissolved properly. This bad solubility characteristic afforded very inhomogeneous films with a high degree of defects and led to un-precious control on the weight ratio. As shown in Figure 42, the V<sub>oc</sub> of PBCDPP is significantly lower than the other 3 three polymers. This is most likely due to two aspects, firstly the poor film formation affords shunt resistances, that will result in a low V<sub>oc</sub>, this combined with the unfavorable high HOMO of -5.14 eV can explanation of the V<sub>oc</sub> around 0.35V. Jo *et al.* [109] reported an array of carbazol analogs to PBCDPP polymer, consisting of a 2,7-linked carbazole and DPP derivatives, these polymers had a maximum performance of 3.64% with a V<sub>oc</sub> of 0.77V, a J<sub>sc</sub> of 9.03 mAcm<sup>-2</sup>. This shows that the OPV devices and polymer reported by Jo *et al.* outperformed the BC derivative on every parameter.

Table 15: *IV characteristics of the devices from the polymer PBCDPP with PC<sub>71</sub>BM as acceptor weight ratio of 1:1. Devices are spin coated from o-DCB.*

Spin speed [rpm]	DIO [%]	V <sub>oc</sub> [V]	J <sub>sc</sub> [mAcm <sup>-2</sup> ]	FF [%]	PCE[%]
<b>1000</b>	-	<b>0.35</b>	<b>3.59</b>	<b>32.28</b>	<b>0.410</b>
	1	0.36	3.25	34.2	0.401
	2	0.22	2.19	31.4	0.155
	3	0.17	1.00	29.6	0.051
1500	-	0.38	2.90	33.3	0.365
	1	0.08	2.00	25.83	0.042
	2	0.24	2.23	32.1	0.173
	3	0.16	1.43	28.9	0.065
2000	-	0.35	2.38	32.6	0.275
3000	-	0.29	1.85	32.0	0.173

This again is ascribed to the pseudo-A/A polymer type, which does not afford low enough HOMO to give a decent V<sub>oc</sub> whilst the LUMO level is comparable with the other polymers reported here.

In order to evaluate the device performance of the EQE, measurements have been conducted to observe and determine the progression of absorbance and conversion of light into electricity. These EQE measurements are conducted on the two best performing devices, being PBCBDTTT/PC<sub>71</sub>BM 1:3 and PBCQT/PC<sub>71</sub>BM 1:3 as can be seen in Figure 47. The EQE shows maximum conversion efficiency 53% for the PBCBDTTT devices and is around 410 nm which acceptably does not correspond to the maximum absorbance point of the native polymer shown in Figure 41, due to the presence of the acceptor material PC<sub>71</sub>BM in the blended active layer materials. The secondary maximum at 480 nm (51%) corresponds to the maximum absorbance of the polymer. For the PBCQT device the maximum peaks are located around 390 nm (~28%) and 470 nm (28%), and again the first maximum is not related to the maximum absorbance of the native polymer because of the extra absorption from PC<sub>71</sub>BM, while the second maximum is associated to maximum absorbance of the polymer.

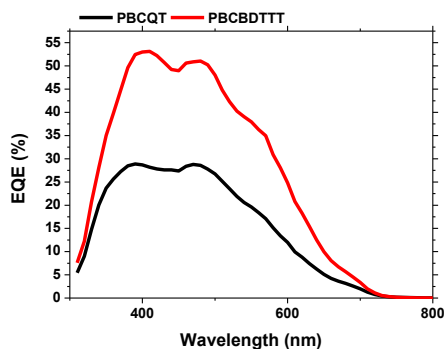


Figure 47: EQE performance of the device from PBCQT:PC<sub>71</sub>BM (black) and PBCQT:PC<sub>71</sub>BM (red) with the weight ratio 1:3. Devices are spin coated from *o*-DCB at, 1500 rpm and 3000 rpm, respectively. Adapted from paper III.

Ultimately the active morphology is essential to the performance of the device, as the surface smoothness of the film indicates a good mixing between the two blended compounds. The AFM images of the BC based polymers, can be seen in Figure 48. The homogeneity of the polymer acceptor blends are essential as the charge dissociation occurs at the interface between the two phases, and this interface is increased when the materials are mixed well. The root-mean-squared roughness (RMSR) of the film are given by the apparatus as defined in the ISO 25178 series, the RMSR is 0.52nm, 0.40 nm, 1.2nm, and 0.75 nm for the PBCBDTTT, PBCQT, P3HTBCBT, and PBCDPP, respectively. These RMSR are very low indicating a good mixing between the dual phases. The two best performing devices have a lower RMSR than the other two worst performing ones; resulting a higher FF for their relatively high PCE in this series of polymers. For all the analyzed materials, it is clearly seen that there are some areas where the height is significantly higher than others; this is taken as an indication of large aggregates formed by either impurities or insoluble polymers residues. These aggregates were also apparent, where centrifugal patterns emerged when spin coating PBCDPP resulted in a large degree of flawed devices.

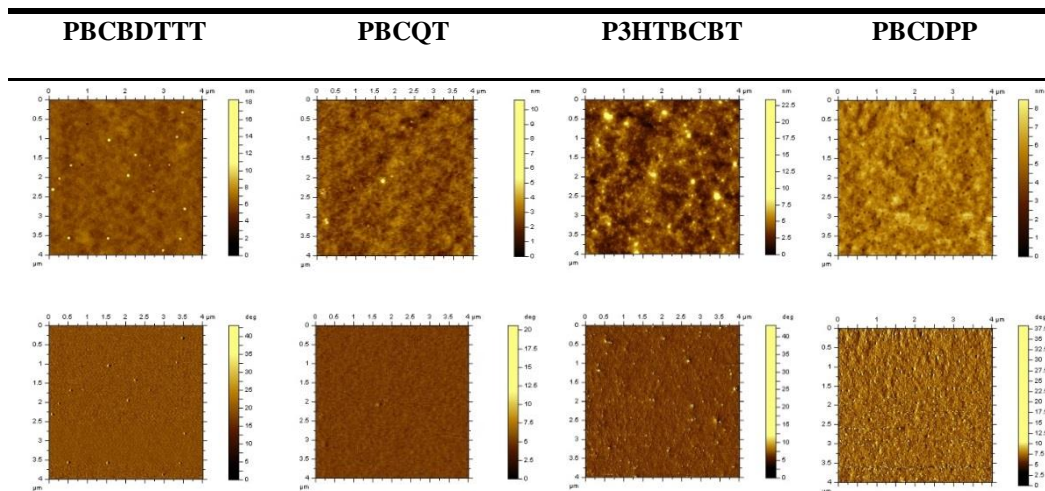


Figure 48: Atomic force microscopy images obtained via height tapping mode, the upper row is the topographic images and the lower is the phase images of the four polymers noted above. All images are of the optimized polymer:PC<sub>71</sub>BM blend.

### 3.4.1. ROLLCOATED DEVICES

Efforts in testing the scalability of PV devices from the two best performing polymers were made via roll-coating (RC) as previously described (2.2.1.3). However no success of such roll-coated fabrication was gained due to unexplainable dewetting of the polymer film, as shown in Figure 49.

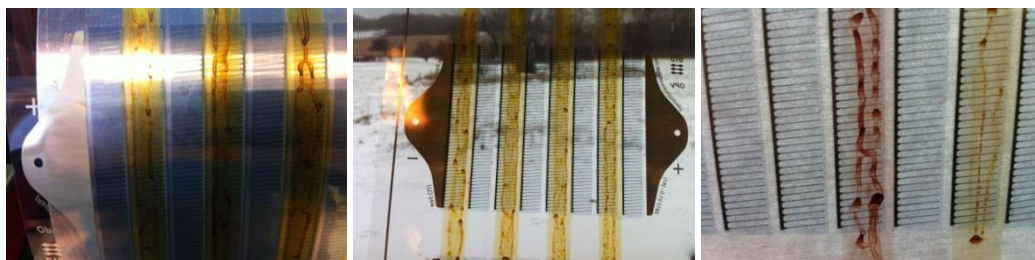


Figure 49: Photographs of the attempt to make RC devices, the yellowish polymer is PBCBDTTT and the red is PBCQT.

Such dewetting could be addressed by certain additives that could reduce the surface tension of between the polymer blend and the flextrode, but this was not carried on due to scarcity of the materials.

### 3.5. SUMMARIZATION

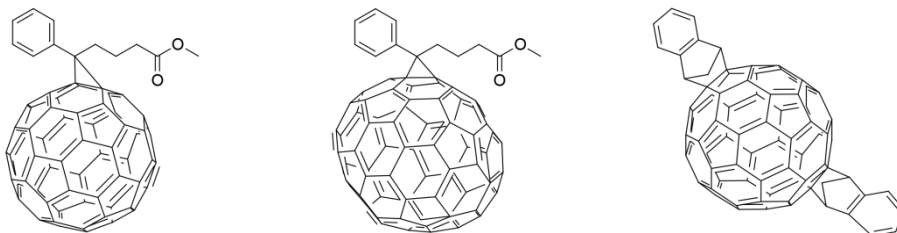
In this study, the novel boron containing monomer, 3,6-dibromo-*N*-(dimesitylboryl) carbazole (BC) was synthesized and the structure had been confirmed via FTIR and <sup>1</sup>HNMR studies. The FTIR data was held against the molecular dynamics simulated vibrational data acquired using DFT B3LYP/6-31G(d,p). The versatility of the novel monomer as pseudo acceptor moiety was shown by polymerizing it with an array of different donor units: a.) with 3,3''-didodecyl-2,2':5',2'':5'',2''':5'''-quaterthiophene (QT) by Kumada cross-coupling with *in situ* formation of Grignard reagent; b.) with 2,6-bis(trimethyltin)-4,8-di(5-(2-ethylhexyl)thiophene-2-yl)benzo[1,2-b:4,5-b']dithiophene (BDTTT) via Stille cross-coupling; c.) with 3,6-bis(5-boronic acid pinacol ester thiophen-2-yl)-2,5-bis(2-ethylhexyl)-6-(thiophen-2-yl)pyrrolo[3,4-c]pyrrol e-1,4(2H,5H)-dion (DPP) via a Suzuki cross-coupling; and d.) lastly with 2,5-dibromo-3-hexylthiophene and 2,1,3-Benzothiadiazole-4,7-bis(boronic acid pinacol ester) via random Suzuki cross-coupling polymerization, affording the polymers of PBCBDTTT, PBCQT, PBCDPP and P3HTBCBT, respectively. Molecular simulations of PBCBDTTT, PBCQT, and PBCDPP showed an interesting distribution of the LUMO orbitals. For PBCBDTTT and PBCQT, the LUMO was partly distributed on the boron atom of the BC moiety, while this was not as predominant on the PBCDPP polymer. The molecular simulations also showed no effects on the dihedral angle between the BC moiety and comonomer, compared to the analogs found in literature. This LUMO interaction of the BC moiety is ascribed to the vacant  $\pi$ -orbitals of the boron moiety affording a pseudo-acceptor when interacting with the N-atom of the carbazole. This interesting characteristic is also seen in the absorbance spectra of the molecules. Where a secondary absorbance maximum is observed below 330 nm, this is ascribed to the absorbance of the boron of the BC. Despite the quasi-A/D polymer, the afforded polymers had rather wide band gaps being 2.07, 2.23, 1.77 and 1.92 eV, for the polymers PBCBDTTT, PBCQT, PBCDPP and P3HTBCBT, respectively. These bandgaps afforded the frontier orbitals like ( $E_{\text{HOMO}}/E_{\text{LUMO}}$ ) -5.52 eV/-3.45 eV, -5.56 eV/-3.33 eV, -5.14 eV/-3.37 eV, and -5.60 eV/-3.68 eV for PBCBDTTT, PBCQT, PBCDPP, PBCDPP, and P3HTBCBT, respectively. The notion of the ambipolar effects of the dimesitylboryl functionality is supported when observing a ca. 0.4 eV lowered  $E_{\text{HOMO}}$  and  $E_{\text{LUMO}}$  on the polymer PBCQT. All polymers showed excellent hole and electron mobilities ( $\mu_{\text{hole}}$  and  $\mu_{\text{electrons}}$ ) in the order of  $10^{-4}$  cm<sup>2</sup>V<sup>-1</sup>s<sup>-1</sup> (except the hole mobility of PBCQT), determined by means of the SCLC method.

The optimized devices afford the following results; PCE of 3.82%, with a  $V_{\text{oc}}$  1.00 V,  $J_{\text{sc}}$  of 8.31 mAcm<sup>-2</sup> and a FF of 45.7% for PBCBDTTT; PCE of 1.45% with a  $V_{\text{oc}}$  of 0.79V,  $J_{\text{sc}}$  of 4.88 mAcm<sup>-2</sup> and FF of 37.2% for PBCQT; PCE of 0.410%, with a  $V_{\text{oc}}$  of 0.35V,  $J_{\text{sc}}$  of 3.59 mAcm<sup>-2</sup> and a FF of 32.28% for PBCDPP; and PCE of 0.407 % with a  $V_{\text{oc}}$  of 0.66V, a  $J_{\text{sc}}$  of 2.32 mAcm<sup>-2</sup> and FF of 26.5% for P3HTBCBT. However roll-coated devices for further scaling-up OPV fabrication were attempted but could not be made with success due to an unexplainable dewetting.

# CHAPTER 4. SMALL MOLECULE ACCEPTORS: GOING FROM SMALL TO LARGE AREA OPVS

## 4.1. INTRODUCTION

As discussed in the introduction, the relatively low dielectric constants ( $\epsilon \sim 3$ ) and high exciton binding energies result in short diffusion lengths (<20nm) of the generated excitons (when light is absorbed by the organic chromophore)[117]. In order to diminish the electron-hole's recombination, an efficient charge separation of the exciton becomes indispensable. Therefore an essential component of the active layer materials in an OPV device, i.e. the electron acceptor had been sparked by C.W. Tang[118], such an electron acceptor, differs from the electron deficient acceptor moiety in the previously discussed structure of a low bandgap donor-acceptor (D-A) polymer or small molecule (SM) of D-A type. Without using an electron acceptor, the obtainable efficiency of a device is in the range of 0.1% [8], [119]. The state-of-art electron acceptor is derivatives of the Buckminsterfullerene[120], [121] due to its high electron affinity[122] and high electron mobility[123], [124] (in all three dimensions[125]). This isoelectric nature of the fullerene facilitates a favorable morphology from the solution-coated active layers[126]–[128]. The mostly used Buckminsterfullerene derivatives are the soluble PC<sub>61</sub>BM, PC<sub>71</sub>BM or indene-C60-bisadduct (ICBA), seen in Scheme 17.

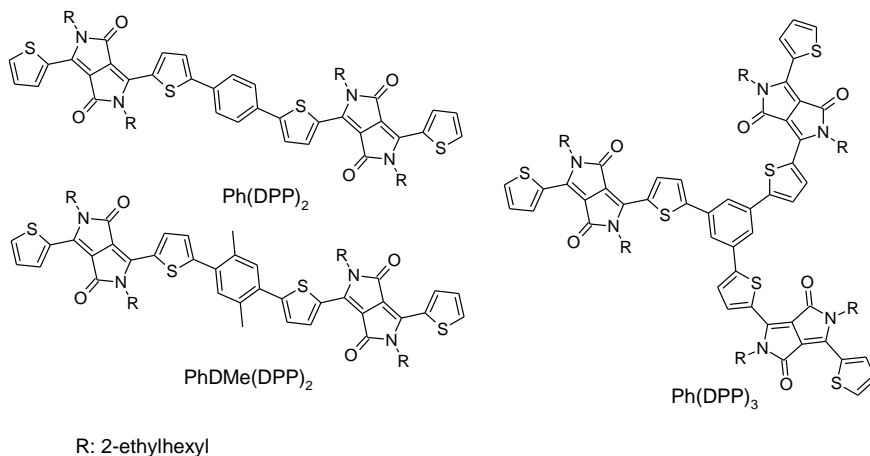


Scheme 17: Buckminster fullerene derivatives PC<sub>61</sub>BM, PC<sub>71</sub>BM and ICBA

Despite all the merits of the fullerene based acceptors, they all have some major drawbacks: a.) a large mismatch between their optical absorption and the solar radiation, combined with their low absorption coefficients being disadvantageous as the introduction of the fullerene will only limited participating directly in the generation of the photocurrent; b.) an inherent difficulty in manipulating the frontier orbitals, thus the fine-tuning of the band gap is troublesome. Bloking *et al.*[129] discussed another vital limitation of the fullerene acceptor in regards to the  $V_{oc}$ , arguing that there is a upper limit of 1 V. This upper  $V_{oc}$  limit will result in a large current drop when exceed, due to inability to split the generated excitons into free charge carriers[129]. In addition to the mentioned intrinsic flaw of the fullerene based OPVs, fullerene derivatives also suffer from some insufficiencies: Firstly, due to polar interactions, they diffuse towards the PEDOT:PSS layer, this has been shown by Brand *et al.* [130], such diffusion affords a lowering of the fracture resistance of the film and can ultimately result in a delamination of the active layer as shown by Dupont *et al.* [131]. Secondly, from a

commercialization perspective, large energy input in the production materials such as PC<sub>61</sub>BM which has an embodied energy of 64.7 GJkg<sup>-1</sup> and for other fullerene derivatives such as PC<sub>71</sub>BM, the energy input is even higher like 90.2 GJkg<sup>-1</sup>[132]. Therefore it would be advantageous to substitute the fullerene based electron acceptors with a non-fullerene based acceptor, e.g., organic ones. The most important, the fixed energy level of frontier orbitals (LUMO) (together with the required fixed energy level difference between the LUMO of the donor materials and them) strictly limits the choice of possible donor materials. Despite there being several ways to circumvent the use of fullerene based acceptors, the use of either n-type polymers or n-type SMs has become the most dominant one. In regards to these two, the SM has a higher uniformity and the well-defined structural composition with no batch to batch variations, making it a more interesting design strategy than the electron accepting polymers. The SM can be easily tuned in regard of the level of the frontier orbitals, by functionalization, by certain substituents. SM acceptors tend to be planar molecules with strong  $\pi$ - $\pi$  interactions, when oriented co-facially. These  $\pi$ - $\pi$  stacking based strong interactions will promote phase separation resulting in structured domains within the active layer matrix[133], [134]. Intermolecular orientation among SMs is directly opposite to the behavior of the fullerene acceptors, as these do not phase separate in the active layer matrix. For SM these structural interactions results in a good orbital overlap that in turns will afford a high mobility, while fullerenes do not [133], [134]. A promising SM acceptor moiety candidate is diketopyrrolopyrrole (DPP), as this chromophore shows a strong absorbance, excellent thermal stability and can be modified quite easily at the amide-nitrogen of the DPP unit, affording an readily path to increase the solubility[45], [117]. The DPP chromophore is generally flanked by two aromatic extensions, being either phenyl or thienyl[135], [136]; in this work only the DPP with the adjacent thiophenes have been utilized, therefore when discussing the DPP, we prospectively refer to the thiophene-DPP derivative. The DPP moiety is very planar showing a tendency towards high degree of  $\pi$ - $\pi$  stacking[45], [117]. There are two predominant strategies when designing DPP containing SM acceptors; one being the DPP center moiety with adjacent functionalization as reported by Sonar *et al.*[137] or by a flanking a central donor moiety by DPP reported by the group of Zhan[138], [139]. The design strategy applied by Sonar *et al.*[137] were focused on flanking a DPP center moiety with electron deficient phenyl moieties being groups such as *p*-(trifluoromethyl)phenyl group and *trans*-2-[4-(trifluoromethyl)phenyl]vinyl. The SM acceptors were tested against P3HT as the donor of the active layer matrix, which is the state-of-art donor polymer used to test against these novel acceptors. DPP flanked by *trans*-2-[4-(trifluoromethyl)phenyl]vinyl afforded an efficiency of 0.58% with a  $V_{oc}$  of 0.64 V and  $J_{sc}$  of 1.7 mAcm<sup>-2</sup>, while the DPP flanked by *p*-(trifluoromethyl)phenyl claimed a PCE of 1.00% with a  $V_{oc}$  of 0.81 V and  $J_{sc}$  of 2.36 mAcm<sup>-2</sup>. The band gaps of the two molecules were 1.81 eV (592 nm) and 1.94 eV (599 nm), respectively. Lin *et al.*[138] in 2012 reported a triphenylamine (TPA) center donor moiety[140] flanked by DPP to afford a star-shaped SM acceptor. This SM was tested against P3HT, obtaining an efficiency of 1.20 %, with a  $V_{oc}$  of 1.18 V and  $J_{sc}$  of 2.68 mAcm<sup>-2</sup>. This work showed the potential of a  $V_{oc}$  exceeding 1 V, which is not affordable for fullerene based acceptors. The usage of a donor center moiety was further improved by dibenzosilole from Lin *et al.*[139] in 2013. This dibenzosilole (DBS) flanked by DPP offered an efficiency of 2.05%, with a  $V_{oc}$  0.97 V and 4.91 mA cm<sup>-2</sup>, which is the highest performing DPP SM containing non-fullerene acceptor. The LUMO levels of TPA-DPP and DBS-DPP reported by Lin *et al.*, were -3.26 eV and -3.28 eV, respectively[138], [139]. So despite the similar LUMO levels, the efficiencies of these are rather different, which most likely derives from difference in the formed morphology.

This notion that the intermolecular interactions are quite dictating for the photovoltaic performance of a given device is also shown by Sherman *et al.*[133]. They found via a systematic studied an array of small molecule acceptors, and found that almost planar, amorphous non-fullerene acceptors were disadvantageous for applications in BHJ OPVs. It was shown that an ordered structure would facilitate a higher mobility, thus a lower degree of recombination affording more efficient devices.



Scheme 18: The three DPP based non-fullerene small molecule acceptors  $\text{Ph(DPP)}_2$ ,  $\text{PhDMe(DPP)}_2$ , and  $\text{Ph(DPP)}_3$ .

Considering the above mentioned molecular design, an array of simple non-fullerene acceptors has been proposed in this thesis. In this work we focus on a center moiety being either phenyl, 2,5-dimethyl-1,4-phenylene or a 1,3,5-phenylene flanked by either two or three alkylated DPP, as seen in Scheme 18. The design idea is to gradually increase the disorder via torsion between the center moieties going from native benzene ( $\text{Ph(DPP)}_2$ ), to the 2,5-dimethyl-1,4-phenylene ( $\text{PhDMe(DPP)}_2$ ) to the tri-substituted 1,3,5-phenylene forming a star-shaped molecule ( $\text{Ph(DPP)}_3$ ). While the degree of disorder or degree of planarity is decreased, the frontier orbitals are not expected to change, thus keeping the same fundamental building blocks to ensure a degree of comparability within the different molecules and the device performance.

There has been a large progress in the utilization of SM acceptors, efficiencies for bilayer OPV devices using SM acceptors have reached a PCE of 8.4 % [141] and for BHJ devices a PCE of 7.16 % has been obtained [142]. For the device with a PCE of 8.4% the active layer was processed using sublimation techniques which are not appropriate for upscaling and ultimately commercialization of the OPV technologies. For the device with a PCE of 7.16% reported by Sun *et al.*, the potential is larger, as the materials are solution processed but the choice of electrodes being ITO and the application of Ca as an interface layer will, due to previous stated reason, be far from advantageous [31], [143]. The previously mentioned SM acceptors based on DPP had active area ranging from 4 mm<sup>2</sup> to 9 mm<sup>2</sup>. There has been little work done in investigating the upscaling of the SM based devices from the mm<sup>2</sup> range to cm<sup>2</sup> range. The first attempt on this was conducted by Chen *et al.* [144] that, with limited success, produced SM based device had a PCE of 0.067%. This was done by utilizing SM donor

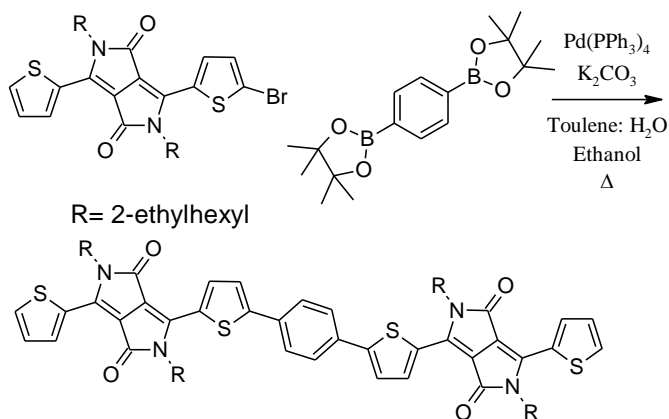
against PCBM as acceptor using a device design without the application of ITO or vacuum techniques. The first attempt to utilize a SM acceptor together with a P3HT in such a vacuum- and ITO-free setup was conducted by Liu *et al.* [145] where a polymer performing 3.17% in its PCE in a small area (0.054 cm<sup>2</sup>) spin coated device and a PCE of 0.65% in a medium area device setup (1 cm<sup>2</sup>). The work presented by Liu *et al.* is the best performing adaptation of the SM going from small to large area [145]. In this work the three previously mentioned SM acceptor candidates will be tested both in a conventional setup and in the large area setup.

## 4.1. MATERIALS AND METHODS

### 4.1.1.1 Materials

Chemicals used were of commercial grade, and used without further purification, if not state otherwise. The synthesis is also shown in paper **II** and **IV**.

### 4.1.1.2 Syntheses

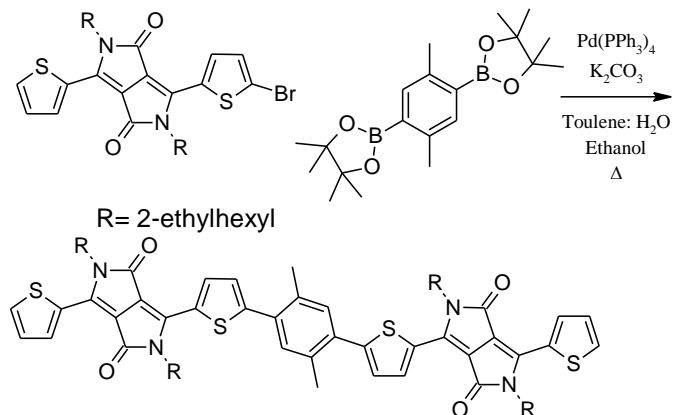


*Scheme 19: Suzuki cross-coupling between 3-(5-bromothiophen-2-yl)-2,5-bis(2-ethylhexyl)-6-(thiophen-2-yl)pyrrolo[3,4-c]pyrrole-1,4(2H,5H)-dione and 1,4-bis(4,4,5,5-tetramethyl-1,3,2-dioxaborolan-2-yl)benzene to afford Ph(DPP)<sub>2</sub>.*

**Ph(DPP)<sub>2</sub>:** To a three-necked round bottom flask were added 3-(5-bromothiophen-2-yl)-2,5-bis(2-ethylhexyl)-6-(thiophen-2-yl)pyrrolo[3,4-c]pyrrole-1,4(2H,5H)-dione (1 g, 1.66 mmol), 1,4-bis(4,4,5,5-tetramethyl-1,3,2-dioxaborolan-2-yl)benzene (0.24 g, 0.72 mmol), potassium carbonate (1.99 g, 14.4 mmol), demineralized water (7.2 mL), ethanol (2.9 mL) and toluene (50 mL). The mixture was degassed with nitrogen for 15 min. Pd(PPh<sub>3</sub>)<sub>4</sub> (0.067 g, 0.058 mmol) was added under nitrogen as shown in Scheme 19. The mixture was heated at 80 °C for 24 h and subsequently cooled to ambient temperature. The mixture was extracted with dichloromethane (DCM) and washed with saturated sodium chloride aqueous solution (brine). The organic phase was dried over anhydrous MgSO<sub>4</sub> and filtered. After removing the solvent from filtrate, the residue was purified by column chromatography on silica gel using DCM as eluent yielding a dark blue solid (0.68 g, 84 %).

<sup>1</sup>H NMR (600 MHz, CDCl<sub>3</sub>, δ) 9.00 (d, J = 4.1 Hz, 2H), 8.93 (dd, J<sub>1</sub> = 3.9 Hz, J<sub>2</sub> = 0.9 Hz, 2H), 7.73 (s, 4H), 7.65 (dd, J<sub>1</sub> = 5.0 Hz, J<sub>2</sub> = 0.9 Hz, 2H), 7.54 (d, J = 4.1 Hz, 2H), 7.29 (dd, J<sub>1</sub> = 5.0

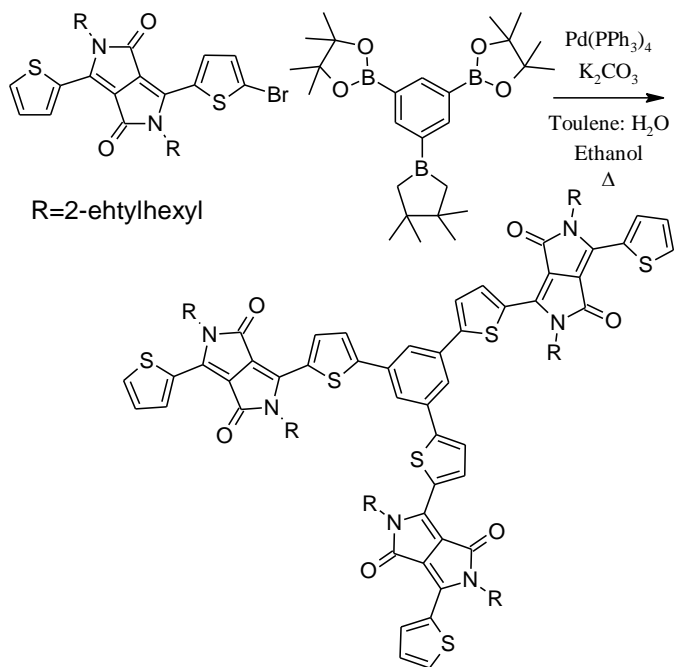
Hz,  $J_2=3.9$  Hz, 2H), 4.16–4.01 (m, 8H), 2.00–1.86 (m, 4H), 1.48–1.22 (m, 32H), 0.97–0.86(m, 24H);  $^{13}\text{C}$  NMR (600 MHz,  $\text{CDCl}_3$ , d): 161.76,161.67, 148.54, 140.21, 139.94, 136.89, 135.35, 133.38, 130.57, 129.89, 129.26, 128.47,126.62, 124.83, 108.29, 108.13, 45.95, 39.30,39.12, 30.38,30.25, 28.57,28.37,23.71,23.57, 23.12, 23.09, 14.10,14.04 10.61, 10.52, 10.51; MS (MALDI):  $m/z$  1123.43 ( $\text{M}^+$ )



Scheme 20: Suzuki cross-coupling between 3-(5-bromothiophen-2-yl)-2,5-bis(2-ethylhexyl)-6-(thiophen-2-yl)pyrrolo[3,4-c]pyrrole-1,4(2H,5H)-dione and 2,2'-(2,5-dimethyl-1,4-phenylene)bis(4,4,5,5-tetramethyl-1,3,2-dioxaborolane) to afford PhDMe(DPP)<sub>2</sub>

**PhDMe(DPP)<sub>2</sub>**: To a three-necked round bottom flask were added then compounds 3-(5-bromothiophen-2-yl)-2,5-bis(2-ethylhexyl)-6-(thiophen-2-yl)pyrrolo[3,4-c]pyrrole-1,4(2H,5H)-dione (1 g, 1.66 mmol), 2,2'-(2,5-dimethyl-1,4-phenylene)bis(4,4,5,5-tetramethyl-1,3,2-dioxaborolane) (0.26 g, 0.72 mmol), potassium carbonate(1.99 g,14.4 mmol), demineralized water (7.2 mL), ethanol (2.9 mL) and toluene (50 mL).The mixture was degassed with nitrogen for 15 min. The catalyst  $\text{Pd}(\text{PPh}_3)_4$  (0.067 g, 0.058 mmol) was added under counter flow of nitrogen, as shown in Scheme 20. The mixture was heated to 80 °C for kept at this temperature for 24 h and then allowed to ambient temperature. The mixture was extracted with DCM and washed with saturated sodium chloride aqueous solution. The organic phase was dried over anhydrous  $\text{MgSO}_4$  and filtered. After removing the solvent from filtrate, the residue was purified by column chromatography on silica gel using DCM as eluent yielding a purple red solid (0.71 g, 86%).

$^1\text{H}$  NMR (600 MHz,  $\text{CDCl}_3$ ,  $\delta$ ) 9.02 (d,  $J = 4.0$  Hz, 2H), 8.93 (dd,  $J_1 = 3.8\text{Hz}$ ,  $J_2=1.1$  Hz, 2H), 7.66 (dd,  $J_1 = 5.0\text{Hz}$ ,  $J_2=1.1\text{Hz}$ , 2H), 7.46 (s, 2H), 7.34(d,  $J = 4.0$  Hz, 2H), 7.30 (dd,  $J_1 = 5.0\text{Hz}$ ,  $J_2=3.8$  Hz, 2H), 4.14–4.03 (m, 8H), 2.55(s, 6H), 2.01–1.86 (m, 4H), 1.48–1.21(m, 32H), 0.96–0.86(m, 24H);  $^{13}\text{C}$  NMR (600 MHz,  $\text{CDCl}_3$ , d): 161.81,161.76, 148.09, 140.30, 140.18, 136.09, 135.29, 133.83, 133.15, 132.88, 130.54, 129.90,129.68, 128.47, 128.21,108.09, 108.00, 45.95, 39.30,39.10, 30.29, 30.22, 28.54 ,28.38, 23.56, 23.15, 23.10,20.94, 14.10,14.07,10.53, 10.52, 10.51; MS (MALDI):  $m/z$  1151.47 ( $\text{M}^+$ ).



Scheme 21: Suzuki cross-coupling between 3-(5-bromothiophen-2-yl)-2,5-bis(2-ethylhexyl)-6-(thiophen-2-yl)pyrrolo[3,4-c]pyrrole-1,4(2H,5H)-dione and 1,3,5-tris(4,4,5,5-tetramethyl-1,3,2-dioxaborolan-2-yl)benzene to afford Ph(DPP)<sub>3</sub>

**Ph(DPP)<sub>3</sub>:** To a three-necked round bottom flask were added 3-(5-bromothiophen-2-yl)-2,5-bis(2-ethylhexyl)-6-(thiophen-2-yl)pyrrolo[3,4-c]pyrrole-1,4(2H,5H)-dione (1.7 g, 2.82 mmol), 1,3,5-tris(4,4,5,5-tetramethyl-1,3,2-dioxaborolan-2-yl)benzene (0.28 g, 0.62 mmol), potassium carbonate(2.60 g, 18.8 mmol), deionized water (10 mL), ethanol (8 mL) and toluene (80 mL). The mixture was deoxygenated with nitrogen for 15 min. Pd(PPh<sub>3</sub>)<sub>4</sub> (0.087 g, 0.075 mmol) was added under nitrogen, as shown in Scheme 21. The mixture was heated to 80°C and kept here for 24 h and then cooled down to room temperature. The mixture was extracted with DCM and washed with saturated sodium chloride aqueous solution. The organic phase was dried over anhydrous MgSO<sub>4</sub> and filtered. After removing the solvent from filtrate, the residue was purified by column chromatography on silica gel using DCM as eluent yielding a red solid (0.76 g, 74%).

<sup>1</sup>H NMR (600 MHz, CDCl<sub>3</sub>, δ) 8.97 (d, J = 4.2 Hz, 3H), 8.96 (d, J = 3.6 Hz, 3H), 7.89 (s, 3H), 7.67 (d, J = 4.8 Hz, 3H), 7.60 (d, J = 3.6 Hz, 3H), 7.31-7.29 (m, 3H), 4.15-4.02 (m, 12H), 2.00-1.87 (m, 6H), 1.48-1.22 (m, 48H), 0.99-0.97 (t, J = 7.8, Hz 9H), 0.93-0.85 (m, 17H); <sup>13</sup>C NMR (600 MHz, CDCl<sub>3</sub>, d): 161.74, 161.69, 147.37, 140.70, 139.57, 136.43, 135.56, 135.22, 130.78, 129.94, 129.83, 128.51, 125.61, 123.76, 108.61, 108.05, 45.95, 39.28, 39.11, 30.34, 30.22, 28.54, 28.37, 23.78, 23.57, 23.09, 14.07, 14.04, 10.68, 10.53; MS (MALDI): *m/z* 1646.66 (M<sup>+</sup>).

#### 4.1.1.3 Methods

<sup>1</sup>H and <sup>13</sup>C NMR was conducted as described in 2.1.1.3. MALDI-TOF MS spectra were recorded on a Bruker's Daltonics flex Analysis ultraflex TOF mass spectrometry. All other

methods were similarly to previously described (2.2.1.3). The topographic images (AFM) of the films were obtained on a Veeco MultiMode atomic force microscopy (AFM) in the tapping mode using an etched silicon cantilever at a nominal load of approximately 2 nN, and the scanning rate for a 5  $\mu\text{m}$  x 5  $\mu\text{m}$  image size was 1.0 Hz.

The spin coated small area devices were prepared as followed: ITO glass was pre-cleaned by detergent, deionized water, isopropanol, acetone, and ethanol in ultrasonic bath for 15min, sequentially. After dried by the  $\text{N}_2$  gas flow, these substrates were spin-coated with PEDOT:PSS (Baytron P4083, Germany) for 60s. The thickness of the PEDOT:PSS layer was about 30 nm. The photoactive layer was spin-cast at 4000 rpm from a solution of P3HT and DPP derivative in chloroform at a total solid concentration of 20  $\text{mgmL}^{-1}$  and followed by 10 min annealing at different temperatures in  $\text{N}_2$  atmosphere. A 5-nm-thick poly [(9,9-bis(3'-(N,N-dimethylamino)propyl)-2,7-fluorene)-alt-2,7-(9,9-dioctylfluorene)] (PFN) film was deposited as the cathode buffer layer by spin-coating solution of 0.4  $\text{mgmL}^{-1}$  PFN in methanol in order to reduce the work function of the cathode. At last, a 100 nm thick Al film was deposited on the active layer under vacuum of approximately  $4 \cdot 10^{-4}$  Pa. The active area of OSCs is 9  $\text{mm}^2$ . The roll coated devices were made using the method described in section 2.2.1.3.

## 4.2. MATERIALS CHARACTERIZATION

The three small molecule acceptors, were characterized by  $^1\text{H}$  and  $^{13}\text{C}$  NMR and the resulting chemical shifts are shown under the synthetic procedure alongside the mass determined by MS.

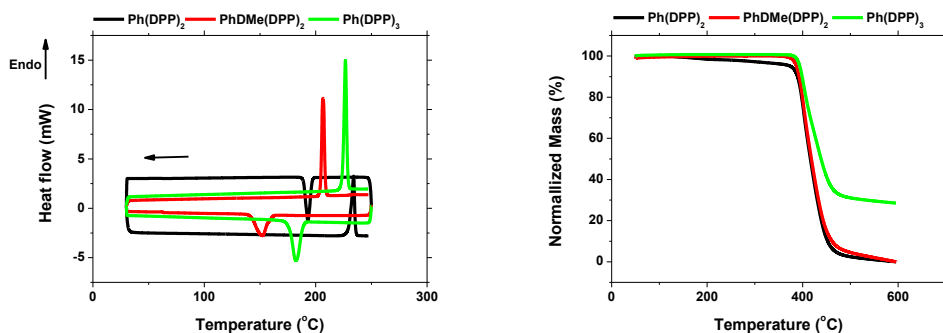


Figure 50: Differential scanning calorimetry (DSC, left) and thermo gravimetric analysis (TGA, right) scan of the three SM: Ph(DPP)<sub>2</sub> (black), PhDMe(DPP)<sub>2</sub> (red) and Ph(DPP)<sub>3</sub> (green). Adapted from paper II and IV.

The three materials Ph(DPP)<sub>2</sub>, PhDMe(DPP)<sub>2</sub> and Ph(DPP)<sub>3</sub> showed all a comparable thermal stability, with a thermal decomposition temperature around 380 °C, which is sufficient for solution processing of OPV devices and thermo annealing. The melting points are 234 °C, 206 °C, and 226 °C for Ph(DPP)<sub>2</sub>, PhDMe(DPP)<sub>2</sub> and Ph(DPP)<sub>3</sub>, respectively. All melting ranges of the three compounds indicate high purity of all the three synthesized materials and good crystallization properties.

## 4.2.1. MOLECULAR SIMULATIONS

To investigate planarity and electron density distribution of the frontier orbitals of the molecules, theoretical calculations have been performed via density function at the B3LYP/6-31G(d) level. It should be noted that the side chains of the DPP moieties are reduced to methyl in order to reduce the computational load. The geometry of the small molecules can be seen in Figure 51.

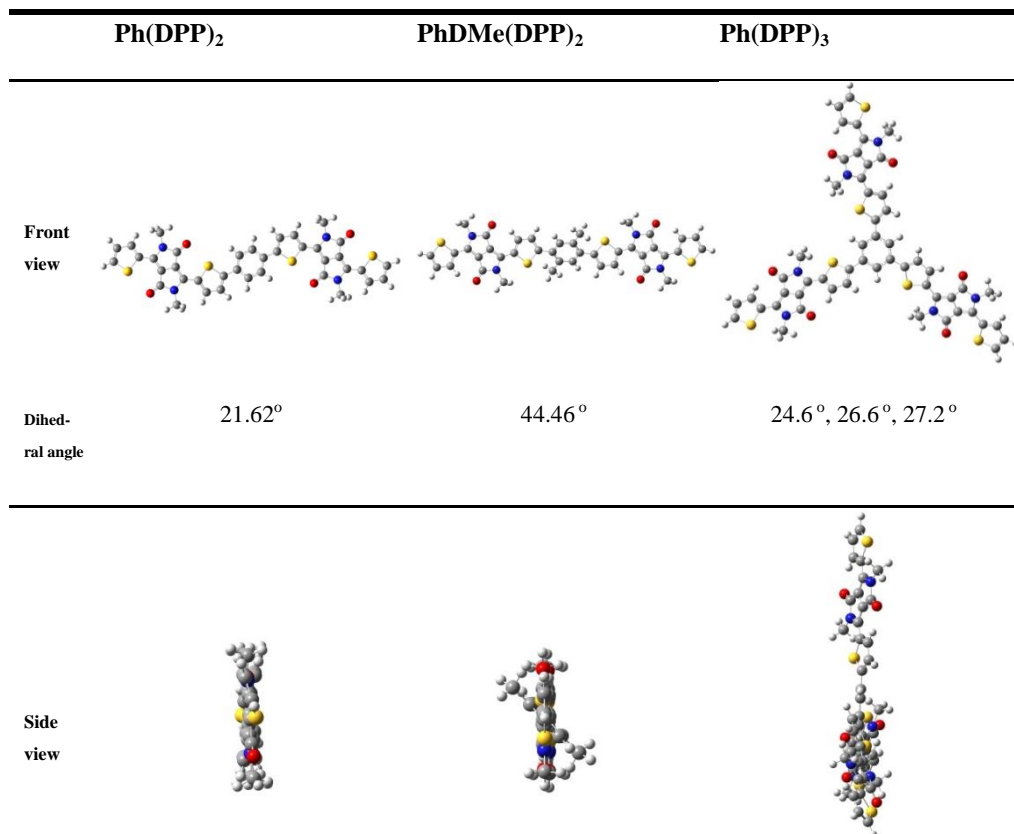


Figure 51: The optimized geometric structure of the three molecule Ph(DPP)<sub>2</sub>, PhDMe(DPP)<sub>2</sub> and Ph(DPP)<sub>3</sub>.

The dihedral angle, noting the angle between the central phenyl moiety and the DPP moiety, was determined by using the GaussView tool, and was found to be 21.62° for Ph(DPP)<sub>2</sub>, 44.46° for PhDMe(DPP)<sub>2</sub> and ranging from 24.6° to 27.2° for Ph(DPP)<sub>3</sub>. As it can be seen, the introduction of the two methyl groups on the phenyl unit increases the dihedral angle from 21.62° to 44.46° as expected, due to the spatial interactions between the methyl groups and the thiophene units of the adjacent DPP. Such introduction of torsion has an effect on the intermolecular interactions of the molecules, as torsion is expected to reduce  $\pi$ - $\pi$  stacking due to steric hindrance of the DPP moieties. This combined with the effect of a larger torsion angle that will also result in a higher band gap, as a large torsion angle will break not only the  $\pi$ - $\pi$  stacking but also the conjugation of the molecules as the orientation of the  $\pi$ -orbitals are

altered. Meanwhile DFT simulations of the  $\text{Ph}(\text{DPP})_3$  molecule announced slightly larger angle than  $\text{Ph}(\text{DPP})_2$ , proving similar torsions among the DPP and the central phenyl moiety, even though owning one more DPP unit. This reveals that spatial arrangement is still not sterically hindered among the 3 DPP units in  $\text{Ph}(\text{DPP})_3$ . Such similar torsions lead to comparable band gap energy between  $\text{Ph}(\text{DPP})_2$  and  $\text{Ph}(\text{DPP})_3$  as well. They would afford a higher degree of intermolecular stacking than  $\text{PhDMe}(\text{DPP})_2$ . Location of the frontier orbitals is shown in Figure 52. It has been argued by Sherman *et al.*[133] that the usage of completely planar acceptors might be disadvantageous, as planarity has a tendency to facilitate phase separation without the increase in mobility when dealing with amorphous materials, which in turn reduces that D/A interface between D and A in the active layer blends.

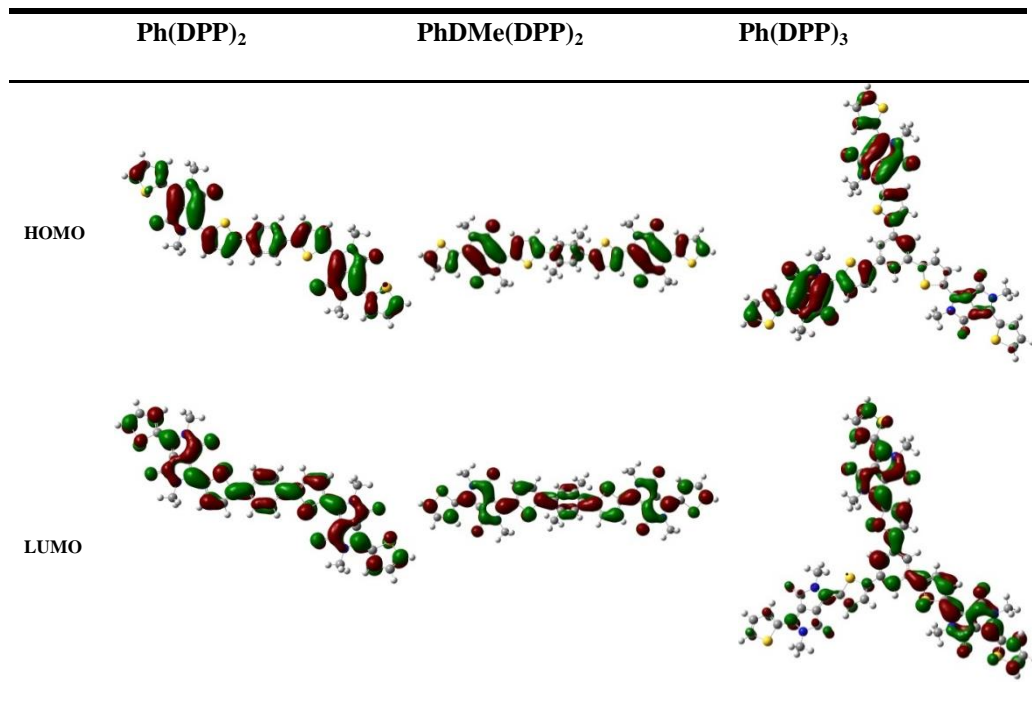


Figure 52: The theoretical distribution of the frontier orbitals (HOMO and LUMO) for the three molecules:  $\text{Ph}(\text{DPP})_2$ ,  $\text{PhDMe}(\text{DPP})_2$  and  $\text{Ph}(\text{DPP})_3$

The frontier orbitals (both HOMO and LUMO) are spread across the molecules, in regard to the  $\text{Ph}(\text{DPP})_2$  and  $\text{PhDMe}(\text{DPP})_2$ . There is actually a plan of symmetry across on the central benzene moiety, which was also shown in literature to be associated with a uniform (cross molecular) distribution of the frontier orbitals[146], [147]. The overlapping of the LUMO- and HOMO-orbitals, is expected to facilitate the HOMO to LUMO electronic transition ( $\pi \rightarrow \pi^*$ ) of the molecules[146]. The energy levels of the modelled frontier orbitals are shown in Table 16. Here it can be seen that the  $E_g$  of the three molecules are arranged  $\text{PhDMe}(\text{DPP})_2 < \text{Ph}(\text{DPP})_2 < \text{Ph}(\text{DPP})_3$ .

Table 16: The summarized modelling data for the frontier orbitals of the three small molecules;  $\text{Ph(DPP)}_2$ ,  $\text{PhDMe(DPP)}_2$  and  $\text{Ph(DPP)}_3$ . The DFT data is obtained using the B3LYP with the basis set 6-31G(d)

Material	$E_{\text{HOMO-THEO}}$ [eV]	$E_{\text{LUMO-THEO}}$ [eV]	$E_{\text{g-THEO}}$ [eV]
$\text{Ph(DPP)}_2$	-4.86	-2.71	2.15
$\text{PhDMe(DPP)}_2$	-4.44	-2.68	1.76
$\text{Ph(DPP)}_3$	-4.99	-2.71	2.28

This ranking of the band gap is interesting as it would be expected that the torsion of  $\text{Ph(DPP)}_3$  is slightly higher than that of  $\text{Ph(DPP)}_2$ , while  $\text{PhDMe(DPP)}_2$  possess the largest torsion. Therefore the larger planar conjugation, the lower band gap could be expected. Then ranking of  $E_{\text{g}}$  could be:  $\text{Ph(DPP)}_2 < \text{Ph(DPP)}_3 < \text{PhDMe(DPP)}_2$ . The  $E_{\text{g}}$  deviation on  $\text{PhDMe(DPP)}_2$  could be caused by underestimating of the torsion angles and the resulted misalignment of the  $\pi$ -orbitals. The three estimated LUMO levels are in the same level as they only deviate by 0.03 eV. While the difference on the  $E_{\text{g}}$  derives from the very different calculated HOMO levels of the molecules. This difference is assumed to derive from the introduction of the dihedral angle in the molecules. The molecular modeling results, showed breaking of the planarity of the molecule, which might afford some positive effects on the molecular geometry in regards to the application in OPVs devices.

#### 4.2.2. PHOTOPHYSICAL PROPERTIES

The absorbance properties of the three synthesized molecules have been recorded, both in solutions ( $\text{CHCl}_3$ ) and in films. These absorbance spectra can be seen in Figure 53 and Figure 54, for the solution and the film, respectively. The solution containing  $\text{PhDMe(DPP)}_2$  and  $\text{Ph(DPP)}_3$  showed similar absorbance characteristics, with an onset of 630 and 620 nm, respectively. Whilst the absorbance onset of the  $\text{Ph(DPP)}_2$  is 655 nm indicating a better conjugated planarity, as agreed by its lowest dihedral angle from DFT calculations. But all three molecules show the same overall progression with two local maximas in the short wavelength region of the spectrum ranging from 400-250 nm. Since the molecular design of the three SM acceptors does contain a strong donor, the two distinctive smaller local maxima in the high energy part of the spectrum, indicates a degree of  $\pi \rightarrow \pi^*$  interactions that normally derive from the absorbance of donor component of a given D/A structure. This is also why two high energy maxima are observed, as these both derive from the HOMO excitation of the phenyl along with that of the DPP moieties[148]. The absorption at higher wavelength region (>450nm) for all the three compounds reflects the electron push-pull effects (the intra-chain charge transfer) between the central phenyl units (donor) and flanked DPP moiety (acceptor).

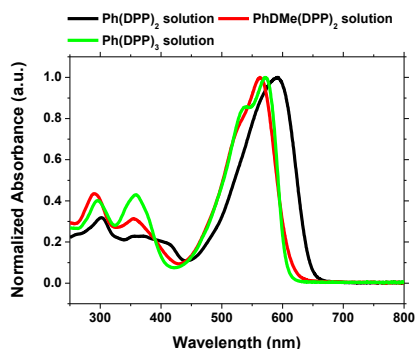


Figure 53: The UV-vis absorbance spectra of the three molecules;  $Ph(DPP)_2$  (black),  $PhDMe(DPP)_2$  (red) and  $Ph(DPP)_3$  (green) in  $CHCl_3$  solution. Adapted from paper II and IV.

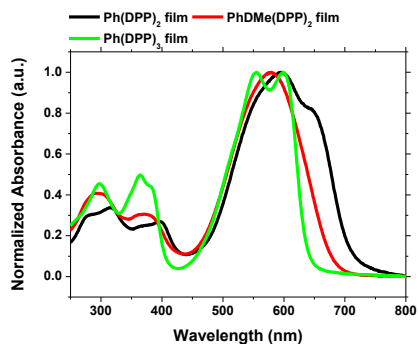


Figure 54: The UV-vis absorbance spectra of the three molecules;  $Ph(DPP)_2$  (black),  $PhDMe(DPP)_2$  (red) and  $Ph(DPP)_3$  (green) in film. Adapted from paper II and IV.

It is no surprise that the  $Ph(DPP)_2$  exhibits the lowest bandgap, as the torsion of this given molecule is much lower than  $PhDMe(DPP)_2$  and slightly lower than  $Ph(DPP)_3$ . When observing  $Ph(DPP)_3$ , the relative higher bandgap of  $Ph(DPP)_3$  comes from the slightly higher torsion as a result of the slightly higher dihedral angle. The visual appearance of the three different SMs can be seen in Figure 55 (the left image), where it can be seen that the color of  $Ph(DPP)_3$  is red, while  $Ph(DPP)_2$  is dark blue, and  $PhDMe(DPP)_2$  exhibits a purple color. For the film absorbance seen in Figure 54,  $Ph(DPP)_2$  has an approximately 60 nm red shift of the onset, with a film absorbance onset of 708 nm, with a clear vibronic shoulder at 650 nm deriving from  $\pi$ - $\pi$  interactions of the planar  $Ph(DPP)_2$ .  $PhDMe(DPP)_2$  also shows a red-shift going from 630 nm to 680 nm, so despite the introduced torsion the  $\pi$ - $\pi$  stacking in films is still occurring and result in a red shift of  $PhDMe(DPP)_2$ . It becomes clear when observing  $Ph(DPP)_3$ , it has the smallest red shift among the three SMs. The red shift of 17 nm going from 620 nm to 637 nm, which proves the steric hindrance of  $Ph(DPP)_3$  that prevents the  $\pi$ - $\pi$  stacking and thus prevents as large a redshift as  $Ph(DPP)_2$  and  $PhDMe(DPP)_2$  has. The band gaps of the SM have been determined using the absorbance onset being; 1.75, 1.82 and 1.95 eV, for  $Ph(DPP)_2$ ,  $PhDMe(DPP)_2$  and  $Ph(DPP)_3$ , respectively.

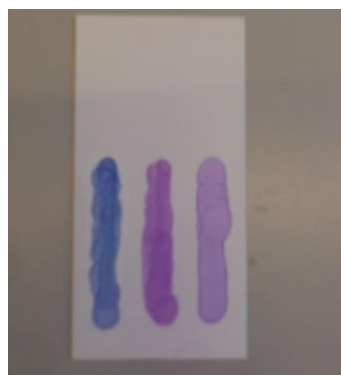


Figure 55: The visual appearance of the three molecules;  $Ph(DPP)_2$  (left),  $PhDMe(DPP)_2$  (middle) and  $Ph(DPP)_3$  (right) in solution and on a TLC plate.

The right image in Figure 55 is shown the solid film absorbance of the three materials on a silica TLC plate. The Ph(DPP)<sub>2</sub> has a blue color; PhDMe(DPP)<sub>2</sub> has a purple color which both corresponds to the color of the solutions. More interestingly Ph(DPP)<sub>3</sub> goes from a redish color in solution to a purple color on the silica. Using CV, the frontier orbitals of the molecules have been determined. The HOMO level of the SM has been determined to be -5.16 eV, -5.18 eV, and -5.24 eV, for Ph(DPP)<sub>2</sub>, PhDMe(DPP)<sub>2</sub>, and Ph(DPP)<sub>3</sub>, respectively. Combining the determined HOMO levels, with the optically determined bandgap, affords the LUMO level of -3.41 eV, -3.36 eV and -3.29 eV, for Ph(DPP)<sub>2</sub>, PhDMe(DPP)<sub>2</sub> and Ph(DPP)<sub>3</sub>, respectively. The frontier orbitals obtained by combining the electrochemical HOMO and the optical bandgap afforded a LUMO level, which is not deep enough for the SMs to work efficient as an acceptor for the donor polymer P3HT. As the energy levels of P3HT has been determined to be -3.20 eV and -5.14 eV, for the LUMO and HOMO, respectively. While the 0.3 eV criterion is not met by LUMO levels determined by the optical bandgap, using the LUMO levels obtained by CV afforded slightly different LUMO levels being -3.52 eV, -3.65 eV and -3.55 eV, for Ph(DPP)<sub>2</sub>, PhDMe(DPP)<sub>2</sub> and Ph(DPP)<sub>3</sub>, respectively. These electrochemically obtained LUMO levels, meets the criteria, thus it is expected to facilitate an efficient energy transfer, therefore being suitable acceptors to blend with the state-of-art light harvesting materials P3HT.

Table 17: The summarized photo-physical data for the three small molecules Ph(DPP)<sub>2</sub>, PhDMe(DPP)<sub>2</sub> and Ph(DPP)<sub>3</sub>.

Name	$\lambda_{\text{onset}}$	$E_{\text{g}}^{\text{optical}}$ [eV]	$E_{\text{HOMO}}$ [eV]	$E_{\text{LUMO-opt}}$ [eV]	$E_{\text{LUMO-cv}}$ [eV] <sup>a</sup>	$E_{\text{g}}^{\text{cv}}$ [eV] <sup>b</sup>
Ph(DPP) <sub>2</sub>	707.6	1.75	-5.16	-3.41	-3.52	1.64
PhDMe(DPP) <sub>2</sub>	679.6	1.82	-5.18	-3.36	-3.65	1.53
Ph(DPP) <sub>3</sub>	637.4	1.95	-5.24	-3.29	-3.55	1.69

<sup>a</sup>) calculated from reduction by formula  $E_{\text{LUMO}} = -(E_{\text{red}} + 4.8 - 0.4) \text{ eV}$ , the 0.4 being the halfway potential of fc/fc+ redox-pair <sup>b</sup>)  $E_{\text{g}}^{\text{cv}} = E_{\text{HOMO}} - E_{\text{LUMO}}$

The electrochemically obtained LUMO levels in turn result in electrochemical bandgap, which is quite different from the optical acquired bandgap of 1.64 eV / 756 nm, 1.53 eV/810 nm and 1.69 eV / 733 nm, for Ph(DPP)<sub>2</sub>, PhDMe(DPP)<sub>2</sub> and Ph(DPP)<sub>3</sub>, respectively. The reason to the apparent decreased electrochemical bandgap compared to the optical ones, are mainly caused by strong intermolecular interactions ( $\pi$ - $\pi$  stacking) in films where the SMs were casted on the electrode.

#### 4.2.3. DEVICE PERFORMANCE

Small area spin coated PV devices were fabricated for investigation on active layer materials composed of P3HT and our synthesized acceptor materials, Medium area sized roll coated devices were also made for scaling up PV cells for the future.

### 4.2.3.1 Small area spincoated devices

As described in 4.1.1.3, the small area devices were constructed using the device structure: ITO/PEDOT:PSS/AL/PFN/Al. The SMs are tested against P3HT as donor. The summarized device data can be seen in Table 18, it was found via optimization that the optimal ratio between the donor (P3HT) and acceptor (the SM) was 1:1.5 weight equivalents. This optimum is determined using PhDMe(DPP)<sub>2</sub> and was then applied to the two other materials.

Table 18: The summarized spin coated device data for the three small molecules Ph(DPP)<sub>2</sub>, PhDMe(DPP)<sub>2</sub> and Ph(DPP)<sub>3</sub> with various D:A weight ratios (the D being P3HT). The active layer was spin coated from CHCl<sub>3</sub> unless stated.

Material	Ratio [D:A]	Annealing[°C]	V <sub>oc</sub> [V]	I <sub>sc</sub> [mAcm <sup>-2</sup> ]	FF[%]	PCE[%]
PhDMe(DPP) <sub>2</sub>	1:1	-	0.83	0.16	28.7	0.04
		80	0.81	1.30	31.0	0.33
		100	1.02	1.01	33.2	0.34
	1:1.5	-	1.13	0.31	26.4	0.04
		<b>80</b>	<b>1.13</b>	<b>1.54</b>	<b>37.3</b>	<b>0.65</b>
		90	1.14	1.26	41.1	0.61
		90 <sup>a</sup>	1.15	1.23	43.2	0.61
		90 <sup>b</sup>	1.09	0.86	38.7	0.36
		100	0.99	1.17	33.6	0.39
		100	0.99	1.17	33.6	0.39
	1:2	-	0.80	0.09	27.5	0.02
		80	0.36	1.33	29.0	0.14
100		0.89	0.94	33.8	0.29	
Ph(DPP) <sub>2</sub>	1:1.5	-	1.13	0.27	26.0	0.08
		80	1.10	1.25	28.4	0.39
		<b>90</b>	<b>1.10</b>	<b>1.45</b>	<b>30.0</b>	<b>0.48</b>
Ph(DPP) <sub>3</sub>	1:1.5	-	1.18	0.15	26.7	0.05
		80	1.18	0.84	23.4	0.23
		<b>90</b>	<b>1.17</b>	<b>1.07</b>	<b>24.8</b>	<b>0.31</b>

<sup>a</sup>) Solvent chlorobenzene (CB) <sup>b</sup>) Solvent dichlorobenzene (DCB)

Different annealing temperatures have been tested and the optimum annealing temperature was found to be 90°C. The maximum performance obtained for any of the three SM acceptors was of 0.65% for PhDMe(DPP)<sub>2</sub> with a  $V_{oc}$  of 1.13 V,  $J_{sc}$  of 1.54  $\text{mAcm}^{-2}$  and a fill factor of 37.3 %. The highest  $V_{oc}$  obtained for PhDMe(DPP)<sub>2</sub> was obtained using CB as solvent rather than  $\text{CHCl}_3$ , with a  $V_{oc}$  of 1.15 V. The second highest performing material was the Ph(DPP)<sub>2</sub> with an efficiency of 0.48 % under the similar conditions as PhDMe(DPP)<sub>2</sub>, the efficiency was obtained with a  $V_{oc}$  of 1.10 V, a  $J_{sc}$  of 1.45  $\text{mAcm}^{-2}$  and a fill factor of 30.0%. This being higher than the efficiency obtained for the Ph(DPP)<sub>3</sub>; that only achieved an efficiency of 0.31%, with a  $V_{oc}$  of 1.17,  $J_{sc}$  of 1.07  $\text{mAcm}^{-2}$  and a FF of 24.8%. The reason that Ph(DPP)<sub>3</sub> has the highest  $V_{oc}$  derives from the relative deeper HOMO compared to the two other SM materials.

Generally the  $V_{oc}$  of these small molecule acceptors are high, all exceeding 1.1 V. This increase in  $V_{oc}$  derives from the deep LUMO levels of the SM acceptors, and the low HOMO of P3HT. But despite for very high  $V_{oc}$ , the issue with the performance is primarily associate with the low  $J_{sc}$  which only reaches a mere 1.54  $\text{mAcm}^{-2}$  (for PhDMe(DPP)<sub>2</sub>) this is assumed to derive either from an unfavorable film morphology (resulting in a small D/A interface), or a lack of  $|\Delta\text{LUMO}_{\text{acceptor}} - \text{LUMO}_{\text{donor}}|$  potential.

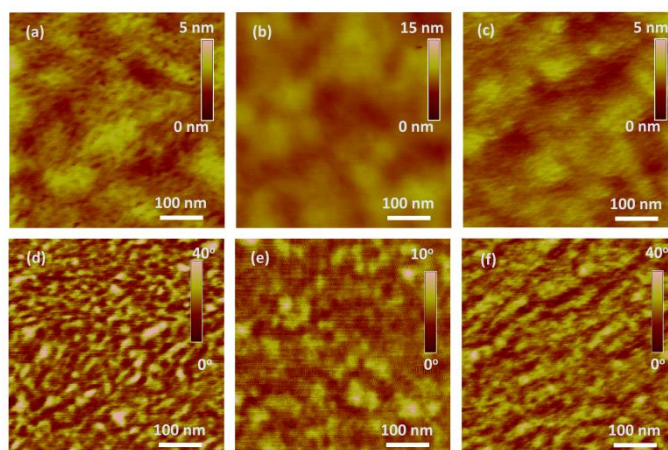


Figure 56: The AFM images both topographic (a, b and c) and phase (d, e and f) of the SM films were of the SM; Ph(DPP)<sub>2</sub> (a,d), PhDMe(DPP)<sub>2</sub> (b,e) and Ph(DPP)<sub>3</sub> (c,f). The films were of the best performing devices.

As indicated from the AFM images in Figure 56, there is not a large phase separation, even though some slightly elongated phases are present in the images of the matrix containing Ph(DPP)<sub>3</sub> (c and f). Meaning that the low performance must derive from the lack of potential to ensure charge separation. This lack of charge separation potential strengthens the notion that using the optical bandgap to estimate the LUMO level, as according to the electrochemical LUMO the  $|\Delta\text{LUMO}_{\text{acceptor}} - \text{LUMO}_{\text{donor}}|$  difference was all above the optimal difference of approximately 0.3 eV. While the optical showed  $|\Delta\text{LUMO}_{\text{acceptor}} - \text{LUMO}_{\text{donor}}|$  difference of 0.09-0.2 eV thus explaining the lack of current in the devices.

Despite the relative low performance of the devices, the goal of this study was to increase the active area of the device from the 9 mm<sup>2</sup> to 1cm<sup>2</sup>. Therefore using the optimal ratio, roll-coated devices were made.

#### 4.2.3.2 Roll coated devices

Using the procedure described in section 2.2.1.3, Roll-coated devices have been fabricated, the devices where of the inverted geometry, and were constructed using either a 3 layer top electrode or a single layer top electrode (as described before (2.1.3)).

The OPV performance can be seen in Table 19 and Figure 57, it can be seen that the highest performance achieved was 0.229 % for Ph(DPP)<sub>3</sub> while the lowest maximum efficiency was PhDMe(DPP)<sub>2</sub> with a performance 0.022%. This is interesting as the ranking of these are the opposite of the findings for the spin coated devices, were the order of most efficient was PhDMe(DPP)<sub>2</sub>>Ph(DPP)<sub>2</sub>>Ph(DPP)<sub>3</sub>.

*Table 19: The summarization of performance data of the roll-coated OPV (all in the D:A ratio of 1:1.5), the values are the average of 4 measured devices*

Material	J <sub>sc</sub> [mAcm <sup>-2</sup> ]	V <sub>oc</sub> [V]	FF[%]	PCE[%]	PCE [%](best)
Ph(DPP) <sub>3</sub>	-0.833±0.039	0.690±0.026	36.38±2.58	0.204±0.023	0.229
PhDMe(DPP) <sub>2</sub>	-0.148±0.009	0.398±0.048	32.34±1.99	0.019±0.002	0.022
Ph(DPP) <sub>2</sub>	-0.577±0.072	0.646±0.006	32.72±0.51	0.122±0.015	0.135

Ph(DPP)<sub>3</sub> obtained an average PCE of 0.20 % with a V<sub>oc</sub> of 0.69 V, a J<sub>sc</sub> of 0.83 mAcm<sup>-2</sup> and FF of 36%, Ph(DPP)<sub>2</sub> gained an average PCE of 0.12 % with a V<sub>oc</sub> of 0.65 V, J<sub>sc</sub> of 0.58 mAcm<sup>-2</sup> and FF 33 % and lastly the PhDMe(DPP)<sub>2</sub> achieved an average PCE 0.02% via a V<sub>oc</sub> of 0.40 V, J<sub>sc</sub> of 0.15 mAcm<sup>-2</sup> and a FF of 32%. Both the J<sub>sc</sub> and the V<sub>oc</sub> is lower than the ones obtained for spin coated devices. The characteristic that was praised mostly was the high V<sub>oc</sub> exceeding 1.1 V for the spin coated cells, however those were not maintained in the roll-coated devices which reached a maximum V<sub>oc</sub> of 0.69V. This lower voltage could derive from an increased shut resistance as a result of either silver spikes of the applied electrode or bad film formation; or possibly also being a combination of both these. The loss could also simply derive from the change in device geometry.

It should be noted that the roll coated devices are without uses of ITO electrode as the front electrode or the application vacuum deposited back electrodes. This seen in the light of the change of order in regards of efficiency, this could also be derived from a change the morphology of the film.

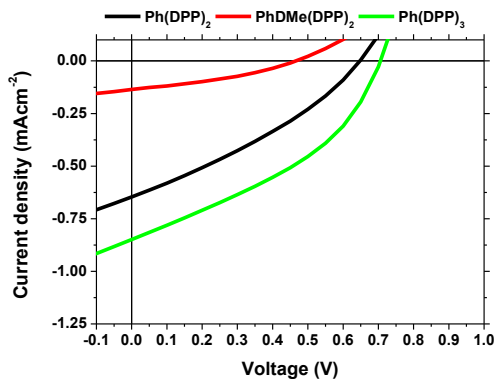


Figure 57: I-V characteristics of the roll coated devices with the active layer consisting P3HT : Small molecule acceptor in the ratio 1:1.5 ( $\text{Ph(DPP)}_2$  (black),  $\text{PhDMe(DPP)}_2$  (red) and  $\text{Ph(DPP)}_3$  (green)) coated from  $\text{CHCl}_3$ . Adapted from paper IV.

The  $J_{\text{sc}}$  is a result of multiple factors of the active layer of the device; therefore the change in hierarchy of materials most likely does not lead to the charge separation potential of the different SM acceptors, but most likely from either the different device geometries or the different processing technologies. Changing the device geometry primarily switches the direction of the current in the devices and the electrode materials. The changes of electrode materials will in certain change the maximum obtainable potential and therefore maximal obtainable PCE. But this again should not change the order of efficiency as it will not affect the active layer dynamics in regards to the internal charge separation. Therefore the largest difference between (neglecting the different change in area) is the evaporation speed of the active layer in the roll coated and spin coated devices, respectively. The evaporation of the active layer solution in the spin coating is nearly instantly, while the evaporation rate is slightly lower in roll coated procedure this will most likely result in a larger phase separation for the molecules that have the largest intermolecular interactions, this being the planar  $\text{Ph(DPP)}_2$ ; thus affording a lower D/A phase interface-area resulting in a lower current. But again this does not fully explain the observed current characteristics, as  $\text{Ph(DPP)}_2$  and  $\text{Ph(DPP)}_3$  performs superior to  $\text{PhDMe(DPP)}_2$ .

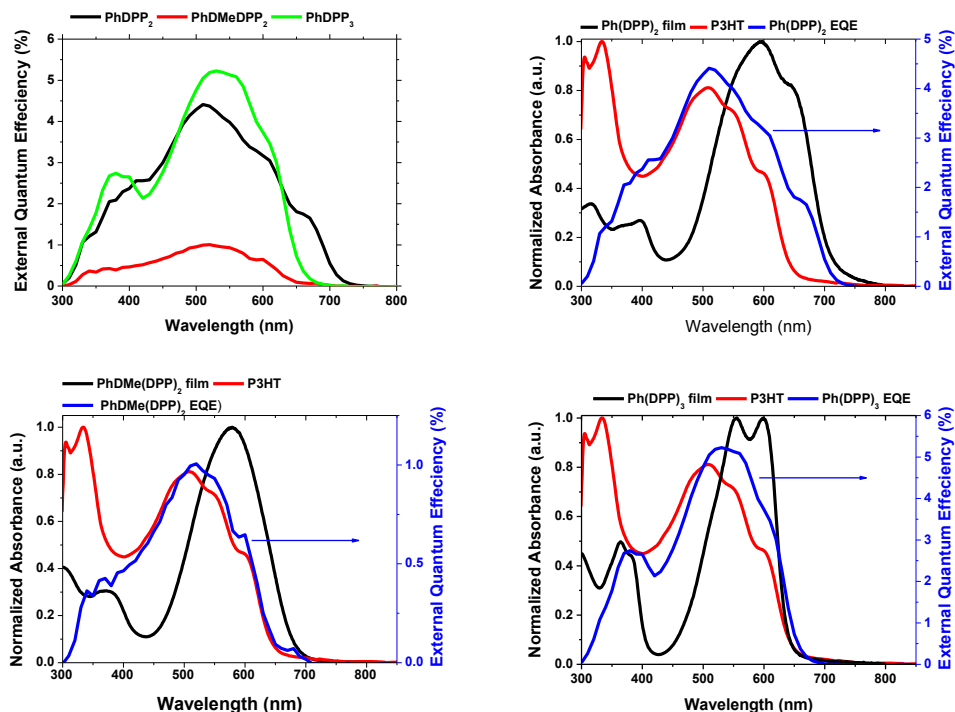


Figure 58: In the upper left corner, the external quantum efficiency (EQE) for the best performing SM devices containing  $(\text{Ph}(\text{DPP})_2)$  (black),  $\text{PhDMe}(\text{DPP})_2$  (red) and  $\text{Ph}(\text{DPP})_3$  (green) coated from  $\text{CHCl}_3$  adapted from paper IV. The upper right, and lower left and right are the EQE plots (blue) of the respective polymers, together with the absorbance of P3HT (red) and the given SM (black).

The difference could be found in what extent the SM is involved in the generation of photocurrent; this can be quantified using EQE measurements as seen in Figure 58. In Figure 58 (the upper left) it is clear that the maximum obtained EQE is for  $\text{Ph}(\text{DPP})_3$  (~5.5 % at 525 nm), followed by  $\text{Ph}(\text{DPP})_2$  (~4.5% at 500 nm), and  $\text{PhDMe}(\text{DPP})_2$  (~1% at 510 nm). The differences between the materials are especially interesting when observing the correlation between absorbance and the three different SMs and the donor P3HT. It can be seen that the onset of the EQE of  $\text{Ph}(\text{DPP})_2$  containing devices (upper right in Figure 58) correlates with the absorbance of the SM, thus showing that the SM is actively participate in the absorbance of photons, and thus increasing the overall efficiency of these devices. While this is also the case for  $\text{Ph}(\text{DPP})_2$ . For the device containing  $\text{PhDMe}(\text{DPP})_2$  (lower left in Figure 58) the progression of the EQE only correlates with the P3HT in these devices affording an explanation of low performance of these devices. The lack of involvement of the  $\text{PhDMe}(\text{DPP})_2$  is especially clear, as the onset of the EQE is approximately 50 nm lower than that  $\text{PhDMe}(\text{DPP})_2$ . For the device utilizing the  $\text{Ph}(\text{DPP})_3$  as acceptor (lower right in Figure 58), the onset of the EQE and the absorbance of  $\text{Ph}(\text{DPP})_3$  correlates, but as the onset of  $\text{Ph}(\text{DPP})_3$  and P3HT are comparable, the effect of the SM acceptor in regards to the generation of photocurrent is not definitively observed. But the effect and involvement is observed due to the secondary maximum at 380 nm of the measured EQE, still which is combined with the relative higher EQE of  $\text{Ph}(\text{DPP})_3$ .

Another important parameter of the OPV technology is the lifetime of these device, these can be used to estimate the stability of the SM acceptors. The results of the lifetime studies can be seen in Figure 59 and the maximum performance for the three devices can be seen in Table 20.

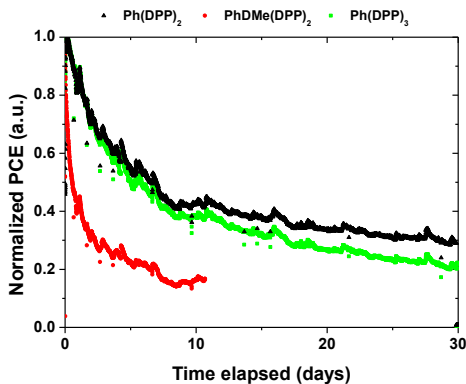


Figure 59: The normalized PCE as function of time for the devices containing the three small molecules acceptors:  $(Ph(DPP)_2)$  (black),  $PhDMe(DPP)_2$  (red) and  $Ph(DPP)_3$  (green). The  $PhDMe(DPP)_2$  device lost connection approximately at the 11<sup>th</sup> day. Adapted from paper IV.

The devices tested in ambient conditions under a continuous illumination of a 1.5 AM sun simulator, and after 11 days  $PhDMe(DPP)_2$  suffered a fatal defect and disconnected from the testing system. But what is notable is that the efficiency of all the devices initially increased as function of the exposure to the light; the efficiency increases from 0.022 % to 0.04 % for  $PhDMe(DPP)_2$ , 0.135% to 0.429% for  $Ph(DPP)_2$  and 0.229% to 0.538% for  $Ph(DPP)_3$ . This increment derives from both an increase in  $J_{sc}$  and  $V_{oc}$  as seen in Table 20, where  $Ph(DPP)_3$  obtained a  $V_{oc}$  of 0.82V and  $J_{sc}$  of  $-1.5 \text{ mAcm}^{-2}$ ,  $Ph(DPP)_2$  obtained a  $V_{oc}$  of 0.80V and  $J_{sc}$  of  $-1.2 \text{ mAcm}^{-2}$ , and  $PhDMe(DPP)_2$  afforded a  $V_{oc}$  of 0.54V and  $J_{sc}$  of  $-0.19 \text{ mAcm}^{-2}$ . Lafalce *et al.*[149] described that this increase basically involved three processes; the photo induced desorption of adsorbed oxygen, filling of charges traps and thermal activation of trapped charges. The initial desorption of oxygen afforded by the illumination can according to Lafalce *et al.* result in a reversible oxidation of the active layer that results in a p-doping, this was shown for P3HT (the donor of this system) resulting in an initial increase of efficiency [149]. But this is counter acted by the irreversible oxidation of the active layer that reduces the efficiency and finally becomes fatal for the device performance. The findings of this study shows the same trends as the processes discussed by Lafalce *et al.*, as for all the devices an initial spike in efficiency is observed and followed by the burn-in period of about ten days for the device. The large efficiency spike which is suspected to derive from desorption of oxygen falls well in line with these devices were fabricated under ambient atmosphere.

Table 20: The maximum obtained data from the lifetime experiments of three SM acceptor devices. Adapted from paper IV.

Device	Time [s] (hrs)	Isc[mAcm <sup>-2</sup> ]	Voc[V]	FF[%]	PCE[%]
Ph(DPP) <sub>3</sub>	16750 (4.65)	-1.484	0.815	35.76	0.538
PhDMe(DPP) <sub>2</sub>	564 (0.16)	-0.185	0.543	32.59	0.040
Ph(DPP) <sub>2</sub>	16470 (4.57)	-1.219	0.802	350	0.429

### 4.3. SUMMARZATION

Three simple none-fullerene acceptors have been successfully synthesized. The small molecules were obtained via Suzuki cross-coupling between 3-(5-bromothiophen-2-yl)-2,5-bis(2-ethylhexyl)-6-(thiophen-2-yl)pyrrolo[3,4-c]pyrrole-1,4(2H,5H)-dione and a boron acid ester; 1,4-bis(4,4,5,5-tetramethyl-1,3,2-dioxaborolan-2-yl)benzene to afford Ph(DPP)<sub>2</sub>, 2,2'-(2,5-dimethyl-1,4-phenylene)bis(4,4,5,5-tetramethyl-1,3,2-dioxaborolane) to afford PhDMe(DPP)<sub>2</sub> and 1,3,5-tris(4,4,5,5-tetramethyl-1,3,2-dioxaborolan-2-yl)benzene to afford Ph(DPP)<sub>3</sub>. The molecular structure of these three small molecules have been investigated and confirmed by <sup>1</sup>H and <sup>13</sup>C NMR and MALDI-TOF MS. The materials showed melting points of 234 °C, 206 °C and 226 °C for Ph(DPP)<sub>2</sub>, PhDMe(DPP)<sub>2</sub> and Ph(DPP)<sub>3</sub>, respectively, indicating their purity and crystallization ability. Their thermal stabilities are exceeding 300 °C. Molecular simulations showed dihedral angles from the center moiety to the DPPs to be 21.6°, 44.6° and approximately 26°, for Ph(DPP)<sub>2</sub>, PhDMe(DPP)<sub>2</sub> and Ph(DPP)<sub>3</sub>, respectively. This increase in angle showed an effect on the molecular dynamics of the molecules. The frontier orbital of the small molecule acceptors where determined to be (HOMO/LUMO) -5.15 eV/-3.41 eV, -5.16 eV/-3.36 eV and -5.24 eV / -3.29 eV, for Ph(DPP)<sub>2</sub>, PhDMe(DPP)<sub>2</sub> and Ph(DPP)<sub>3</sub>, respectively. The optical bandgaps where determined to be; 707 nm/1.75 eV, 679 nm/1.82 eV and 637 nm/1.95 eV for Ph(DPP)<sub>2</sub>, PhDMe(DPP)<sub>2</sub> and Ph(DPP)<sub>3</sub>, respectively. The SMs were tested both in a convention normal geometry small area spin coated device and the inverted geometry medium area roll coated device which were ITO free and produced in ambient conditions without the usage of vacuum techniques.

The SMs were tested as acceptor against P3HT. The maximum performance obtained for any of the three SM acceptors was of 0.65% for PhDMe(DPP)<sub>2</sub> with a V<sub>oc</sub> of 1.13 V, J<sub>sc</sub> of 1.54 mAcm<sup>-2</sup> and a FF of 37.3 %. While Ph(DPP)<sub>2</sub> obtained an PCE of 0.48 % with a V<sub>oc</sub> of 1.10 V, a J<sub>sc</sub> of 1.45 mAcm<sup>-2</sup> and a FF of 30.0% and Ph(DPP)<sub>3</sub> only achieved an efficiency of 0.31%, with a V<sub>oc</sub> of 1.17 V, a J<sub>sc</sub> of 1.07 mAcm<sup>-2</sup> and a FF of 24.8%. Interestingly all three molecules showed high V<sub>oc</sub> all exceeding 1.1 V, which is expected to derive from the deep homo levels of SM acceptors. The reasons for the relative low efficiencies derive from low photo currents, which most likely derive from a low potential difference between the LUMO<sub>donor</sub> and LUMO<sub>acceptor</sub>. Despite the relative low efficiencies, the SM where still tested in roll coated devices. These afforded the following PCEs for; Ph(DPP)<sub>3</sub> obtained an average PCE of 0.20 % with a Voc of 0.69 V, a J<sub>sc</sub> of 0.83 mAcm<sup>-2</sup> and FF of 36%, Ph(DPP)<sub>2</sub> gained

an average PCE of 0.12 % with a  $V_{oc}$  of 0.65 V,  $J_{sc}$  of  $0.58 \text{ mAcm}^{-2}$  and FF 33 % and lastly the PhDMe(DPP)<sub>2</sub> achieved an average PCE 0.02% via a  $V_{oc}$  of 0.40 V, a  $J_{sc}$  of  $0.15 \text{ mAcm}^{-2}$  and a FF of 32%. As it can be seen the SM that performed the worst in the spin coated device (Ph(DPP)<sub>3</sub>) performed the best in the roll coated devices, and vice versa. It should be noted that the high  $V_{oc}$  found for the spin coated devices were not found in the roll coated devices, as the  $V_{oc}$  obtained was 0.65 V, 0.40 V and 0.69 V, for Ph(DPP)<sub>2</sub>, PhDMe(DPP)<sub>2</sub> and Ph(DPP)<sub>3</sub>, respectively, while all exceeded 1.1 V in the spin coated devices.

An EQE experiment showed that for Ph(DPP)<sub>2</sub>, and Ph(DPP)<sub>3</sub>, the SM contributed to the generation of the photocurrent, this was not the case for PhDMe(DPP)<sub>2</sub>, explaining the relative lower efficiency of this SM compared to the others in the roll coated devices. A life-time study was conducted and it was found that after an during burn in period the efficiency of the tested devices increases from 0.022 % to 0.04 % for PhDMe(DPP)<sub>2</sub>, 0.135% to 0.429% for PhDPP<sub>2</sub> and 0.229% to 0.538% for Ph(DPP)<sub>3</sub>. This increase is followed by a slower decrease in efficiency. These tendencies are all ascribed to the processing in ambient atmosphere. Interestingly the  $V_{oc}$  of these devices increased to 0.80V, 0.54 V and 0.82V for Ph(DPP)<sub>2</sub>, PhDMe(DPP)<sub>2</sub> and Ph(DPP)<sub>3</sub>, respectively, the origin of this increase is unclear. The synthesis and testing of the small array of SM none-fullerene acceptors show that aligning the energy levels is enough when designing a SM acceptor. The molecular geometry also plays an important role in the performance of these devices.

# CHAPTER 5. NANOPARTICLES VIA *IN SITU* MICRO-EMULSION POLYMERIZATION TOWARDS WATER PROCESSABLE OPVS

## 5.1. MOTIVATION

When discussing the commercialization of OPV, the first and most pressing issue is certainly the relative low performance and poor stability of the OPVs compared to the readily available inorganic counterparts. But as often mentioned throughout this entire thesis, there is and have been continuous focus on the development of well performing devices with efficiencies exceeding 10 % for BHJ based devices. While groups such as F.C. Krebs (at Technical University of Denmark) have pioneered the out-phasing of ITO based electrodes, as the embodied energy and scarcity of ITO would be a large issue in regards to the energy pay-back time (EPBT) of OPV devices[31], [143]. This change in electrodes from ITO to a suitable electrode constellation in combination with the vacuum-free utilization has lowered the embodied energy significantly. But a large factor that still has to be addressed is the usage of organic solvents such as chloroform, chlorobenzene (CB), di-chlorobenzene, toluene, isopropanol, or acetone. These solvents are not only non-environmental friendly, but also a health risk as some of these solvents are suspected of being carcinogenic. Another very important parameter of the organic solvents that need to be considered is their embodied energy, for example, 36.5 MJ kg<sup>-1</sup> for isopropanol[150], 21.42 MJ kg<sup>-1</sup> for toluene[151], and 159 MJ kg<sup>-1</sup> for CB [143]. Comparing these embodied energies to that of water, being 19 kJ kg<sup>-1</sup> [152], there certainly is some energy to be saved, from circumventing the application of these energy intensive solvents. Therefore, it could be advantageous to investigate different strategies for applying an aqueous processing to avoid some or the majority of these undesirable solvents.

Generally, there are two concepts to move the materials towards water based processing. First, modifying the monomers, via the introducing of either non-ionic sidechains such as PEG[153] or hydroxy functionality, or via introduction of ionic side chains such as carboxylic acid, ammonium [154], phosphates[155], sulfuric acids or even zwitterion functionality [156]. In 2011 Søndergaard *et al.*[153] showed an example of the firstly mentioned technique; where a polythiophene modified with a thermo-cleavable PEG sidechain, which is allowed for water processing while removing sidechain components during post processing. The resulting device had an efficiency of 0.7%. More recently Zhang *et al.*[157] reported an application of a water/alcohol-soluble conjugated copolymer consisting of a 9,9-bis(6'-(N-diethylamino)propyl)-fluorene and 9,9-bis(3-ethyl(oxetane-3-ethyloxy)-hexyl)-fluorene, while this polymer is not incorporated in the active layer, the polymer itself is processable in water and used as an interface-layer between the active layer and the electron transport layer, the resulting devices had an efficiency of 9.28%. A major disadvantage with the monomer modification approach is that when doing so, it results in large changes in the film morphology that in turn will change the approach of which the film morphology is formed. Therefore, it would be advantageous to employ native unmodified  $\pi$ -conjugated polymers through two major design-strategies being via precipitation and micro-emulsion.

### 5.1.1. PRECIPITATION TECHNIQUE

The most straight forward approach is called reprecipitation or even nano-precipitation. This technique is basically to pour a polymer solution in a good solvent (often THF[158], [159]) into a non-solvent, which could be water for the conjugated polymers. The non-solvent should be miscibility with the good one. The concept (seen in Figure 60) is that the sudden drop in solubility, going from a good to a poor solvent mixture will result in precipitation and particle size control could be obtained under given high enough shear, this could afford a precipitate in nanometer-scale[158]. This technique has been reported by Szymanski *et al.*[160] in 2005; where they showed that using the above mentioned technique on poly[2-methoxy-5-((2-ethylhexyl)oxy)-*p*-phenylenevinylene] (MEH-PPV) afforded nanoparticles in the diameter range of 5-30 nm with the majority of the particles populating the diameter range of 5-10 nm, indicating that these consist of only one polymer molecule, according to Szymanski *et al.*[160]. In 2007 Wu *et al.*[161] showed the versatility of the method by preparing nanoparticles of the homopolymer poly(9,9-dihexylfluorenyl-2,7-diyl) and the copolymer poly[(9,9-dioctyl-2,7-divinylene-fluorenylene)-alt-co-(2-methoxy-5-(2-ethylhexyloxy)-1,4-phenylene)] (PFPV) affording particles in a diameter range of 5-50 nm. It is worth noticing that none of the polymers mentioned above has been involved in any modification/functionalization. The formation of these nano-scale precipitates are mainly attributed to the hydrophobic effect, induced by the rapid change of solvations [158]. The particle diameter is primarily controlled by the polymer concentration in the good solvent. The origin of the stabilizing effects are unclear, as there are not employed any emulsifier/surfactant, that ensures the thermodynamically stabilization of the particles[159]. As the stabilization on particle sizes is an issue and the concentration of the final material is rather low, this will potentially be problematic in fabrication of OPV devices.

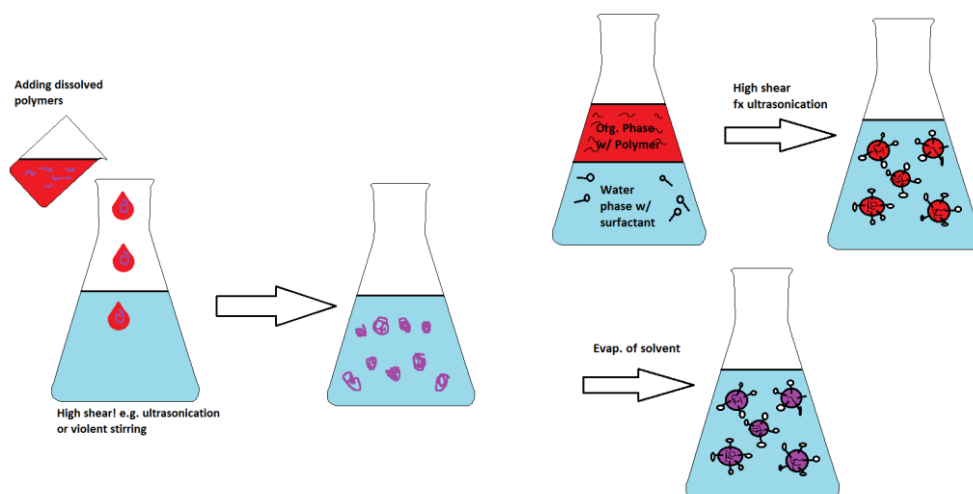


Figure 60: A schematic illustration of precipitation technique (left) and the micro-emulsion technique (right), both are inspired by Tuncel and Demir [158].

### 5.1.2. MICRO-EMULSION TECHNIQUE

This method was pioneered by Landfester and co-workers who presented the versatility of the method in the fabrication of nanometer scaled particles[162], [163]. The micro-emulsion technique is rather similar to that of the precipitation (seen in 5.1.1), the two major differences being the presence of a surfactant in the water phase and the application of a water immiscible solvent for the emulsion technique (shown in Figure 60). A standard procedure is: a solution of a given polymer in a minimum amount of solvent like CB or chloroform is added into an aqueous solution of surfactant usually the ionic sodium dodecyl sulfate (SDS) or non-ionic surfactant such as polyoxyethylene or sorbitan monolaurate (polysorbate, TWEEN). The addition of the polymer solution is done under shear induced by stirring and sometimes via the exposure to sonication, after the sonication the solvent can be removed by elevating the temperature for an extended period of time, affording solid nanoparticles consisting of conjugated polymer and surfactant. The aggregation is prevented either by electro static charges of the surface of the particles (applying ionic surfactants) or by steric hindering, these surfactants are normally amphiphilic meaning they have both a lipophilic and a hydrophilic part, thus the material located in the water – oil interface. In the case of hydrophobic materials in nanoparticles, the lipophilic parts will be oriented facing inwards while the hydrophobic part will face outwards. This orientation affords colloidal stabile nanoparticles. In 2003 Kietzke *et al.* [162] showed the fabrication of nanoparticles consisting of polymer blends and further more showed the potential towards the usage of these in OPV. They showed that forming nanoparticles and then subsequently process these from an organic solvent, would maintain the morphology of the particles. The organic solvent used was xylene which is a relative poor solvent for conjugated polymers. And issue with this approach is that, despite succeeding in producing these nanoparticles, the relative large amounts of organic solvents during the production, which though should be recyclable.

The first successfully full R2R aqueous processed LBG polymer particles where reported by Andersen *et al.* [36] in 2011 showing functional devices. This was done using the basics of the method presented by the Landfester group[162]. Andersen *et al.* showed fully R2R processed devices with a PCE around 0.55% for the poly[(4,4`-bis(2-ethylhexyl)-dithieno[3,2-b:2',3'-d]silole)-2,6-diyl-alt-(2,1,3-benzothiadiazole)-4,7-diyl] in combination with PC<sub>61</sub>BM as the acceptor, the area of the measured devices are 4 cm<sup>2</sup>[36]. Although the work of Andersen *et al.* showed a tremendous potential, it still involved conjugated polymers, obtained via large number of synthetic steps and extensive purification, and large amount of these organic solvents (though it should be noted that these solvents can be recycled[36]).

### 5.1.3. MICRO-EMULSION POLYMERIZATION

The micro-emulsion methodology in combination with polymerization techniques could show a promising path away from the solvent intensive processing methods for conventional uses. Traditional emulsion polymerization has been limited to the chain reaction of vinyl polymerization[164]. Baier *et al.*[164] in 2009 showed that conjugated polymer could be synthesized in an aqueous system via the Glaser coupling of different biethynyl-substituted aromatic monomers, affording fluorescent nanoparticles.

The copper-based catalyst utilized hydrophobic ligands to ensure solubility in the organic phase. This approach afforded high molecular weight polymers, some of these polymers exhibited a low solubility when tried to resolubilized in organic solvents[164]. The synthesized particles showed diameters in the range of 30 nm. Using the same procedure, Huber *et al.* [165] reported Sonogashira polymerization of diethynyl and dibromo monomers for D-A style polymers with a Pd-based catalyst. They further highlights the advances of efficiently fabricated polymers that become insoluble after the processing steps, such as coating[165]. Compared to the work of Søndergaard *et al.* where the polymer was rendered insoluble via thermal cleavage, this elaborated synthesis might be avoidable via the usage of micro-emulsion approach[153]. Both the discussed micro-emulsion systems involves the usage of diethynyl monomers, which are not the frequently used monomers, as the majority of the D-A polymers reported for OPV applications, are polymerized using Stille or Suzuki cross-coupling procedures.

Wang *et al.* [166] reported the polymerization of a toluene-based micro emulsion, using the non-ionic surfactant Tween 80. One of the polymers obtained was the D-A copolymer of 2,1,3-benzothiadiazole and 9,9-dioctyl-2,7-yl-flourene, resulting in particles with diameters in the range of 200-300 nm [166]. The D-A copolymer showed similar absorbance spectrum to a control polymer, with the same structure [167][168]. Combination of the methods of Andersen *et al.*[36] and Wang *et al.*[166] for an all-in-one *in situ* polymerized nano-particles would be interesting, as this could reduce the number of overall steps for the syntheses of the nano-particles.

In this chapter the nano-particles consisting of poly(4,7-(2,1,3-benzothiadiazole)-alt-2,7(9,9-dioctylflourene)) (PBTFI) nano-particles with and without incorporating PC<sub>61</sub>BM into the nanoparticle matrix is proposed, as illustrated in Figure 61.

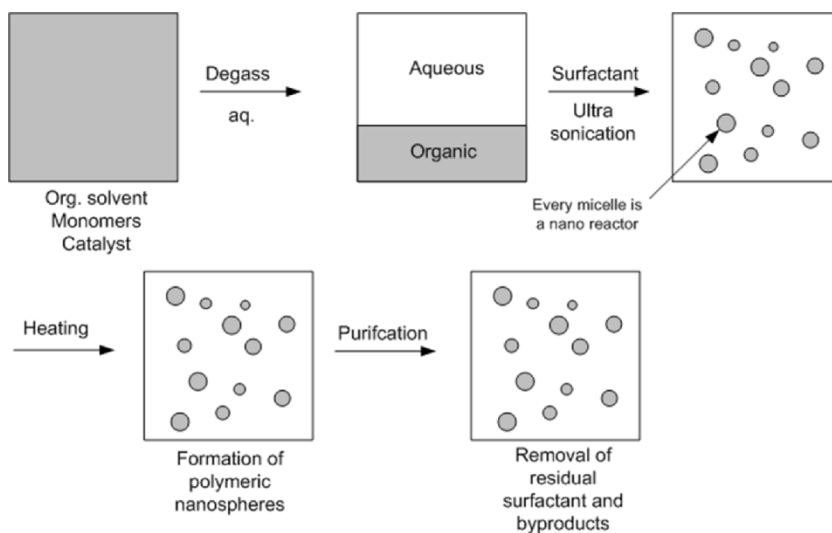


Figure 61: Flowchart of the synthesis of PBTFI nanoparticles in micro emulsion system.

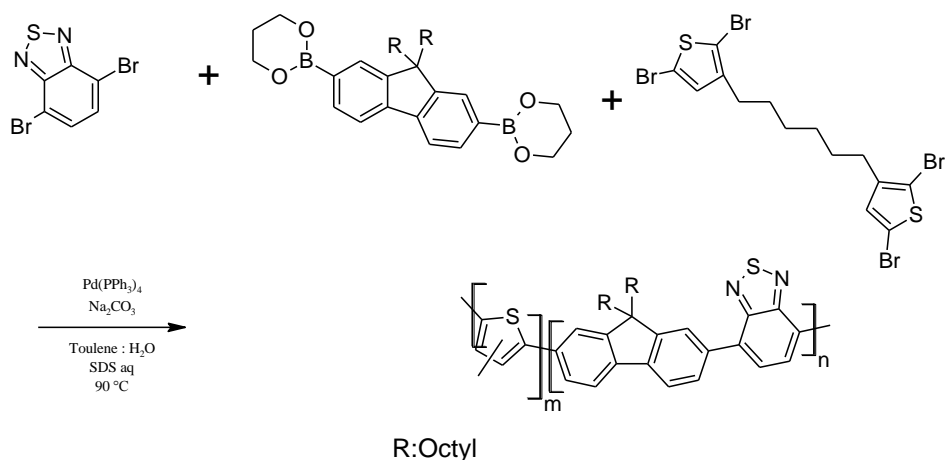
After the organic components have been completely dissolved and degassed, a degassed aqueous solution of detergent and base is added and subsequently treated by ultra-sonication (ultra sound bath). The reaction mixture is then heated for a certain reaction time. The resulting nano-spheres are then purified by means of dialysis.

## 5.2. MATERIALS AND METHODS

### 5.2.1.1 Materials

Chemicals used were of commercial grade, and used without further purification, if not state otherwise. 3,3'-hexane-1,6-diylbis(2,5-dibromothiophene) was synthesized according to literature procedure[169]. Our synthetic procedure of the micro emulsion polymerization (inspired by Wang *et al.*[166]) has been improved in regards to the use of crosslinking agent and a different surfactant.

### 5.2.1.2 Synthetic procedure



*Scheme 22: Synthesis of poly (4,7-(2,1,3-benzothiadiazole)-alt-2,7(9,9-dioctylfluorene))with the cross linker 3,3'-hexane-1,6-diylbis(2,5-dibromothiophene)via a Suzuki-cross coupling in micro emulsion.*

**PBTFI:** As shown in Scheme 22, 9,9-dioctylfluorene-2,7-bis(propanionboronate) (60 mg, 0.1 mmol), 4,7-dibromo-2,1,3-benzothiadiazole (30 mg, 0.1 mmol) and 3,3'-hexane-1,6-diylbis(2,5-dibromothiophene) (3 mg, 0.005 mmol), were dissolved in toluene (1.5 mL). Then an aqueous solution of degassed alkaline surfactant (25 mL, Na<sub>2</sub>CO<sub>3</sub> (1M) and SDS (3 w/w%)) was added. The flask was degassed twice by two consecutive freeze-pump-thaw cycles. Hereafter a catalytic amount of Pd(PPh<sub>3</sub>)<sub>4</sub> (6 mg, 5 mol%) was added under nitrogen counter flow, followed by resealing of the flask. The sealed flask was then degassed by one freeze-pump-thaw cycles. The entire solution was placed in a ultrasound bath for 1 h. The mixture was kept 48 hours in darkness at 85 °C and under nitrogen. The resulted suspension was then dialyzed against 1 L deionized water, using a cutoff of 3.5kDa. The water was changed daily for two days. The resulting polymeric solution was fluorescent yellow.

**PBTfI+PCBM:** The experimental procedure was identical with that of **PBTfI** but PC<sub>61</sub>BM (225 mg) was added together with the monomers. The resulting polymeric solution was low fluorescent yellow, and slightly darker than the PBTfI solution.

### 5.2.1.3 Methods

The particles size was determined via dynamic light scattering (DLS) on a Zetasizer Nano Z system (Malvern, USA). Scanning electron microscopy images were obtained on a Zeiss 1540XB (Carl Zeiss NTS GmbH, Germany). Fluorescence emission spectra were recorded on Varian Cary Eclipse fluorescence spectrophotometer. The absorbance spectra were obtained on a Varian Cary Eclipse absorbance spectrophotometer.

## 5.3. RESULTS AND DISCUSSION

### 5.3.1. CHARACTERIZATION OF PARTICLES

The diameter of the fabricated particles are shown in Table 21, it can be seen that the particle diameter (Z-average) are comparable, 121 nm and 132 nm, for PBTfI and PBTfI+PCBM.

Table 21: The obtained DLS data for the two polymer nanoparticles with and without PC<sub>61</sub>BM.

Sample name	PdI	PdI Width [nm]*	Z-average [nm]*
PBTfI	0.262	61.9	120.9
PBTfI+PCBM	0.302	72.4	131.8

\*diameter

The particles were slightly smaller than the ones reported by Wang *et al.* [166], which is attributed to the usage of SDS (3 w/w%) as a different surfactant, due to non-reproducibility of their work. After communication with the authors, it was found that the “TWEEN 80” used by them did not correspond to the datasheet acquired at the manufacturer of the surfactant. The one used in Wang *et al.*[166] was colorless whilst “TWEEN 80” according to the manufacturer is amber yellow [170]. The change to SDS is due to the promising results shown by Andersen *et al.* by employing it as the surfactant to afford OPVs from aqueous solutions[36].

The morphology of the synthesized polymer nano-particles were further investigated by SEM (Figure 62), the images revealed spheres with a diameter less than 200 nm.

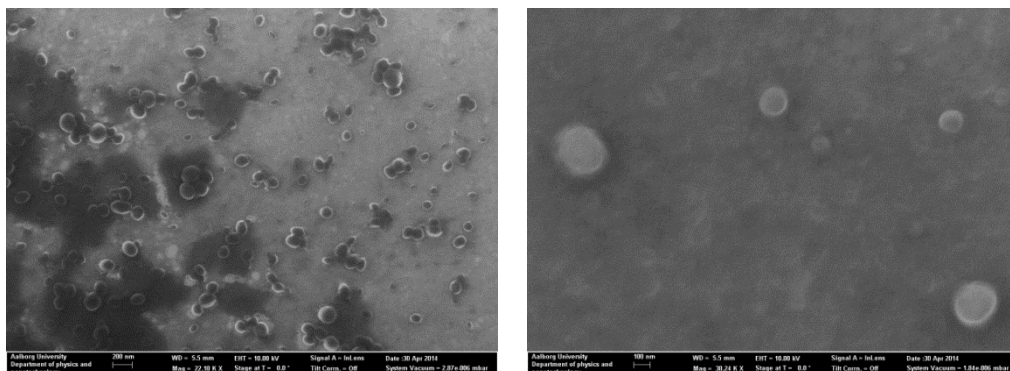


Figure 62: SEM images of the synthesized nanoparticles, the left image being of PBTFI with a scale bar of 200 nm and the right image is of the PBTFI+PCBM with a scale bar of 100 nm.

For the PBTFI particles it is evident that aggregations are, as the particles are distributed in small clusters. This is not the case for the PBTFI+PCBM particles, where the particles apparently are more uniformly distributed.

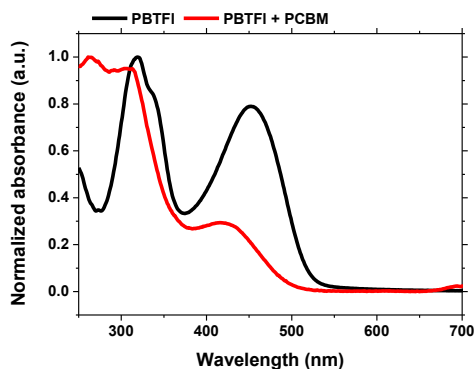


Figure 63: The absorbance spectrum of the two absorbance particle suspensions in water; PBTFI (Black) and PBTFI+PCBM (red)

In Figure 63 the absorbance spectra of the two particle suspensions are shown. The onsets of approximately 550 nm (2.25 eV) for the native PBTFI particles, are comparable with those reported in literature[171], [172]. The onset of the fullerene containing particles, are slightly lower than that of the native PBTFI particles, i.e. approximately 530 nm (2.34 eV). The lower onset of the PCBM containing particles could be due to the relative lower amount of monomer in each particle, caused by the higher overall dry matter content of the organic phase. Due to the low solubility deriving from the introduction of the crosslinking agent, SEC experiments were not performed, thus the molecular weight obtained particles where not determined. A common approach to evaluate the charge transfer is to observe, whether the excitation can be quenched by the presence of a material that efficiently result in alternative recombination route than emission of light. Therefore, fluorescence spectroscopy experiments have been conducted, where the water suspension of nano-particles have been excited at different

excitation wavelengths and the resulting emission spectrum have been recorded, as can be seen in Figure 64.

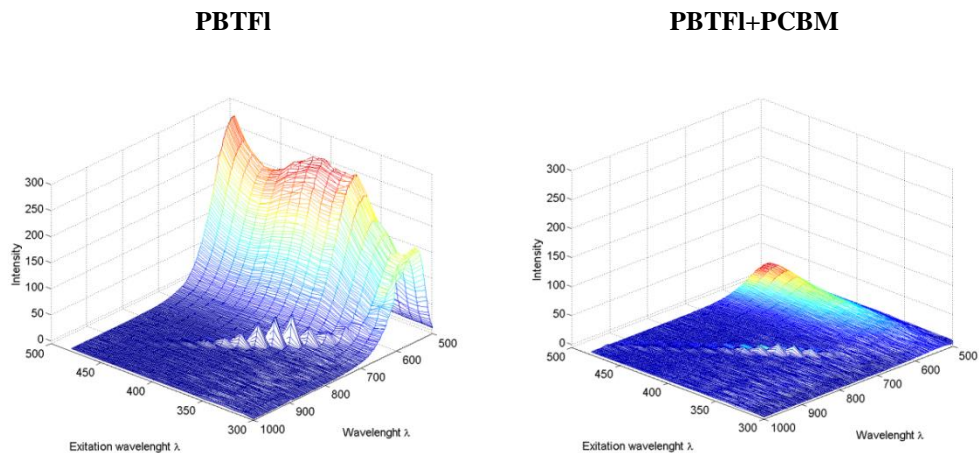


Figure 64: The Emission spectra of the two nano-particle suspensions PBTfI (left) and PBTfI+PCBM (right). The notation wavelength ( $\lambda$ ) refers to emission wavelength.

The emission spectra of the native PBTfI particles, showed two maxima in emissions intensity at excitation wavelengths 400 nm and 525 nm. The maximum wavelength of the emissions is at 550nm which corresponds to the onset of the absorbance, the intensity of the emission depends on the excitation wavelength. Which can be found to be lowered significantly as a result the incorporation of fullerene in the particles. The emission maximum at an excitation wavelength of 400 nm is nearly completely quenched, indicating a charge transfer from the excited polymer onto the fullerene within the formed nanoparticles. This charge transfer is in regards to the further usage in OPV devices, as it is essential for the functionality of the device.

### 5.3.2. ATTEMPTS TO MAKE NANOPARTICLE DEVICES

As a result of the apparent good fluorescence quenching, representing a high degree of charge transfer, OPV devices were constructed. The devices were constructed similar to that presented in 2.2.1.3. In order to coat the particles, the different additives where tested, being FSO-300, FSO-100 (FSO is an ethoxylated fluorosurfactant) and ethylene glycol (EG). It was found that a combination of FSO-100 (5 volume%) and EG (5 volume%) afforded a homogenous film. The coating was also conducted at a 90°C. Despite the overall good films the I-V characteristics of the fabricated devices did not show any photocurrent and functioned as a resistor rather than a semiconductor, this is seen in Figure 65.

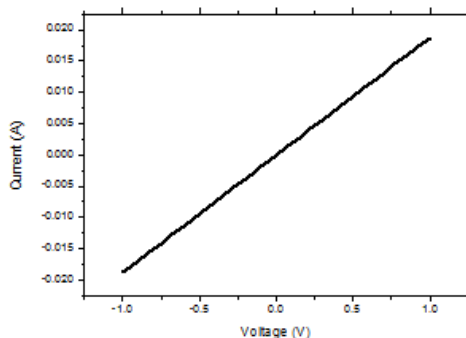


Figure 65: The I-V characteristics of a roll coated all-in-one nanoparticle based ink of PBTF1+PCBM

## 5.4. SUMMARY

In this study all-in-one nanoparticles have been synthesized via *in situ* micro-emulsion Suzuki cross-coupling polymerization to afford poly (4,7-(2,1,3-benzothiadiazole)-alt-2,7(9,9-dioctylfluorene)) with a small amount (5mol%) of crosslinker (3,3'-hexane-1,6-diylbis(2,5-dibromothiophene)) in the absence and the presence of PC<sub>61</sub>BM. The resulting nanoparticles had a diameter of 121 nm and 132 nm, for particles without and with PC<sub>61</sub>BM, respectively. These particles sizes were determined using DLS and the dimensions were further investigated with SEM, proved the presence of particles in the same size range. The absorbance of the native nano-particles suggested the same progression as a control polymer. Due to the presence of the cross-linker making the polymer particles insoluble, the molecular weight was not measured. To investigate the charge transfer from conjugated polymer to the fullerene within the particles, a fluorescence experiment was conducted. This showed a near complete quenching of the fluorescence, which is an indication of a good charge transfer. But when devices were fabricated, there were no photocurrent detected. This could be explained by the incorporation of the catalyst in the *in situ* formed nano-particles, it has been shown in the literature; that the effect of residual catalyst can have a fatal impact on the devices [173]. If the catalyst is the largest obstacle in the fabrication of the devices, this might be circumvented by applying a water soluble catalyst which could lead to a lower Pd content of the resulting particles. Due to time limitations this was not pursued.



# CHAPTER 6. CONCLUSION AND PERSPECTIVE

As introduced (in section 1.6), there have been three overall topics throughout this thesis. Firstly, the syntheses of novel conjugated polymers for applications in both small area OPVs and large area roll-coated OPV devices. A series of D-A polymers employing benzodipyrrolidone (BDPDP) as the acceptor combined with an array of donors: 4,8-bis(5-(2'-alkyl)thiophen-2-yl)benzo[1,2-b;4,5-b']dithiophene (BDTTT), 9-(9-heptadecanyl)-9H-carbazole (C), 9,9-dioctylfluorene (F), and the previously published N-(1-pentylhexyl)dithieno[3,2-b:2',3'-d]-pyrrole (DTP). The resulting polymers did not perform well with efficiencies ranging from 0.007% to 0.682% in small area spin coated OPVs, depending on the D-A combination. Attempts to fabricate roll-coated OPVs using the BDPDP polymers have been made, but with limited success. Surprisingly the PBDPDPDTP performed significantly worse in roll-coated devices than the results from spin-coated devices reported in literature. This is ascribed to the different branched alkyl sidechain applied, from 2-octyl-dodecyl while in this work to 2-ethyl-hexyl in literature, emphasizing the importance of alkyl-sidechain.

Two novel Isoindigo based D-A polymers have also been constructed, whose donor component were 9,9-dioctylfluorene and N-(1-pentylhexyl)dithieno[3,2-b:2',3'-d]-pyrrole. The polymer consisting of 9,9-dioctylfluorene and Isoindigo were tested in small area spin coated OPVs against PC<sub>71</sub>BM, but resulted in low PCEs. The underlying issue was ascribed to the morphology, as TEM images showed a large degree of phase separation, and was therefore not investigated further. The D-A polymer consisting of isoindigo and DTP (PDTPI) was tested in both spin-coated small area devices and as roll-coated large area devices. A good scalability was found as the PCE increased from 0.72% to 0.99% in this transition. This good scalability combined with a good optical match with the polymers P3HT and PBDTTTz-4 led to the testing of the PDTPI in a fully roll coated tandem solar cell stack. The best performing device was PDTPI combined with PBDTTTz-4 that resulted in a tandem device with a PCE of 1.73%, more importantly under ITO- and vacuum-free conditions.

A novel conjugated monomer has been presented, the 3,6-dibromo-N-(dimesitylboryl)carbazole (BC) monomer, which via molecular simulations were found to be a pseudo-acceptor. The BC monomer was combined with 3,3''-didodecyl-2,2':5',2'':5'',2''''-quaterthiophene (QT) and 4,8-di(5-(2-ethylhexyl)thiophene-2-yl)benzo[1,2-b:4,5-b']dithiophene (BDTTT) to form a quasi D-A type polymers and with 2,5-bis(2-ethylhexyl)-6-(thiophen-2-yl)pyrrolo[3,4-c]pyrrole-1,4(2H,5H)-dione (DPP). The versatility of the BC monomer was found not only for participating in both Suzuki and Stille cross-coupling polymerizations but also in direct arylation polymerization. A ternary polymer consisting of BC, 2,5-dibromo-3-hexylthiophene, and 2,1,3-Benzothiadiazole-4,7-bis(boronic acid pinacol ester) to affording a random copolymer called P3HTBCBT. All four different polymers have been electrochemically and photophysically characterized and OPV devices were made. The BC based polymers were tested against PC<sub>71</sub>BM in small area OPV devices. The best was PBCBDTTT polymer with a PCE of 3.82%, this high PCE shows the great potential of the BC moiety and this is, to the best of knowledge, the highest PCE obtained for a boron containing polymer. Attempts on making large area devices via RC processing were abandoned due to

dewetting. As perspectives for the BC, it could be relevant to synthesize a large array of quasi D-A polymers, implementing units such as DTP or other stronger donors to further investigate the potential of this novel monomer. An even more interesting issue with the BC is the dewetting, the origin of this dewetting must be addressed for larger area devices fabrication on BC based polymers. This is essential to ultimately evaluate the potential of the BC monomer and polymer system of it, in a future commercialization of the OPV technology.

Another important aspect in designing low bandgap polymers is to align the LUMO levels of the electron donor molecule and the electron acceptor molecule in the active layer in an OPV device. This issue derives from the difficulty in modifying the band gap and more importantly the LUMO level of the state-of-art fullerene based electron acceptors. In this thesis, three simple DPP based small molecule non-fullerene acceptors have been design, synthesized, and characterized. The three simple molecules consisted of a benzene ring flanked by either two or three DPP moieties. The small molecule acceptors were: with benzene moiety centered, 1,4-substituted (Ph(DPP)<sub>2</sub>); with 2,5-dimethyl-benzene moiety centered, 1,4-substituted (PhDMe(DPP)<sub>2</sub>); and finally benzene moiety centered, 1,3,5- substituted (Ph(DPP)<sub>3</sub>). These small molecule acceptors were all tested against P3HT, the standard donor polymer. Molecular simulation have shown that the introduction of the methyl groups of the PhDMe(DPP)<sub>2</sub> increases the dihedral angle between the center moiety and flanking DPP to 44.5° from the 21.6° found in both Ph(DPP)<sub>2</sub> and Ph(DPP)<sub>3</sub>. The three SM acceptors have been fully characterized in regards photo-physical and electronic properties. Despite the similar building blocks of these acceptors, the color changes from blue purple going from Ph(DPP)<sub>2</sub> to Ph(DPP)<sub>3</sub>, giving an indication of the impact of molecular geometry on SM acceptors. The SM acceptors have been tested in both a small area spin-coated devices and in large area fully roll-coated devices. The maximum performance (PCE) achieved with the SM acceptors was 0.65 % for PhDMe(DPP)<sub>2</sub> and 0.31% for Ph(DPP)<sub>3</sub>. Interestingly the opposite as observed for roll coated devices, where the Ph(DPP)<sub>3</sub> outperformed with a PCE of 0.23% compared to PhDMe(DPP)<sub>2</sub> with a PCE of only 0.02%. EQE of the roll coated devices showed that the photocurrent of the PhDMe(DPP)<sub>2</sub> is primarily driven by the P3HT, while the SM acceptor in both Ph(DPP)<sub>2</sub> and Ph(DPP)<sub>3</sub> contributes to the generation of the photocurrent, which at least for the roll coated devices explains the hierarchy, but does not enlighten the underlying reason. Upon extended exposure to the light, during a life time study, a PCE of 0.54% was achieved for t Ph(DPP)<sub>3</sub> while PhDMe(DPP)<sub>2</sub> also performed better, reaching a PCE of 0.04%. The underlining reason for the ranking of the three similar SM acceptors are not fully understood, but are suspected to derive from the different processing approaches being either roll-coating or spin-coating. But this study clearly underlines the impact and importance of not only the energy levels of a given molecule but also morphology that it gives rise to. This should therefore be further investigated.

In order to achieve a well-defined morphology in nanometer scale and to reduce the number of processing steps; *in situ* micro emulsion polymerized nano-particles could be a potential method to achieve this. In this thesis, a Suzuki coupling based *in situ* polymerization method has been explored for making nanoparticles consisting of the conjugated D-A polymer of poly(4,7-(2,1,3-benzothiadiazole)-alt-2,7(9,9-dioctylflourene) which showed the same absorbance in the particle form, as a control polymer with the same structure. The sizes of the particles were investigated via DLS, determining a diameter of approximately ~130 nm, which was further confirmed by SEM images. As mentioned the absorbance of the polymer is not affected by the formed nanoparticles compared to conventionally polymerized ones, which

indicated a decent molecular weight being large enough, but due to the introduction of a crosslinking agent, the molecular weight determinations of these polymers were impossible. To achieve a prearranged morphology, both nanoparticles with and without PC<sub>61</sub>BM incorporated were synthesized. The impact of this incorporation, was that the fluorescence was nearly completely quenched, proving a strong charge transfer. Despite the apparently good charge separation the device constructed from the nanoparticles with the PC<sub>61</sub>BM incorporated did not show any photocurrent. This is ascribed to the disadvantageous incorporation of the Pd-catalyst, which in literature, has been shown to be fatal for the photovoltaic effect. This might be circumvented by employing a water soluble catalyst, which can be removed more efficiently.



# REFERENCES

- [1] I.E Agency (IEA), *2014 Snapshot of global PV Markets*. 2015.
- [2] E. Becquerel, “Mémoire sur les effets électriques produits sous l’influence des rayons solaires,” *Comptes rendus*, no. 9, pp. 561–567, 1839.
- [3] A. Chodos, “April 25, 1954: Bell Labs Demonstrates the First Practical Silicon Solar Cell,” *APS News - This month in Physics history*, 2009. [Online]. Available: <http://www.aps.org/publications/apsnews/200904/physicshistory.cfm>. [Accessed: 20-Jan-2016].
- [4] M. A. Green, K. Emery, Y. Hishikawa, W. Warta, and E. D. Dunlop, “Solar cell efficiency tables (Version 45),” *Prog. Photovoltaics Res. Appl.*, vol. 23, no. 1, pp. 1–9, Jan. 2015.
- [5] Solar Direct, “Solar Electric Photovoltaic Modules,” 2015. [Online]. Available: <http://solardirect.com/pv/pvlist/pvlist.htm>. [Accessed: 20-Jan-2016].
- [6] First Solar, “First Solar (TM) PV Modules.” [Online]. Available: <http://firstsolar.com/Home/Technologies-and-Capabilities/PV-Modules/First-Solar-Series-3-Black-Module>. [Accessed: 20-Jan-2016].
- [7] T. Meng, “Inorganic Photovoltaic Solar Cells: Silicon and Beyond,” *Electrochem. Soc. Interface*, vol. Winter, pp. 30–35, 2008.
- [8] H. Spanggaard and F. C. Krebs, “A brief history of the development of organic and polymeric photovoltaics,” *Sol. Energy Mater. Sol. Cells*, vol. 83, no. 2–3, pp. 125–146, Jun. 2004.
- [9] C. Jonathan, G. Nick, and W. Stuart, *Organic Chemistry*, 2nd Editio. Oxford University Press, 2012.
- [10] J. L. Delgado, P.-A. Bouit, S. Filippone, M. A. Herranz, and N. Martín, “Organic photovoltaics: a chemical approach,” *Chem. Commun. (Camb)*, vol. 46, no. 27, pp. 4853–65, Jul. 2010.
- [11] K. Emery, “Reference Solar Spectral Irradiance: Air Mass 1.5,” *About the Reference AM 1.5 Spectra*, 2015. [Online]. Available: <http://rredc.nrel.gov/solar/spectra/am1.5/>. [Accessed: 20-Jan-2016].
- [12] E. Bundgaard and F. Krebs, “Low band gap polymers for organic photovoltaics,” *Sol. Energy Mater. Sol. Cells*, vol. 91, no. 11, pp. 954–985, Jul. 2007.
- [13] C. Winder and N. S. Sariciftci, “Low bandgap polymers for photon harvesting in bulk heterojunction solar cells,” *J. Mater. Chem.*, vol. 14, no. 7, p. 1077, 2004.

- [14] C. L. Jones and S. J. Higgins, "Some in situ reflectance Fourier transform infrared studies of electrochemically prepared polybenzo[c]thiophene and poly-5-fluorobenzo[c]thiophene films," *J. Mater. Chem.*, vol. 12, no. 3, pp. 758–764, 2002.
- [15] H.-Y. Chen, J. Hou, S. Zhang, Y. Liang, G. Yang, Y. Yang, L. Yu, Y. Wu, and G. Li, "Polymer solar cells with enhanced open-circuit voltage and efficiency," *Nat. Photonics*, vol. 3, no. 11, pp. 649–653, Nov. 2009.
- [16] A. Pivrikas, N. S. Sariciftci, G. Juška, and R. Österbacka, "A review of charge transport and recombination in polymer/fullerene organic solar cells," *Prog. Photovoltaics Res. Appl.*, vol. 15, no. 8, pp. 677–696, Dec. 2007.
- [17] J. Xue, "Perspectives on Organic Photovoltaics," *Polym. Rev.*, vol. 50, no. 4, pp. 411–419, Oct. 2010.
- [18] B. Kippelen and J.-L. Brédas, "Organic photovoltaics," *Energy Environ. Sci.*, vol. 2, no. 3, p. 251, 2009.
- [19] S. Günes, H. Neugebauer, and N. S. Sariciftci, "Conjugated polymer-based organic solar cells," *Chem. Rev.*, vol. 107, no. 4, pp. 1324–38, Apr. 2007.
- [20] W. Shockley and H. J. Queisser, "Detailed Balance Limit of Efficiency of p-n Junction Solar Cells," *J. Appl. Phys.*, vol. 32, no. 3, p. 510, 1961.
- [21] G. Dennler, M. C. Scharber, and C. J. Brabec, "Polymer-Fullerene Bulk-Heterojunction Solar Cells," *Adv. Mater.*, vol. 21, no. 13, pp. 1323–1338, Apr. 2009.
- [22] T. Ameri, G. Dennler, C. Lungenschmied, and C. J. Brabec, "Organic tandem solar cells: A review," *Energy Environ. Sci.*, vol. 2, no. 4, p. 347, 2009.
- [23] K. Vandewal, A. Gadisa, W. D. Oosterbaan, S. Bertho, F. Banishoeib, I. Van Severen, L. Lutsen, T. J. Cleij, D. Vanderzande, and J. V. Manca, "The Relation Between Open-Circuit Voltage and the Onset of Photocurrent Generation by Charge-Transfer Absorption in Polymer : Fullerene Bulk Heterojunction Solar Cells," *Adv. Funct. Mater.*, vol. 18, no. 14, pp. 2064–2070, Jul. 2008.
- [24] A. Cravino, "Origin of the open circuit voltage of donor-acceptor solar cells: Do polaronic energy levels play a role?," *Appl. Phys. Lett.*, vol. 91, no. 24, p. 243502, 2007.
- [25] D. Konios, G. Kakavelakis, C. Petridis, K. Savva, E. Stratakis, and E. Kymakis, "Highly efficient organic photovoltaic devices utilizing work-function tuned graphene oxide derivatives as the anode and cathode charge extraction layers," *J. Mater. Chem. A*, 2016.
- [26] M. C. Scharber and N. S. Sariciftci, "Efficiency of bulk-heterojunction organic solar cells," *Prog. Polym. Sci.*, vol. 38, no. 12, pp. 1929–1940, Dec. 2013.
- [27] A. De Vos, "Detailed balance limit of the efficiency of tandem solar cells," *J. Phys. D. Appl. Phys.*, vol. 13, no. 5, pp. 839–846, May 1980.

- [28] P. Cheng, L. Ye, X. Zhao, J. Hou, Y. Li, and X. Zhan, "Binary additives synergistically boost the efficiency of all-polymer solar cells up to 3.45%," *Energy Environ. Sci.*, vol. 7, no. 4, pp. 1351–1356, 2014.
- [29] R. Singh, E. Aluicio-Sarduy, Z. Kan, T. Ye, R. C. I. MacKenzie, and P. E. Keivanidis, "Fullerene-free organic solar cells with an efficiency of 3.7% based on a low-cost geometrically planar perylene diimide monomer," *J. Mater. Chem. A*, vol. 2, no. 35, p. 14348, Jul. 2014.
- [30] Y. Zhou, T. Kurosawa, W. Ma, Y. Guo, L. Fang, K. Vandewal, Y. Diao, C. Wang, Q. Yan, J. Reinspach, J. Mei, A. L. Appleton, G. I. Koleilat, Y. Gao, S. C. B. Mannsfeld, A. Salleo, H. Ade, D. Zhao, and Z. Bao, "High Performance All-Polymer Solar Cell via Polymer Side-Chain Engineering," *Adv. Mater.*, vol. 26, no. 22, pp. 3767–3772, Jun. 2014.
- [31] N. Espinosa, F. O. Lenzmann, S. Ryley, D. Angmo, M. Hösel, R. R. Søndergaard, D. Huss, S. Dafinger, S. Gritsch, J. M. Kroon, M. Jørgensen, and F. C. Krebs, "OPV for mobile applications: an evaluation of roll-to-roll processed indium and silver free polymer solar cells through analysis of life cycle, cost and layer quality using inline optical and functional inspection tools," *J. Mater. Chem. A*, vol. 1, no. 24, p. 7037, 2013.
- [32] F. C. Krebs and M. Jørgensen, "Polymer and organic solar cells viewed as thin film technologies: What it will take for them to become a success outside academia," *Sol. Energy Mater. Sol. Cells*, vol. 119, pp. 73–76, Dec. 2013.
- [33] R. Søndergaard, M. Hösel, D. Angmo, T. T. Larsen-Olsen, and F. C. Krebs, "Roll-to-roll fabrication of polymer solar cells," *Mater. Today*, vol. 15, no. 1–2, pp. 36–49, Jan. 2012.
- [34] R. R. Søndergaard, M. Hösel, and F. C. Krebs, "Roll-to-Roll fabrication of large area functional organic materials," *J. Polym. Sci. Part B Polym. Phys.*, vol. 51, no. 1, pp. 16–34, Jan. 2013.
- [35] D. Angmo, I. Gonzalez-Valls, S. Veenstra, W. Verhees, S. Sapkota, S. Schiefer, B. Zimmermann, Y. Galagan, J. Sweelssen, M. Lira-Cantu, R. Andriessen, J. M. Kroon, and F. C. Krebs, "Low-cost upscaling compatibility of five different ITO-free architectures for polymer solar cells," *J. Appl. Polym. Sci.*, vol. 130, no. 2, pp. 944–954, Oct. 2013.
- [36] T. R. Andersen, T. T. Larsen-Olsen, B. Andreasen, A. P. L. Böttiger, J. E. Carlé, M. Helgesen, E. Bundgaard, K. Norrman, J. W. Andreasen, M. Jørgensen, and F. C. Krebs, "Aqueous processing of low-band-gap polymer solar cells using roll-to-roll methods.," *ACS Nano*, vol. 5, no. 5, pp. 4188–96, May 2011.
- [37] T. Yokozawa, H. Kohno, Y. Ohta, and A. Yokoyama, "Catalyst-Transfer Suzuki–Miyaura Coupling Polymerization for Precision Synthesis of Poly(p-phenylene)," *Macromolecules*, vol. 43, no. 17, pp. 7095–7100, Sep. 2010.

- [38] Z. Bao, W. Chan, and L. Yu, "Synthesis of conjugated polymer by the stille coupling reaction," *Chem. Mater.*, vol. 5, no. 1, pp. 2–3, 1993.
- [39] E. Lim, S. Lee, and K. K. Lee, "Improved OPV Efficiency of Fluorene-Thiophene-Based Copolymers with Hole- and Electron-Transporting Units in the Main Chain," *Mol. Cryst. Liq. Cryst.*, vol. 538, no. 1, pp. 157–163, May 2011.
- [40] M. Lai, J. Tsai, C. Chueh, C. Wang, and W. Chen, "Syntheses of New 3,6-Carbazole-Based Donor / Acceptor Conjugated Copolymers for Optoelectronic Device Applications a," *Macromol. Chem. Phys.*, vol. 211, no. 18, pp. 2017–2025, 2010.
- [41] J. Li and A. C. Grimsdale, "Carbazole-based polymers for organic photovoltaic devices.," *Chem. Soc. Rev.*, vol. 39, no. 7, pp. 2399–410, Jul. 2010.
- [42] P. Gao, D. Cho, X. Yang, V. Enkelmann, M. Baumgarten, and K. Müllen, "Heteroheptacenes with fused thiophene and pyrrole rings.," *Chemistry*, vol. 16, no. 17, pp. 5119–28, 2010.
- [43] F. Boon, N. Hergué, G. Deshayes, D. Moerman, S. Desbief, J. De Winter, P. Gerbaux, Y. H. Geerts, R. Lazzaroni, and P. Dubois, "Synthesis of poly[(4,4'-(dihexyl)dithieno(3,2-b;2',3'-d)silole)] and copolymerization with 3-hexylthiophene: new semiconducting materials with extended optical absorption," *Polym. Chem.*, vol. 4, no. 16, p. 4303, 2013.
- [44] H. Zhou, L. Yang, and W. You, "Rational Design of High Performance Conjugated Polymers for Organic Solar Cells," *Macromolecules*, vol. 45, pp. 607–632, 2012.
- [45] S. Qu and H. Tian, "Diketopyrrolopyrrole (DPP)-based materials for organic photovoltaics.," *Chem. Commun. (Camb.)*, vol. 48, no. 25, pp. 3039–51, Mar. 2012.
- [46] S. R. Hammond, W. Braunecker, A. Garcia, R. Larsen, Z. Owczarczyk, D. Olson, and D. Ginley, "Oligomeric dithienopyrrole-thienopyrroledione (DTP-TPD) donor-acceptor copolymer for organic photovoltaics," in *2011 37th IEEE Photovoltaic Specialists Conference*, 2011, pp. 000712–000715.
- [47] H. Zhang and B. Tieke, "Conjugated polymers containing benzo- and naphthodione units in the main chain," *Polym. Chem.*, vol. 5, no. 22, pp. 6391–6406, 2014.
- [48] R. Stalder, C. Grand, J. Subbiah, F. So, and J. R. Reynolds, "An isoindigo and dithieno[3,2-b;2',3'-d]silole copolymer for polymer solar cells," *Polym. Chem.*, vol. 3, no. 1, p. 89, 2012.
- [49] W. Cui, J. Yuen, and F. Wudl, "Benzodipyrrolidones and Their Polymers," *Macromolecules*, vol. 44, no. 20, pp. 7869–7873, 2011.
- [50] X. Guo, A. Facchetti, and T. J. Marks, "Imide- and Amide-Functionalized Polymer Semiconductors," *Chem. Rev.*, vol. 114, no. 18, pp. 8943–9021, 2014.

- [51] C.-W. Chu, V. Shrotriya, G. Li, and Y. Yang, "Tuning acceptor energy level for efficient charge collection in copper-phthalocyanine-based organic solar cells," *Appl. Phys. Lett.*, vol. 88, no. 15, p. 153504, 2006.
- [52] J. W. Rumer, M. Levick, S.-Y. Dai, S. Rossbauer, Z. Huang, L. Biniek, T. D. Anthopoulos, J. R. Durrant, D. J. Procter, and I. McCulloch, "BPTs: thiophene-flanked benzodipyrrolidone conjugated polymers for ambipolar organic transistors," *Chem. Commun.*, vol. 49, no. 40, pp. 4465–4467, 2013.
- [53] W. Cui and F. Wudl, "Dithienylbenzodipyrrolidone: New Acceptor for Donor–Acceptor Low Band Gap Polymers," *Macromolecules*, vol. 46, no. 18, pp. 7232–7238, 2013.
- [54] P. Deng, L. Liu, S. Ren, H. Li, and Q. Zhang, "N-acylation: an effective method for reducing the LUMO energy levels of conjugated polymers containing five-membered lactam units," *Chem. Commun.*, vol. 48, no. 55, p. 6960, 2012.
- [55] J. W. Rumer, B. C. Schroeder, C. B. Nielsen, R. S. Ashraf, D. Beatrup, H. Bronstein, S. J. Cryer, J. E. Donaghey, S. Holliday, M. Hurhangee, D. I. James, S. Lim, I. Meager, W. Zhang, and I. McCulloch, "Bis-lactam-based donor polymers for organic solar cells: Evolution by design," *Thin Solid Films*, vol. 560, no. 0, pp. 82–85, 2014.
- [56] M. J. Robb, S. Y. Ku, F. G. Brunetti, and C. J. Hawker, "A renaissance of color: New structures and building blocks for organic electronics," *J. Polym. Sci. Part A Polym. Chem.*, vol. 51, pp. 1263–1271, 2013.
- [57] W. Hong, C. Guo, Y. Li, Y. Zheng, C. Huang, S. Lu, and A. Facchetti, "Synthesis and thin-film transistor performance of benzodipyrrolinone and bithiophene donor-acceptor copolymers," *J. Mater. Chem.*, vol. 22, no. 41, pp. 22282–22289, 2012.
- [58] K. C. Lee, W.-T. Park, Y.-Y. Noh, and C. Yang, "Benzodipyrrolidone (BDP)-based polymer semiconductors containing a series of chalcogen atoms: comprehensive investigation of the effect of heteroaromatic blocks on intrinsic semiconducting properties," *ACS Appl. Mater. Interfaces*, vol. 6, no. 7, pp. 4872–82, 2014.
- [59] W. Yue, X. Huang, J. Yuan, W. Ma, F. C. Krebs, and D. Yu, "A novel benzodipyrrolidone-based low band gap polymer for organic solar cells," *J. Mater. Chem. a*, vol. 1, no. 35, pp. 10116–10119, 2013.
- [60] M. Yu, L. Zhang, Q. Peng, H. Zhao, and J. Gao, "Narrow-band gap Benzodipyrrolidone (BDPD) based donor conjugated polymer: A theoretical investigation," *Comput. Theor. Chem.*, vol. 1055, pp. 88–93, 2015.
- [61] S. P. Singh, C. P. Kumar, G. D. Sharma, R. Kurchania, and M. S. Roy, "Synthesis of a Modified PC 70 BM and Its Application as an Electron Acceptor with Poly(3-hexylthiophene) as an Electron Donor for Efficient Bulk Heterojunction Solar Cells," *Adv. Funct. Mater.*, vol. 22, no. 19, pp. 4087–4095, Oct. 2012.

- [62] J. Mei, K. R. Graham, R. Stalder, and J. R. Reynolds, "Synthesis of isoindigo-based oligothiophenes for molecular bulk heterojunction solar cells," *Org. Lett.*, vol. 12, no. 4, pp. 660–3, Feb. 2010.
- [63] G. Zhang, Y. Fu, Z. Xie, and Q. Zhang, "Synthesis and Photovoltaic Properties of New Low Bandgap Isoindigo-Based Conjugated Polymers," *Macromolecules*, vol. 44, no. 6, pp. 1414–1420, Mar. 2011.
- [64] B. Liu, Y. Zou, B. Peng, B. Zhao, K. Huang, Y. He, and C. Pan, "Low bandgap isoindigo-based copolymers: design, synthesis and photovoltaic applications," *Polym. Chem.*, vol. 2, no. 5, p. 1156, 2011.
- [65] E. Wang, Z. Ma, Z. Zhang, P. Henriksson, O. Inganäs, F. Zhang, and M. R. Andersson, "An isoindigo-based low band gap polymer for efficient polymer solar cells with high photo-voltage," *Chem. Commun. (Camb)*, vol. 47, no. 17, pp. 4908–10, May 2011.
- [66] Z. Ma, D. Dang, Z. Tang, D. Gedefaw, J. Bergqvist, W. Zhu, W. Mammo, M. R. Andersson, O. Inganäs, F. Zhang, and E. Wang, "A Facile Method to Enhance Photovoltaic Performance of Benzodithiophene-Isoindigo Polymers by Inserting Bithiophene Spacer," *Adv. Energy Mater.*, pp. 1–6, 2013.
- [67] Y. Deng, J. Liu, J. Wang, L. Liu, W. Li, H. Tian, X. Zhang, Z. Xie, Y. Geng, and F. Wang, "Dithienocarbazole and isoindigo based amorphous low bandgap conjugated polymers for efficient polymer solar cells," *Adv. Mater.*, vol. 26, no. 3, pp. 471–6, Jan. 2014.
- [68] R. Stalder, J. Mei, and J. R. Reynolds, "Isoindigo-based donor-acceptor conjugated polymers," *Macromolecules*, vol. 43, no. 20, pp. 8348–8352, Oct. 2010.
- [69] R. Stalder, J. Mei, K. R. Graham, L. a. Estrada, and J. R. Reynolds, "Isoindigo, a versatile electron-deficient unit for high-performance organic electronics," *Chem. Mater.*, vol. 26, no. 1, pp. 664–678, 2014.
- [70] P. Deng and Q. Zhang, "Recent developments on isoindigo-based conjugated polymers," *Polym. Chem.*, vol. 5, no. 10, p. 3298, 2014.
- [71] W. Yue, Y. Zhao, S. Shao, H. Tian, Z. Xie, Y. Geng, and F. Wang, "Novel NIR-absorbing conjugated polymers for efficient polymer solar cells: effect of alkyl chain length on device performance," *J. Mater. Chem.*, vol. 19, no. 15, p. 2199, 2009.
- [72] R. G. Brandt, W. Yue, T. R. Andersen, T. T. Larsen-Olsen, M. Hinge, E. Bundgaard, F. C. Krebs, and D. Yu, "An isoindigo containing donor-acceptor polymer: synthesis and photovoltaic properties of all-solution-processed ITO- and vacuum-free large area roll-coated single junction and tandem solar cells," *J. Mater. Chem. C*, 2015.

- [73] T. R. Andersen, H. F. Dam, B. Andreasen, M. Hösel, M. V. Madsen, S. a. Gevorgyan, R. R. Søndergaard, M. Jørgensen, and F. C. Krebs, "A rational method for developing and testing stable flexible indium- and vacuum-free multilayer tandem polymer solar cells comprising up to twelve roll processed layers," *Sol. Energy Mater. Sol. Cells*, vol. 120, pp. 735–743, Jan. 2014.
- [74] D. Angmo, S. a. Gevorgyan, T. T. Larsen-Olsen, R. R. Søndergaard, M. Hösel, M. Jørgensen, R. Gupta, G. U. Kulkarni, and F. C. Krebs, "Scalability and stability of very thin, roll-to-roll processed, large area, indium-tin-oxide free polymer solar cell modules," *Org. Electron.*, vol. 14, no. 3, pp. 984–994, Mar. 2013.
- [75] S. G. Li, Z. C. Yuan, J. Y. Yuan, P. Deng, Q. Zhang, and B. Q. Sun, "An expanded isoindigo unit as a new building block for a conjugated polymer leading to high-performance solar cells," *J. Mater. Chem. A*, vol. 2, no. 15, pp. 5427–5433, 2014.
- [76] W. Yue, T. T. Larsen-Olsen, X. Hu, M. Shi, H. Chen, M. Hinge, P. Fojan, F. C. Krebs, and D. Yu, "Synthesis and photovoltaic properties from inverted geometry cells and roll-to-roll coated large area cells from dithienopyrrole-based donor–acceptor polymers," *J. Mater. Chem. A*, vol. 1, no. 5, p. 1785, 2013.
- [77] M. M. Wienk, M. Turbiez, J. Gilot, and R. A. J. Janssen, "Narrow-Bandgap Diketo-Pyrrolo-Pyrrole Polymer Solar Cells: The Effect of Processing on the Performance," *Adv. Mater.*, vol. 20, no. 13, pp. 2556–2560, Jul. 2008.
- [78] R. C. Coffin, J. Peet, J. Rogers, and G. C. Bazan, "Streamlined microwave-assisted preparation of narrow-bandgap conjugated polymers for high-performance bulk heterojunction solar cells," *Nat. Chem.*, vol. 1, no. 8, pp. 657–661, Nov. 2009.
- [79] C.-C. Ho, S.-Y. Chang, T.-C. Huang, C.-A. Chen, H.-C. Liao, Y.-F. Chen, and W.-F. Su, "Synthesis, characterization and photovoltaic properties of poly(cyclopentadithiophene-alt-isoindigo)," *Polym. Chem.*, vol. 4, no. 20, p. 5351, 2013.
- [80] J. E. Carlé and F. C. Krebs, "Technological status of organic photovoltaics (OPV)," *Sol. Energy Mater. Sol. Cells*, vol. 119, pp. 309–310, Dec. 2013.
- [81] M. Hösel, R. R. Søndergaard, M. Jørgensen, and F. C. Krebs, "Fast Inline Roll-to-Roll Printing for Indium-Tin-Oxide-Free Polymer Solar Cells Using Automatic Registration," *Energy Technol.*, vol. 1, no. 1, pp. 102–107, Jan. 2013.
- [82] M. Zhang, Y. Sun, X. Guo, C. Cui, Y. He, and Y. Li, "Synthesis and Characterization of Dioctyloxybenzo[1,2- b :4,3- b ' ]dithiophene-Containing Copolymers for Polymer Solar Cells," *Macromolecules*, vol. 44, no. 19, pp. 7625–7631, Oct. 2011.
- [83] M. Helgesen, J. E. Carlé, and F. C. Krebs, "Slot-Die Coating of a High Performance Copolymer in a Readily Scalable Roll Process for Polymer Solar Cells," *Adv. Energy Mater.*, vol. 3, no. 12, pp. 1664–1669, Dec. 2013.

- [84] M. Helgesen, J. E. Carlé, G. A. dos Reis Benatto, R. R. Søndergaard, M. Jørgensen, E. Bundgaard, and F. C. Krebs, "Making Ends Meet: Flow Synthesis as the Answer to Reproducible High-Performance Conjugated Polymers on the Scale that Roll-to-Roll Processing Demands," *Adv. Energy Mater.*, vol. 5, no. 9, p. n/a–n/a, May 2015.
- [85] T. R. Andersen, H. F. Dam, B. Burkhardt, D. Angmo, M. Corazza, B. C. Thompson, and F. C. Krebs, "Medium area, flexible single and tandem junction solar cells based on roll coated semi-random copolymers," *J. Mater. Chem. C*, vol. 2, no. 44, pp. 9412–9415, Oct. 2014.
- [86] F. Jäkle, "Lewis acidic organoboron polymers," *Coord. Chem. Rev.*, vol. 250, no. 9–10, pp. 1107–1121, May 2006.
- [87] J. C. Collings, S.-Y. Poon, C. Le Droumaguet, M. Charlot, C. Katan, L.-O. Pålsson, A. Beeby, J. A. Mosely, H. M. Kaiser, D. Kaufmann, W.-Y. Wong, M. Blanchard-Desce, and T. B. Marder, "The Synthesis and One- and Two-Photon Optical Properties of Dipolar, Quadrupolar and Octupolar Donor-Acceptor Molecules Containing Dimesitylboryl Groups," *Chem. - A Eur. J.*, vol. 15, no. 1, pp. 198–208, Jan. 2009.
- [88] C. D. Entwistle and T. B. Marder, "Applications of three-coordinate organoboron compounds and polymers in optoelectronics," *Chem. Mater.*, vol. 16, pp. 4574–4585, 2004.
- [89] M. J. . Bosdet and W. E. Piers, "B-N as a C-C substitute in aromatic systems," *Can. J. Chem.*, vol. 87, no. 1, pp. 8–29, Jan. 2009.
- [90] N. Matsumi and Y. Chujo, " $\pi$ -Conjugated Organoboron Polymers via the Vacant p-Orbital of the Boron Atom," *Polym. J.*, vol. 40, no. 2, pp. 77–89, Feb. 2008.
- [91] C. D. Entwistle and T. B. Marder, "Boron Chemistry Lights the Way: Optical Properties of Molecular and Polymeric Systems," *Angew. Chemie Int. Ed.*, vol. 41, no. 16, p. 2927, Aug. 2002.
- [92] R. Stahl, C. Lambert, C. Kaiser, R. Wortmann, and R. Jakober, "Electrochemistry and Photophysics of Donor-Substituted Triarylboranes: Symmetry Breaking in Ground and Excited State," *Chem. - A Eur. J.*, vol. 12, no. 8, pp. 2358–2370, Mar. 2006.
- [93] Y. Shirota, M. Kinoshita, T. Noda, K. Okumoto, and T. Ohara, "A Novel Class of Emitting Amorphous Molecular Materials as Bipolar Radical Formants: 2-{4-[Bis(4-methylphenyl)amino]phenyl}-5-(dimesitylboryl)thiophene and 2-{4-[Bis(9,9-dimethylfluorenyl)amino]phenyl}-5-(dimesitylboryl)thiophene," *J. Am. Chem. Soc.*, vol. 122, no. 44, pp. 11021–11022, Nov. 2000.
- [94] H. Doi, M. Kinoshita, K. Okumoto, and Y. Shirota, "A Novel Class of Emitting Amorphous Molecular Materials with Bipolar Character for Electroluminescence," *Chem. Mater.*, vol. 15, no. 5, pp. 1080–1089, Mar. 2003.

- [95] N. Matsumi, K. Naka, and Y. Chujo, "Extension of  $\pi$ -Conjugation Length via the Vacant p-Orbital of the Boron Atom. Synthesis of Novel Electron Deficient  $\pi$ -Conjugated Systems by Hydroboration Polymerization and Their Blue Light Emission," *J. Am. Chem. Soc.*, vol. 120, no. 20, pp. 5112–5113, May 1998.
- [96] A. Sundararaman, M. Victor, R. Varughese, and F. Jäkle, "A Family of Main-Chain Polymeric Lewis Acids: Synthesis and Fluorescent Sensing Properties of Boron-Modified Polythiophenes," *J. Am. Chem. Soc.*, vol. 127, no. 40, pp. 13748–13749, Oct. 2005.
- [97] C.-H. Zhao, A. Wakamiya, and S. Yamaguchi, "Highly Emissive Poly(aryleneethynylene)s Containing 2,5-Diboryl-1,4-phenylene as a Building Unit," *Macromolecules*, vol. 40, no. 11, pp. 3898–3900, May 2007.
- [98] Z. Yuan, J. C. Collings, N. J. Taylor, T. B. Marder, C. Jardin, and J.-F. Halet, "Linear and Nonlinear Optical Properties of Three-Coordinate Organoboron Compounds," *J. Solid State Chem.*, vol. 154, no. 1, pp. 5–12, Oct. 2000.
- [99] D. Reitzenstein and C. Lambert, "Localized versus Backbone Fluorescence in N - p - (Diarylboryl)phenyl-Substituted 2,7- and 3,6-Linked Polycarbazoles," *Macromolecules*, vol. 42, no. 3, pp. 773–782, Feb. 2009.
- [100] A. Lichtblau, H. D. Hausen, W. Schwarz, and W. Kaim, "Inorganic hybrid analogs of Thiele's and Chichibabin's hydrocarbons. Spectroscopy, electrochemistry, and structure," *Inorg. Chem.*, vol. 32, no. 1, pp. 73–78, Jan. 1993.
- [101] J. Chai, C. Wang, L. Jia, Y. Pang, M. Graham, and S. Z. D. Cheng, "Synthesis and electrochemical properties of a new class of boron-containing n-type conjugated polymers," *Synth. Met.*, vol. 159, no. 14, pp. 1443–1449, Jul. 2009.
- [102] T. Taniguchi, J. Wang, S. Irle, and S. Yamaguchi, "TICT fluorescence of N-borylated 2,5-diarylpyrroles: a gear like dual motion in the excited state," *Dalt. Trans.*, vol. 42, no. 3, pp. 620–624, 2013.
- [103] S. G. Sveegaard, "Boron-containing polymers for use in organic solar cells," Aalborg University, 2013.
- [104] Y. Fu, J. Kim, A. Siva, W. S. Shin, S. Moon, and T. Park, "Parameters influencing the molecular weight of 3,6-carbazole-based D- $\pi$ -A-type copolymers," *J. Polym. Sci. Part A Polym. Chem.*, vol. 49, no. 20, pp. 4368–4378, 2011.
- [105] N. Berton, C. Ottone, V. Labet, R. de Bettignies, S. Bailly, A. Grand, C. Morell, S. Sadki, and F. Chandezon, "New Alternating Copolymers of 3,6-Carbazoles and Dithienylbenzothiadiazoles: Synthesis, Characterization, and Application in Photovoltaics," *Macromol. Chem. Phys.*, vol. 212, no. 19, pp. 2127–2141, 2011.

- [106] Y. Fu, H. Cha, G. Y. Lee, B. J. Moon, C. E. Park, and T. Park, “3,6-Carbazole Incorporated into Poly 9,9-dioctylfluorene-alt-(bisthienyl)benzothiadiazole s Improving the Power Conversion Efficiency,” *Macromolecules*, vol. 45, pp. 3004–3009, 2012.
- [107] A. Azazi, A. Mabrouk, and K. Alimi, “Theoretical investigation on the photophysical properties of low-band-gap copolymers for photovoltaic devices,” *Comput. Theor. Chem.*, vol. 978, no. 1–3, pp. 7–15, 2011.
- [108] R. Misra, T. Jadhav, B. Dhokale, and S. M. Mobin, “and cyanide ions using tri and tetra coordinated,” pp. 16052–16060, 2015.
- [109] J. Jo, D. Gendron, A. Najari, J. S. Moon, S. Cho, M. Leclerc, and A. J. Heeger, “Bulk heterojunction solar cells based on a low-bandgap carbazole-diketopyrrolopyrrole copolymer,” *Appl. Phys. Lett.*, vol. 97, no. 20, p. 203303, 2010.
- [110] E. Lim, K. K. Lee, and S. Lee, “Synthesis and Characterization of Carbazole-Thiophene-based Conjugated Polymers for Organic Photovoltaic Cells,” *Mol. Cryst. Liq. Cryst.*, vol. 551, no. 1, pp. 130–137, Nov. 2011.
- [111] B. S. Ong, Y. Wu, P. Liu, and S. Gardner, “High-performance semiconducting polythiophenes for organic thin-film transistors,” *J. Am. Chem. Soc.*, vol. 126, no. 11, pp. 3378–9, Mar. 2004.
- [112] D. Witker and J. R. Reynolds, “Soluble Variable Color Carbazole-Containing Electrochromic Polymers,” *Macromolecules*, vol. 38, no. 18, pp. 7636–7644, Sep. 2005.
- [113] R. Stalder, J. Mei, K. R. Graham, L. A. Estrada, and J. R. Reynolds, “Isoindigo, a Versatile Electron-Deficient Unit For High-Performance Organic Electronics,” *Chem. Mater.*, vol. 26, no. 1, pp. 664–678, Jan. 2014.
- [114] Y.-H. Chen, Y.-Y. Lin, Y.-C. Chen, J. T. Lin, R.-H. Lee, W.-J. Kuo, and R.-J. Jeng, “Carbazole/fluorene copolymers with dimethylboron pendants for blue light-emitting diodes,” *Polymer (Guildf.)*, vol. 52, no. 4, pp. 976–986, Feb. 2011.
- [115] D.-R. Bai, X.-Y. Liu, and S. Wang, “Charge-Transfer Emission Involving Three-Coordinate Organoboron: V-Shape versus U-Shape and Impact of the Spacer on Dual Emission and Fluorescent Sensing,” *Chem. - A Eur. J.*, vol. 13, no. 20, pp. 5713–5723, Jul. 2007.
- [116] J. Kim, Y. S. Kwon, W. S. Shin, S. J. Moon, and T. Park, “Carbazole-based copolymers: Effects of conjugation breaks and steric hindrance,” *Macromolecules*, vol. 44, no. 7, pp. 1909–1919, 2011.
- [117] A. F. Eftaiha, J.-P. Sun, I. G. Hill, and G. C. Welch, “Recent advances of non-fullerene, small molecular acceptors for solution processed bulk heterojunction solar cells,” *J. Mater. Chem. A*, vol. 2, no. 5, pp. 1201–1213, 2014.

- [118]C. W. Tang, "Two-layer organic photovoltaic cell," *Appl. Phys. Lett.*, vol. 48, no. 2, p. 183, 1986.
- [119]H. Hoppe and N. S. Sariciftci, "Organic solar cells: An overview," *J. Mater. Res.*, vol. 19, no. 07, pp. 1924–1945, Mar. 2011.
- [120]P. M. Allemand, A. Koch, F. Wudl, Y. Rubin, F. Diederich, M. M. Alvarez, S. J. Anz, and R. L. Whetten, "Two different fullerenes have the same cyclic voltammetry," *J. Am. Chem. Soc.*, vol. 113, no. 3, pp. 1050–1051, Jan. 1991.
- [121]N. S. Sariciftci, L. Smilowitz, A. J. Heeger, and F. Wudl, "Photoinduced Electron Transfer from a Conducting Polymer to Buckminsterfullerene," *Science (80-. )*, vol. 258, no. 5087, pp. 1474–1476, Nov. 1992.
- [122]V. A. Trukhanov and D. Y. Paraschuk, "Non-fullerene acceptors for organic solar cells," *Polym. Sci. Ser. C*, vol. 56, no. 1, pp. 72–83, Sep. 2014.
- [123]E. von Hauff, V. Dyakonov, and J. Parisi, "Study of field effect mobility in PCBM films and P3HT:PCBM blends," *Sol. Energy Mater. Sol. Cells*, vol. 87, no. 1–4, pp. 149–156, May 2005.
- [124]P. H. Wöbkenberg, D. D. C. Bradley, D. Kronholm, J. C. Hummelen, D. M. de Leeuw, M. Cölle, and T. D. Anthopoulos, "High mobility n-channel organic field-effect transistors based on soluble C60 and C70 fullerene derivatives," *Synth. Met.*, vol. 158, no. 11, pp. 468–472, Jul. 2008.
- [125]D. M. Guldi, "Fullerenes: three dimensional electron acceptor materials," *Chem. Commun.*, no. 5, pp. 321–327, 2000.
- [126]P. Sonar, J. P. Fong Lim, and K. L. Chan, "Organic non-fullerene acceptors for organic photovoltaics," *Energy Environ. Sci.*, vol. 4, no. 5, p. 1558, 2011.
- [127]G. J. Dutton and S. W. Robey, "Non-fullerene acceptors: exciton dissociation with PTCDA versus C<sub>60</sub>," *Phys. Chem. Chem. Phys.*, vol. 17, no. 24, pp. 15953–15962, 2015.
- [128]H. Xin, X. Guo, G. Ren, M. D. Watson, and S. A. Jenekhe, "Efficient Phthalimide Copolymer-Based Bulk Heterojunction Solar Cells: How the Processing Additive Influences Nanoscale Morphology and Photovoltaic Properties," *Adv. Energy Mater.*, vol. 2, no. 5, pp. 575–582, May 2012.
- [129]J. T. Bloking, T. Giovenzana, A. T. Higgs, A. J. Ponc, E. T. Hoke, K. Vandewal, S. Ko, Z. Bao, A. Sellinger, and M. D. McGehee, "Comparing the Device Physics and Morphology of Polymer Solar Cells Employing Fullerenes and Non-Fullerene Acceptors," *Adv. Energy Mater.*, vol. 4, no. 12, Aug. 2014.
- [130]V. Brand, C. Bruner, and R. H. Dauskardt, "Cohesion and device reliability in organic bulk heterojunction photovoltaic cells," *Sol. Energy Mater. Sol. Cells*, vol. 99, pp. 182–189, Apr. 2012.

- [131] S. R. Dupont, M. Oliver, F. C. Krebs, and R. H. Dauskardt, "Interlayer adhesion in roll-to-roll processed flexible inverted polymer solar cells," *Sol. Energy Mater. Sol. Cells*, vol. 97, pp. 171–175, Feb. 2012.
- [132] A. Anctil, C. W. Babbitt, R. P. Raffaele, and B. J. Landi, "Material and Energy Intensity of Fullerene Production," *Environ. Sci. Technol.*, vol. 45, no. 6, pp. 2353–2359, Mar. 2011.
- [133] J. B. Sherman, B. Purushothaman, S. R. Parkin, C. Kim, S. Collins, J. Anthony, T.-Q. Nguyen, and M. L. Chabinyc, "Role of crystallinity of non-fullerene acceptors in bulk heterojunctions," *J. Mater. Chem. A*, vol. 3, pp. 9989–9998, 2015.
- [134] A. J. Ferguson, J. L. Blackburn, and N. Kopidakis, "Fullerenes and carbon nanotubes as acceptor materials in organic photovoltaics," *Mater. Lett.*, vol. 90, pp. 115–125, 2013.
- [135] Z. George, R. Kroon, R. Gehlhaar, G. Gbabode, A. Lundin, S. Hellström, C. Müller, Y. Geerts, P. Heremans, and M. Andersson, "The Influence of Alkoxy Substitutions on the Properties of Diketopyrrolopyrrole-Phenyl Copolymers for Solar Cells," *Materials (Basel)*, vol. 6, no. 7, pp. 3022–3034, Jul. 2013.
- [136] C. Lu and W.-C. Chen, "Diketopyrrolopyrrole-Thiophene-Based Acceptor-Donor-Acceptor Conjugated Materials for High-Performance Field-Effect Transistors," *Chem. - An Asian J.*, vol. 8, no. 11, pp. 2813–2821, Nov. 2013.
- [137] P. Sonar, G. Ng, T. T. Lin, A. Dodabalapur, and Z. Chen, "Solution processable low bandgap diketopyrrolopyrrole (DPP) based derivatives: novel acceptors for organic solar cells," *J. Mater. Chem.*, vol. 20, no. 18, p. 3626, 2010.
- [138] Y. Lin, P. Cheng, Y. Li, and X. Zhan, "A 3D star-shaped non-fullerene acceptor for solution-processed organic solar cells with a high open-circuit voltage of 1.18 V," *Chem. Commun.*, vol. 48, p. 4773, 2012.
- [139] Y. Lin, Y. Li, and X. Zhan, "A solution-processable electron acceptor based on dibenzosilole and diketopyrrolopyrrole for organic solar cells," *Adv. Energy Mater.*, vol. 3, no. 6, pp. 724–728, 2013.
- [140] C. Fan, P. Yang, X. Wang, G. Liu, X. Jiang, H. Chen, X. Tao, M. Wang, and M. Jiang, "Synthesis and organic photovoltaic (OPV) properties of triphenylamine derivatives based on a hexafluorocyclopentene 'core,'" *Sol. Energy Mater. Sol. Cells*, vol. 95, no. 3, pp. 992–1000, Mar. 2011.
- [141] K. Cnops, B. P. Rand, D. Cheyns, B. Verreert, M. A. Empl, and P. Heremans, "8.4% Efficient Fullerene-Free Organic Solar Cells Exploiting Long-Range Exciton Energy Transfer," *Nat. Commun.*, vol. 5, pp. 1–6, 2014.
- [142] D. Sun, D. Meng, Y. Cai, B. Fan, Y. Li, W. Jiang, L. Huo, Y. Sun, and Z. Wang, "Non-Fullerene-Acceptor-Based Bulk-Heterojunction Organic Solar Cells with Efficiency over 7%," *J. Am. Chem. Soc.*, vol. 137, no. 34, pp. 11156–11162, 2015.

- [143] N. Espinosa, R. García-Valverde, A. Urbina, and F. C. Krebs, "A life cycle analysis of polymer solar cell modules prepared using roll-to-roll methods under ambient conditions," *Sol. Energy Mater. Sol. Cells*, vol. 95, no. 5, pp. 1293–1302, May 2011.
- [144] M. R. Chen, C. C. Fan, T. R. Andersen, H. F. Dam, W. F. Fu, Y. Z. Lin, E. Bundgaard, F. C. Krebs, X. W. Zhan, and H. Z. Chen, "Solvent-resistant small molecule solar cells by roll-to-roll fabrication via introduction of azide cross-linkable group," *Synth. Met.*, vol. 195, pp. 299–305, 2014.
- [145] W. Liu, H. Shi, T. R. Andersen, N. K. Zawacka, P. Cheng, E. Bundgaard, M. Shi, X. Zhan, F. C. Krebs, and H. Chen, "Roll-coating fabrication of ITO-free flexible solar cells based on a non-fullerene small molecule acceptor," *RSC Adv.*, vol. 5, no. 45, pp. 36001–36006, 2015.
- [146] S. Arrechea, A. Molina-Ontoria, A. Aljarilla, P. de la Cruz, F. Langa, and L. Echegoyen, "New acceptor- $\pi$ -porphyrin- $\pi$ -acceptor systems for solution-processed small molecule organic solar cells," *Dye. Pigment.*, vol. 121, pp. 109–117, 2015.
- [147] L. R. Rutledge, S. M. McAfee, and G. C. Welch, "Design and computational characterization of non-fullerene acceptors for use in solution-processable solar cells," *J. Phys. Chem. A*, vol. 118, no. 36, pp. 7939–51, 2014.
- [148] S.-Y. Liu, W.-F. Fu, J.-Q. Xu, C.-C. Fan, H. Jiang, M. Shi, H.-Y. Li, J.-W. Chen, Y. Cao, and H.-Z. Chen, "A direct arylation-derived DPP-based small molecule for solution-processed organic solar cells," *Nanotechnology*, vol. 25, no. 1, p. 014006, Jan. 2014.
- [149] E. Lafalce, P. Togli, J. E. Lewis, and X. Jiang, "Photo annealing effect on p-doped inverted organic solar cell," *J. Appl. Phys.*, vol. 115, no. 24, p. 244511, 2014.
- [150] N. Espinosa, R. García-Valverde, A. Urbina, F. Lenzenmann, M. Manceau, D. Angmo, and F. C. Krebs, "Life cycle assessment of ITO-free flexible polymer solar cells prepared by roll-to-roll coating and printing," *Sol. Energy Mater. Sol. Cells*, vol. 97, pp. 3–13, Feb. 2012.
- [151] Office of Energy Efficiency & Renewable Energy, "The BTX Chain: Benzene, Toluene, Xylene," 2000. [Online]. Available: [http://www1.eere.energy.gov/manufacturing/resources/chemicals/pdfs/profile\\_chap4.pdf](http://www1.eere.energy.gov/manufacturing/resources/chemicals/pdfs/profile_chap4.pdf). [Accessed: 22-Jan-2016].
- [152] T. R. Andersen, "Organic Based Solar Cells with Morphology Control," Danish Technical University (DTU), 2013.
- [153] R. Søndergaard, M. Helgesen, M. Jørgensen, and F. C. Krebs, "Fabrication of Polymer Solar Cells Using Aqueous Processing for All Layers Including the Metal Back Electrode," *Adv. Energy Mater.*, vol. 1, no. 1, pp. 68–71, Jan. 2011.

- [154] P. Cai, H. Jia, J. Chen, and Y. Cao, "Organic/Organic Cathode Bi-Interlayers Based on a Water-Soluble Nonconjugated Polymer and an Alcohol-Soluble Conjugated Polymer for High Efficiency Inverted Polymer Solar Cells," *ACS Appl. Mater. Interfaces*, vol. 7, no. 50, pp. 27871–27877, Dec. 2015.
- [155] Z. Hu, K. Zhang, F. Huang, and Y. Cao, "Water/alcohol soluble conjugated polymers for the interface engineering of highly efficient polymer light-emitting diodes and polymer solar cells," *Chem. Commun.*, vol. 51, no. 26, pp. 5572–5585, 2015.
- [156] C. Duan, K. Zhang, X. Guan, C. Zhong, H. Xie, F. Huang, J. Chen, J. Peng, and Y. Cao, "Conjugated zwitterionic polyelectrolyte-based interface modification materials for high performance polymer optoelectronic devices," *Chem. Sci.*, vol. 4, no. 3, p. 1298, 2013.
- [157] K. Zhang, C. Zhong, S. Liu, C. Mu, Z. Li, H. Yan, F. Huang, and Y. Cao, "Highly Efficient Inverted Polymer Solar Cells Based on a Cross-linkable Water-/Alcohol-Soluble Conjugated Polymer Interlayer," *ACS Appl. Mater. Interfaces*, vol. 6, no. 13, pp. 10429–10435, Jul. 2014.
- [158] D. Tuncel and H. V. Demir, "Conjugated polymer nanoparticles.," *Nanoscale*, vol. 2, no. 4, pp. 484–94, Apr. 2010.
- [159] J. Pecher and S. Mecking, "Nanoparticles of conjugated polymers.," *Chem. Rev.*, vol. 110, no. 10, pp. 6260–79, Oct. 2010.
- [160] C. Szymanski, C. Wu, J. Hooper, M. A. Salazar, A. Perdomo, A. Dukes, and J. McNeill, "Single molecule nanoparticles of the conjugated polymer MEH-PPV, preparation and characterization by near-field scanning optical microscopy.," *J. Phys. Chem. B*, vol. 109, no. 18, pp. 8543–6, May 2005.
- [161] C. Wu, C. Szymanski, Z. Cain, and J. McNeill, "Conjugated Polymer Dots for Multiphoton Fluorescence Imaging," *J. Am. Chem. Soc.*, vol. 129, no. 43, pp. 12904–12905, Oct. 2007.
- [162] T. Kietzke, D. Neher, K. Landfester, R. Montenegro, R. Güntner, and U. Scherf, "Novel approaches to polymer blends based on polymer nanoparticles.," *Nat. Mater.*, vol. 2, no. 6, pp. 408–12, Jun. 2003.
- [163] K. Landfester, R. Montenegro, U. Scherf, R. Güntner, U. Asawapirom, S. Patil, D. Neher, and T. Kietzke, "Semiconducting Polymer Nanospheres in Aqueous Dispersion Prepared by a Miniemulsion Process," *Adv. Mater.*, vol. 14, no. 9, pp. 651–655, May 2002.
- [164] M. C. Baier, J. Huber, and S. Mecking, "Fluorescent Conjugated Polymer Nanoparticles by Polymerization in Miniemulsion," *J. Am. Chem. Soc.*, vol. 131, no. 40, pp. 14267–14273, Oct. 2009.
- [165] J. Huber, C. Jung, and S. Mecking, "Nanoparticles of Low Optical Band Gap Conjugated Polymers," *Macromolecules*, vol. 45, no. 19, pp. 7799–7805, Oct. 2012.

- [166] R. Wang, C. Zhang, W. Wang, and T. Liu, "Preparation, morphology, and biolabeling of fluorescent nanoparticles based on conjugated polymers by emulsion polymerization," *J. Polym. Sci. Part A Polym. Chem.*, vol. 48, no. 21, pp. 4867–4874, Sep. 2010.
- [167] P. C. Rodrigues, L. S. Berlim, D. Azevedo, N. C. Saavedra, P. N. Prasad, W. H. Schreiner, T. D. Z. Atvars, and L. Akcelrud, "Electronic Structure and Optical Properties of an Alternated Fluorene–Benzothiadiazole Copolymer: Interplay between Experimental and Theoretical Data," *J. Phys. Chem. A*, vol. 116, no. 14, pp. 3681–3690, Apr. 2012.
- [168] P. Herguth, X. Jiang, M. S. Liu, and A. K.-Y. Jen, "Highly Efficient Fluorene- and Benzothiadiazole-Based Conjugated Copolymers for Polymer Light-Emitting Diodes," *Macromolecules*, vol. 35, no. 16, pp. 6094–6100, Jul. 2002.
- [169] S. Saito, K. Nakakura, and S. Yamaguchi, "Macrocyclic Restriction with Flexible Alkylene Linkers: A Simple Strategy to Control the Solid-State Properties of  $\pi$ -Conjugated Systems," *Angew. Chemie Int. Ed.*, vol. 51, no. 3, pp. 714–717, Jan. 2012.
- [170] W. Peter Wuelfing, K. Kosuda, A. C. Templeton, A. Harman, M. D. Mowery, and R. A. Reed, "Polysorbate 80 UV/vis spectral and chromatographic characteristics – defining boundary conditions for use of the surfactant in dissolution analysis," *J. Pharm. Biomed. Anal.*, vol. 41, no. 3, pp. 774–782, Jun. 2006.
- [171] J. Morgado, E. Moons, R. H. Friend, and F. Cacialli, "Optical and morphological investigations of non-homogeneity in polyfluorene blends," *Synth. Met.*, vol. 124, no. 1, pp. 63–66, Oct. 2001.
- [172] Y. Nakayama, K. Morii, Y. Suzuki, H. Machida, S. Kera, N. Ueno, H. Kitagawa, Y. Noguchi, and H. Ishii, "Origins of Improved Hole-Injection Efficiency by the Deposition of MoO<sub>3</sub> on the Polymeric Semiconductor Poly(dioctylfluorene- alt - benzothiadiazole)," *Adv. Funct. Mater.*, vol. 19, no. 23, pp. 3746–3752, Dec. 2009.
- [173] M. P. Nikiforov, B. Lai, W. Chen, S. Chen, R. D. Schaller, J. Strzalka, J. Maser, and S. B. Darling, "Detection and role of trace impurities in high-performance organic solar cells," *Energy Environ. Sci.*, vol. 6, no. 5, p. 1513, 2013.

ISSN (online): 2246-1248  
ISBN (online): 978-87-7112-518-4

AALBORG UNIVERSITY PRESS